İSTANBUL TECHNICAL UNIVERSITY ★ INSTITUTE OF SCIENCE AND TECHNOLOGY

KELVIN PROBE FORCE MICROSCOPY AND ITS APPLICATIONS

M.Sc. Thesis by
Nihan ÖZKAN

Department : Engineering of Physics

Programme : Engineering of Physics

AUGUST 2010

İSTANBUL TECHNICAL UNIVERSITY ★ INSTITUTE OF SCIENCE AND TECHNOLOGY

KELVIN PROBE FORCE MICROSCOPY AND ITS APPLICATIONS

M.Sc. Thesis by

Nihan ÖZKAN

Date of submission : 20 August 2010

Date of defence examination: 24 August 2010

Supervisor (Chairman) : Assoc. Prof. Dr. H. Özgür ÖZER (İTU)

Members of the Examining Committee : Prof. Dr. Ahmet ORAL (SU)

Asisst. Prof. Dr.Oğuzhan GÜRLÜ(İTU)

AUGUST 2010

İSTANBUL TEKNİK ÜNİVERSİTESİ ★ FEN BİLİMLERİ ENSTİTÜSÜ

KELVIN KUVVET AYGITI MİKROSKOBU VE UYGULAMALARI

YÜKSEK LİSANS TEZİ
Nihan ÖZKAN
(509071110)

Tezin Enstitüye Verildiği Tarih : 07 Mayıs 2010
Tezin Savunulduğu Tarih : 24 Ağustos 2010

Tez Danışmanı : Doç. Dr. H. Özgür ÖZER (İTÜ)
Diğer Jüri Üyeleri : Prof. Dr. Ahmet ORAL (SÜ)
Yrd. Doç. Dr. Oğuzhan GÜRLÜ (İTÜ)

AĞUSTOS 2010

ACKNOWLEDGEMENTS

I would like to express my hearty gratitude to Prof. Dr. Ahmet Oral for his ideas and opportunities supplied for this work. I am grateful to him to allow a chance to work in his group in Sabancı University.

I would like to thank to my advisor Assoc. Prof. Dr. H. Özgür Özer for his continuous support during my master study.

I would like to give special thanks to Ümit Çelik for his contributions to set up the Kelvin probe force microscopy for this work.

I would like to thank Selda Sonuşen and Anıl Günay Demirkol for helping me to prepare samples for this work in Sabancı University. Also i want to thank my other group friends Derya Gemici, Seda Aksoy and Hüsnü Aslan for their helps during my laboratory study.

I would like to thank to Prof. Dr. Mustafa Çulha and his group at Yeditepe University for letting us use the Raman Spectroscopy to characterize our graphene flakes.

I am thankful to the Scientific and Technological Research Council of Turkey (TÜBİTAK) for financial support at the beginning of my academic life.

I would like to give special thanks to my longest time friend Feyzan Özgün Ersoy for sharing all of things and overcoming all troubles with me during my undergraduate and graduate life and my other undergraduate friends from Dokuz Eylül University Hale Sert, Nevin Soylu, Duygu Dörtlemez and Filiz Aksoy for always being by side even they are far away as a distance from me. Also i want to thank Sinem Şalva for her suppport and kind friendship.

I want to give my deepest gratitude to my family for their trust, prayers and patience. Finally I want to give my hearties thanks to my dearest husband for being always with me and for his love and patience.

August 2010 Nihan ÖZKAN

TABLE OF CONTENTS

Page

ABBREVATIONS

AFM	:	Atomic Force Microscopy
STM	:	Scanning Electron Microscopy
SPM	:	Scanning Probe Microscopy
OBD	:	Optical Beam Deflection
PSPD	:	Position Sensitive Photo Detector
VDW	:	Van der Waals
FFM	:	Frictional Force Microscopy
EFM	:	Electrostatic Force Microscopy
KPFM	:	Kelvin Probe Force Microscopy
RMS	:	Root Mean Square
AM-KPFM	:	Amplitude Modulation of Kelvin Probe Force Microscopy
FM-KPFM	:	Force Modulation of Kelvin Probe Force Microscopy
CPD	:	Contact Potential Difference
PLL	:	Phase-Locked Loop
LIA	:	Lock-in Amplifier
PSD	:	Phase-Sensitive Detection
PMMA	:	Poly(methyl methacrylate)
IPA	:	Isopropyl Alcohol
MIBK	:	Methyl Isobutyl Ketone

LIST OF FIGURES

Page

KELVIN PROBE FORCE MICROSCOPY AND ITS APPLICATIONS

SUMMARY

Kelvin Probe Force Microscopy(KPFM) is a modified version of Atomic Force Microscopy(AFM) which measures the local surface potential or work function of different metals with high spatial resolution. It is also known as 'Surface Potential Microcopy'. The difference of KPFM from AFM is that it depends on the principle of Kelvin method and provides work function difference of metals as well as high resolution topography imaging. The work function map obtained from KPFM provides electronic characterization of materials.

In this work we modified the Atomic Force Microscope(AFM) to perform the Kelvin Probe Force Microscopy measurements. There are different KPFM modes commonly employed in the literature. We operated the KPFM in multi-frequency mode in this work, topographical signal and the Kelvin probe signal are simultaneously detected at first and second resonance frequencies of the cantilever, respectively. Thus topography of the surface and work function difference between the sample and tip are simultaneously determined. The first resonance frequency is used to obtain topography image as used in intermittent-contact AFM mode. The second resonance frequency is used to obtain the work function difference image of the sample using a digital Phase Locked Loop or Lock-in Amplifier and a kelvin feedback system.

In this thesis different materials were imaged with KPFM and work function differences between different materials were measured by comparing these work function differences with theoretical values.

KELVİN KUVVET AYGITI MİKROSKOBU VE UYGULAMALARI

ÖZET

Kelvin Kuvvet Aygıtı Mikroskobu (KKAM) yüzeylerin iş fonksiyonlarını atomik ve moleküler ölçekte gözleyebilen atomik kuvvet mikroskobunun (AKM) değişik bir türüdür. Bu yüzden "Yüzey Potansiyeli Mikroskobu" olarak da bilinir. Kelvin Kuvvet Aygıtı Mikroskobu'nun Atomik Kuvvet Mikroskobundan farkı Kelvin metodu prensibine göre çalışması ve yüksek çözünürlüklü topografi bilgisinin yanı sıra yüzeylerin iş fonksiyonları farkını vermesidir. Kelvin Kuvvet Aygıtı Mikroskobu ile sağladığımız iş fonksiyonu haritası, o materyalin yerel yapılarının elektronik durumları ve kompozisyonu hakkında bilgi verir.

Bu çalışmada Kelvin Kuvvet Aygıtı Mikroskobu ölçümleri için Atomik Kuvvet Mikroskobu sistemi üzerinde değişiklik yapılmıştır. Kaynaklara göre farklı Kelvin Kuvvet Aygıtı çalışma kipleri vardır. Biz, bu çalışmada ilk rezonans frekasında topografi sinyalinin ikinci rezonans frekansında ise iş fonksiyonu sinyalinin aynı anda saptandığı çoklu frekans modunda çalıştık. Böylece yüzeyin topografisi ile yüzeyin, mikroskobun iğnesine göre iş fonksiyonu değeri aynı anda belirlenmiş olur. İlk rezonans frekansı, Atomik Kuvvet Mikroskobunun yarı temas kipinde olduğu gibi topografiyi belirlemek için kullanılırken, ikinci rezonans frekansı Faz Kilitleme Döngüsü veya Frekans Kilitlemeli Yükseltici ve Geri Besleme Sistemi ile iş fonksiyonu farkını belirlemek için kullanılır. Bu tez çalışmasında Kelvin Kuvvet Aygıtı Mikroskobu kullanılarak farklı metallar incelenmiş ve bu farklı metaller arasındaki iş fonksiyonları farkı teorideki değerleri ile karşılaştıralarak ölçülmüştür.

1. INTRODUCTION

Fundamentals of scanning probes microscopes rely on 1600's. Isaac Newton studied with inertia and force to understand motion of objects and in 1687 explained three laws of motion which are described these days in physics. In $1881 - 1882$ Hertz published an article about contact mechanics[**1**]. In his work he wanted to work out the relationship between the optical properties of multiple, stacked lenses with the force holding them together. Then profilometers and indenters were developed in 1920's. Developments in quantum mechanics also provided a basis for scanning probe techniques. In 1927 Friedrich Hund discovered the principle of quantum tunneling (quantum mechanical barrier penetration)[**2**]. In 1930's some thoughts about atomic forces were begun to develop. In 1936 London related an interacting two-atom system with van der Waals force which is the interaction between the dipoles occured in the atoms. Then in 1956 Lifshitz developed the macroscopic theory (also called the modern or continuum theory)of van der Waals forces between and within continuous materials[**3**]. In 1970's D. Tabor, R.H.S. Winterton, J.N. Israelachvili developed the first surface forces apparatus for directly measuring the forces between surfaces and for studying other interfacial phenomena at the molecular level. The topografiner is predecessor of scanning tunneling microscope, was invented by Young in 1972[**4**]. It is very similar to scanning tunneling microscope but it relies on the principle of field emission and also the tip should be rather far away from the surface. In the topografiner two scanning piezo elements are used for scanning specimen surface with the emitter which is like sharp tip. In the topografiner the voltage between the emitter and the surface is amplified and applied to a piezoelectric seramic element on which the emitter is mounted. The distance between the emitter and surface is kept constant by a servo system. The vertical and horizontal resolutions of topografiner were limited to 30 Å and 4000 Å. In 1982 Binnig, Rohrer and coworkers have developed first scanning tunneling microscope and received the

Nobel Prize in Physics in 1986 for their discovery [**5**]. The physical basis of the STM is electron tunneling. Binnig and coworkers obtained STM image of clean Au(100) surface and a graphite surface.

STM also has been widely used to atomic manipulation besides imaging the structure and electrical properties of materials. In 1990 Don Eigler manipulated Xe atoms on Ni(110) surface with single atoms by using a STM tip[**6**]. But in atomic manipulation there were some problems in controllably positioning atoms on the surfaces. In manipulation process the force interaction between the tip and adsorbate atom is increased by making the tip-surface distance smaller. This interaction should be stronger for the adsorbate atom to overcome the lateral forces and be able to move along surface. Also not to move the adsorbate atoms from the substrate to the tip, the tip-adsorbate atom interaction should be smaller than the adsorbate-substrate interaction. Therefore the force interaction should be measured to control the atoms on surfaces and in this way to control the manipulation. Also the principle of STM limits the kinds of materials imaging. Only conductor materials can be imaged with STM. Because of these disadvantages atomic force microscope has been constructed with its capability of measuring forces between the surface atoms and tip and imaging of nonconductive materials. Binnig and coworkers has developed the first atomic force microscope in 1986[**7**]. After one year of the invention of AFM, Binnig and coworkers succeeded to image of surface of graphite. In Atomic Force Microscopy the force interaction between the atoms of a sharp tip and sample surface is used to investigate surfaces, just like the tunneling current in STM. Constructing AFM has opened a new challenging area for scientists. In 1991 Nonnenmacher et al.[**21**] developed Kelvin Probe Force Microscopy working with the principle of Kelvin method which was introduced first by Lord Kelvin[**55**] and observed before Alessandro Volta at the beginning of the 19th century.

In Kelvin method two conductors are brought parallel with a small distance between them as a parallel plate capacitor shown in Figure 1.1. When two conductors are first brought into electrical contact, free electrons flow from one with the higher fermi level to the other one with the lower fermi level. When the

system reaches a thermodynamical equilibrium, the resulting potential difference is the Contact Potential Difference(CPD) between the metals and is equal to the difference between their work functions. In this way, the contact potential between the two materials is given by,

$$V_c = \frac{1}{e(\Phi_2 - \Phi_1)} \tag{1.1}$$

where Φ_1 and Φ_2 are the work functions of the conductors. Although the Kelvin

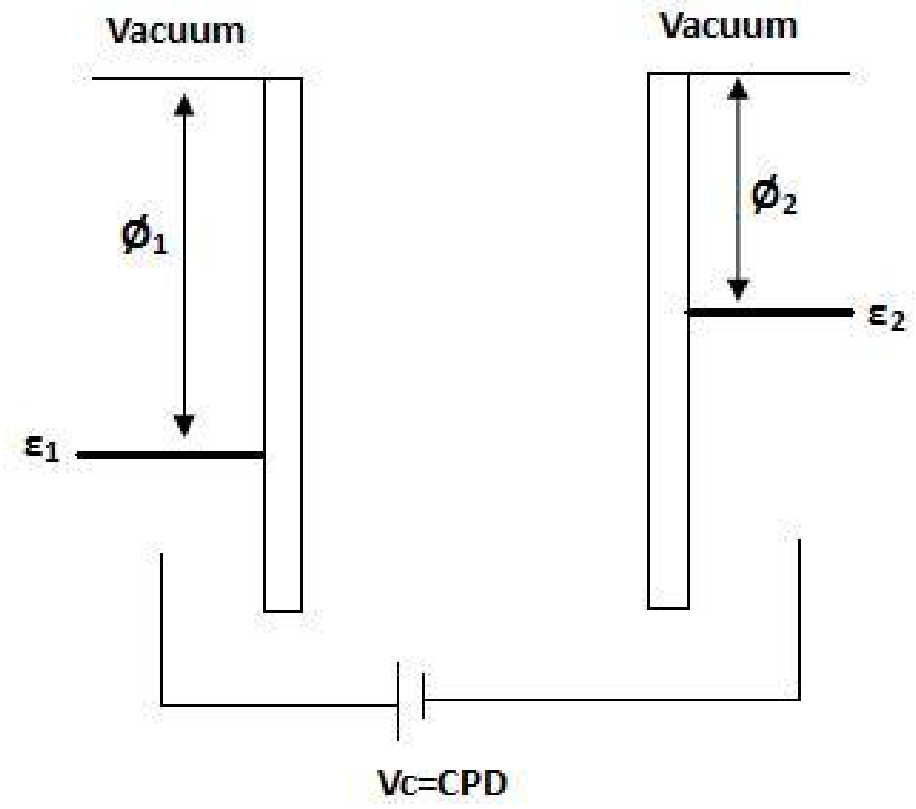

Figure 1.1: The schematic diagram of Kelvin method. ε_1 and ε_2 are the fermi levels of conductors.

method has a high sensitivity for potential measurement, it does not obtain a lateral image of the variation of the CPD on the surface[**21**]. High resolution CPD measurements can be achieved by using KPFM which is a modified version of Scanning Probe Microscopy(SPM).

2. STM AND AFM

2.1 Scanning Tunneling Microscopy

The underlying physical basis of the STM is the tunneling effect. The tunneling effect originates from the wavelike properties of particles in quantum mechanics. When a particle is coming towards to a barrier with a kinetic energy smaller than the potential energy of the barrier, there is classically non-zero probability of passing over the forbidden region and reappearing on the other side of the barrier.

Φ_0 is the potential of a rectangular barrier,E is the kinetic energy of the particle, m is the mass of particle and p is the probability for the particle to pass over the barrier with thickness d is given by,

$$p \propto e^{-2kd} \tag{2.1}$$

where $k = \sqrt{2m(\Phi_0 - E)/\hbar^2}$

The tunneling transmissivity decreases exponentially with the tunneling distance,in vacuum about a factor of 10 every Å.

Figure 2.1 shows the energy of the tunneled particle is the same, only the quantum amplitude is decreased. Hence the probability of the process is also decreased. The principle of electron tunneling was first proposed by Giaever [**8**]. He thought that when a potential difference is applied to two metals separated by a thin insulating film, a current will be occurred between metals with the ability of electrons to penetrate a potential barrier. To be able to measure a tunneling current, the two metals must be so closed(must be spaced no more than 10 nm apart). Binnig and Rohrer were the first to use this formula;

$$I \approx 18 \frac{V_T}{10^4 \Omega} \frac{k}{d} A_{eff} e^{-2kd} \tag{2.2}$$

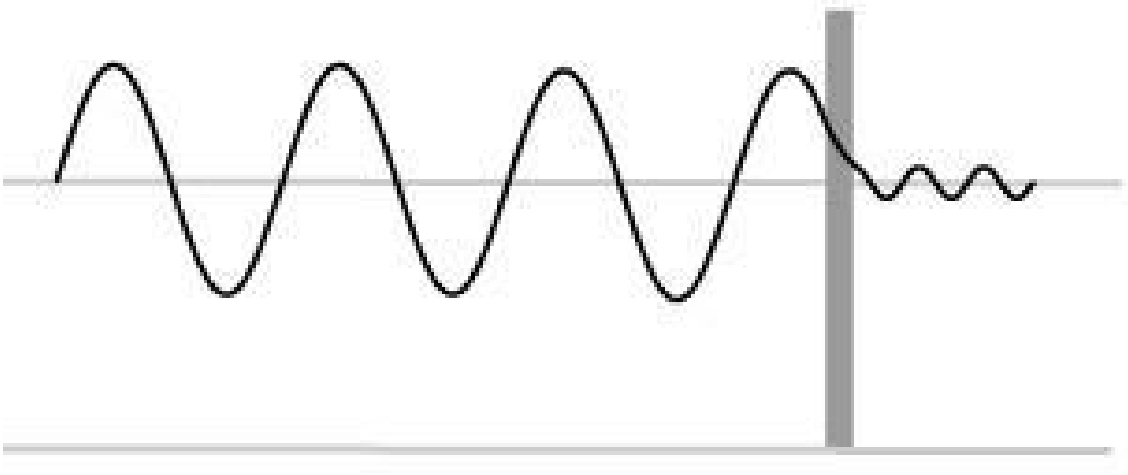

Figure 2.1: Schematic representation of quantum tunneling

where $2k[1/\text{Å}] = 1.025\Phi^{1/2}[eV]$,$\Phi$ is the average work function,V_T is the bias voltage, d is the separation between the tip and the surface and A_{eff} is the effective area determining the lateral resolution.

The tunneling current depends very strongly on the distance between the tip and the surface. A change in separation of tip-surface about 1 Å causes nearly an order of magnitude change in current.

The tip is scanned over the surface, while the tunneling current between it and the surface is measured. There are two STM modes basically; constant current mode and the constant height mode.

Figure 2.2(a) shows the basic constant current mode of operation[**9**]. To keep the current constant, a feedback loop changes the distance between the surface and tip. The feedback loop achieves this by applying suitable voltages to the piezoelectric crystal and the applying voltage to the piezo gives the topographic map of the surface. In the constant height mode (Figure 2.2(b)[**9**]. In this mode the feedback keeps the average current constant. The changes of the tunneling current give the topographic image of the surface. The constant current mode is generally used for atomic-scale images. The constant height mode is not convenient for rough surfaces, because of that it is used for atomically flat surfaces.

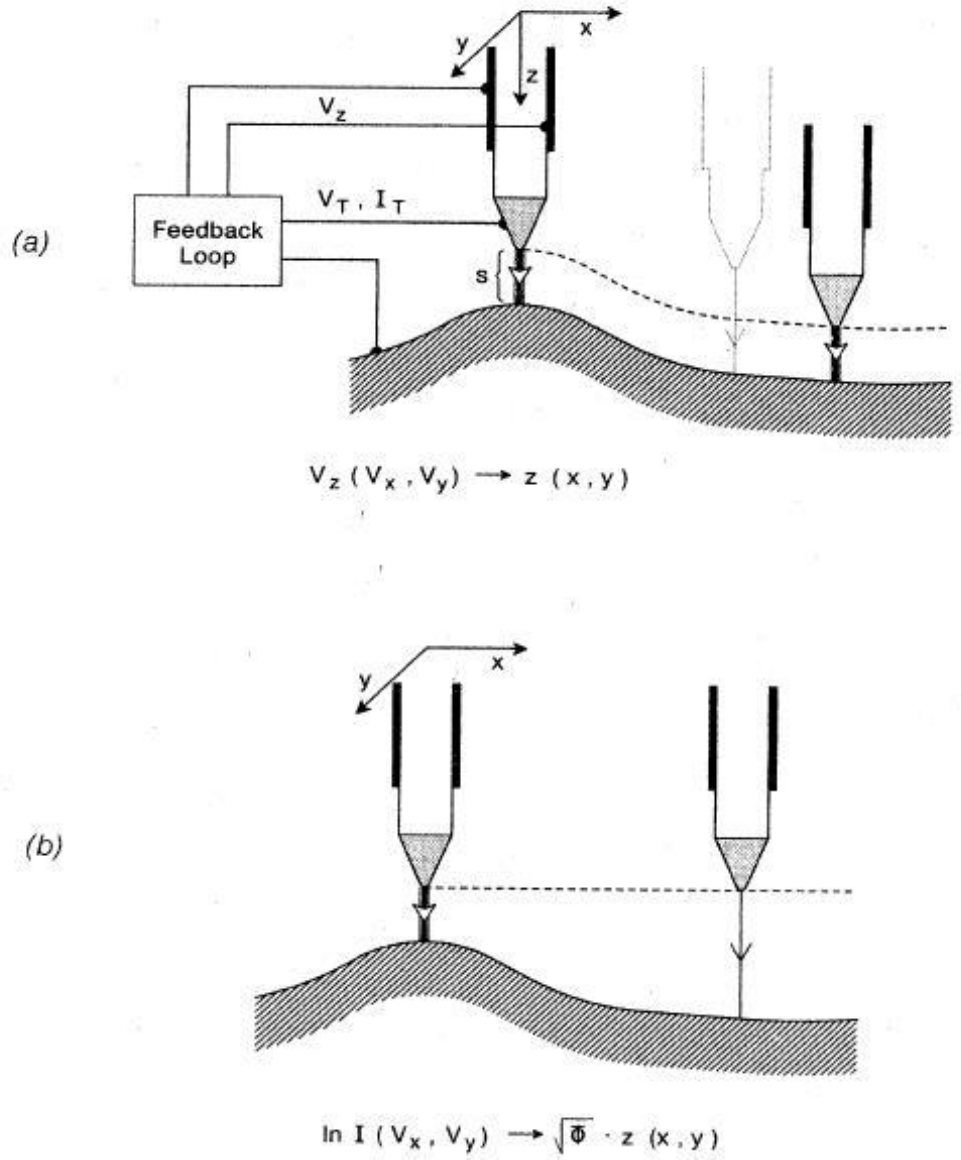

Figure 2.2: An STM can be operated in either the constantcurrent (a) or the constant-height mode (b).

However this mode provides faster scanning images of surfaces to minimize image distortion due to piezoelectric creep and thermal drift.

2.1.1 The STM design of Binnig

Figure 2.3 shows a schematic of an STM designed by Binnig and Rohrer[5]. The tip(T) of the microscope shown in Figure 2.3(a) is scanned over the surface of the sample(S) with a piezoelectric tripod(X,Y,Z). Positioning of the sample is achieved with a piezoelectric 'louse'(L) with electrostatically clamp feet. A vibration filter system(P) protects the system from external vibration and noise.

In the constant current mode a voltage V_z is applied to the Z piezoelectric element and the feedback loop shown in Figure 2.3(b) keeps the tunneling current constant while the tip is scanned over the surface altering V_z and V_y. These altering voltage values give surface topography of the sample.

2.2 Atomic Force Microscopy

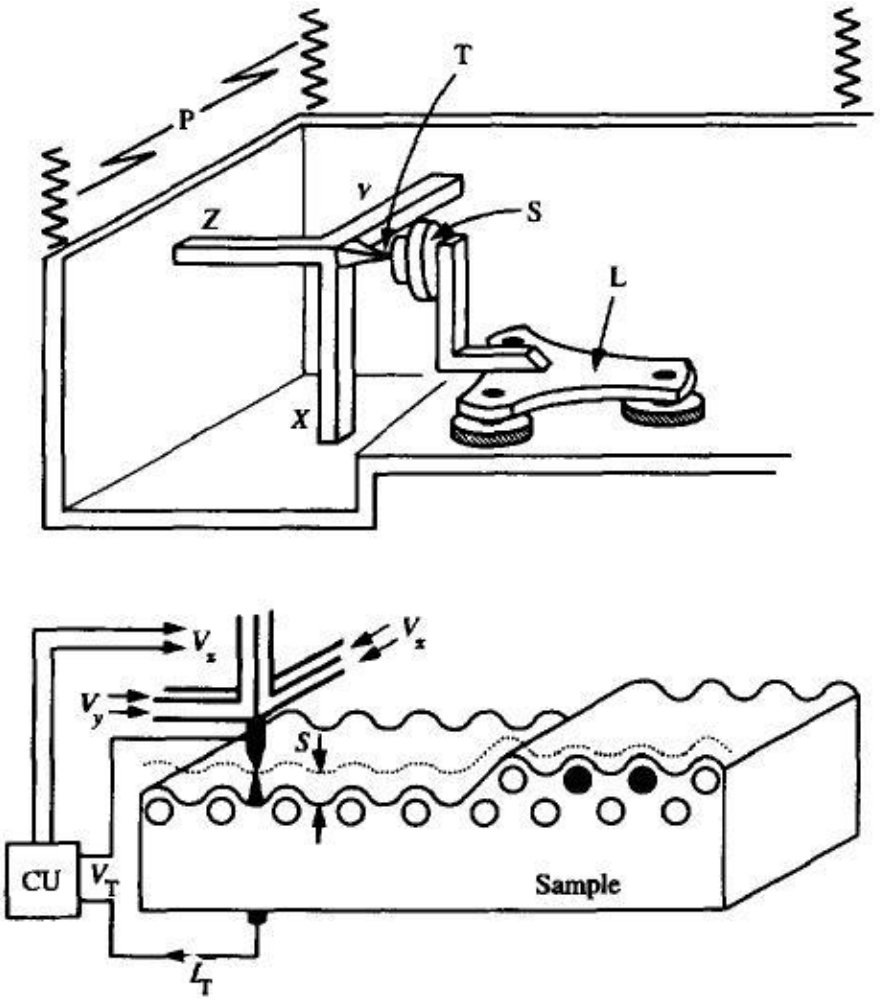

Figure 2.3: Schematic of a scanning tunneling microscope designed by Binnig and its operation

Led Binnig,Quate and Gerber built the first Atomic Force Microscope(AFM) in 1986[**7**]. They made a tiny spring from gold foil and placed a small diamond fragment on the cantilever to act as a tip. They positioned the tip close to the sample and measured the deflection of the cantilever with an STM tip. In this way they were able to measure the force on the diamond tip and obtained images of a ceramic sample.

In an AFM, the force between the sample and tip is used (instead of the tunneling current) to detect the distance between the tip and the sample. The cantilever which is extremely sensitive to weak forces is fixed at one end; the other end has a sharp tip which gently contacts the surface of a sample. The sharp tip scans over the surface within a very short distance. Deflection of the cantilever due to force interaction between the tip and surface is detected with variable deflection techniques and sent to the feedback loop and used as reference in order to obtain topographical images.

2.2.1 Development of the AFM

The first AFM images were taken in repulsive contact between the tip and the surface. Also attractive forces were required to be measured. But some early attempts to measure attractive forces in the AFM by the contact mode of operation method failed [**10**]. Because when the tip and the surface are in contact, attractive forces are much smaller than other interaction forces between the sample and the tip. Martin et al.[**11**] could measure these weak interactions increasing the sensitivity by a factor of Q (the quality factor of cantilever). The cantilever was oscillated near its resonance frequency and changes in oscillation amplitude were measured due to the tip-surface interaction. This work brought an important development of a number of dynamic mode of operation techniques also referred to as intermittent-contact and non-contact modes. These modes are more sensitive than the contact mode of operation.

In the earliest work in AFM, the cantilevers were made by hand from small metal wires by Marti et al.[**12**] or pieces of metal foil by Binnig et al.[**7**]. But they couldn't make the cantilevers smaller than $\approx$ 1mm, so the highest achievable resonant frequencies were only a few kHz. This limits the available bandwidth and causes vibrational problems. Thus, microfabricated cantilevers which can be much smaller and have a higher resonance frequency, were developed. These cantilevers were first made by Binnig et al.[**10**] using etching techniques and the designs and some fabrication processes were developed further by Albrecht et al.[**13**]. These processes include a method for producing SiO_2 or Si_3N_4

cantilevers without tip and a method for producing $SiO_2$and Si_3N_4 cantilevers with integrated tips.

Another significant development in AFM was the measurement of the frictional forces between the tip and the surface. Mate et. al.[**14**] could measure the frictional forces using an AFM by an interferometric detection system which could measure only lateral forces and called as Frictional Force Microscope(FFM).

The most important developments for AFM work were the inventions of detection systems differently from interferometric detection system. Capacitance detection system was invented by Neubauer et al.[**15**] and the optical beam deflection system was devised by Meyer and Amer[**16**]. The optical beam deflection is now commonly used, also it was used in the Atomic Force Microscopy supplied by Nano Magnetics Instruments Ltd. for our work. These cantilever deflection detection techniques will be analyzed in more detail in further sections.

The other significant development in AFM that is particularly relevant to this thesis was the measurement of electrostatic forces. First Martin et al.[**17**] and Erlandsson et al.[**18**] measured electrostatic forces by the method Martin et al.[**11**] described before to increase the sensitivity by a factor of Q. Martin et al.[**17**] also used another technique to measure electrostatic forces as small as 10^{-10}. Then Terris et al.[**19**] measured electrostatic forces by applying an ac voltage between the sample and the tip. In this way Electrostatic Force Microscopy(EFM) was developed by the method in which an ac voltage is applied between the sample and the tip and ac force on the tip was measured.

The final development in EFM instrumentation that is exactly relevant to this thesis came with the development of Kelvin Probe Force Microscopy(KPPFM) by Weaver and Abraham [**20**] and Nonnenmacher et al.[**21**] in 1991. It measures the contact potential difference of different metals with high spatial resolution by the principle of Kelvin Method besides obtaining topographic images.

2.2.2 AFM imaging

The underlying principle of AFM is that the interactions between the tip and the sample cause deflections on the cantilever and these interactions between the

tip and sample are measured by recording the deflection of the cantilever. There are several modes of imaging based on atomic forces. Generally the deflection of the cantilever can be measured associated with the force. Keeping the deflection constant by varying the vertical position of the tip produces constant force image. For instance; when the tip is close to the sample, interactions between the tip and the sample increase and the image represents the topographic structure of the surface. But the deflection is not the most sensitive measurement, it has a relatively small signal-to-noise ratio. There is another more sensitive measurement which uses the vibrational characteristics of the cantilever.

The cantilever is characterized by its spring constant k, resonant frequency f_0 and quality factor Q.The quality factor depends on the damping mechanisms present in the cantilever.

For a rectangular cantilever with dimensions width(w), thickness(t) and length(l), the spring constant k is given by

$$k = \frac{E_Y w t^3}{4l^3} \tag{2.3}$$

where E_Y is the Young's modulus.

The resonant frequency of the cantilever is given by

$$f_0 = \frac{1}{2\pi}\frac{t}{l^2}\sqrt{\frac{E_Y}{\rho}} \tag{2.4}$$

where ρ is the mass density of the cantilever material.

2.2.3 Measuring the cantilever deflection

The AFM is simply one kind of force measuring device,designed to measure particularly small forces (a few nN or less) and therefore small spring displacements. Historically, a lot of different techniques have been used to measure very small displacements,and many of them have been tried in the AFM. In this section a number of the techniques that have been used in the AFM will be described and their advantages and disadvantages will be explained.

2.2.3.1 Electron tunneling detection

In the first AFM set-up an STM tip was used to measure the cantilever deflection[**7**]. The STM tip was positioned behind the AFM tip. The changes in the tunneling current gives the cantilever displacement in the same way as the tip-surface separation is monitored via the exponential dependence of the current on separation in the STM set-up, $I \propto exp(-2kd)$ This method is convenient to set up and high sensitive to the displacement of the cantilever. The high sensitivity is resulting from the exponential distance dependence of the tunneling current an it provides a wide application area. On the other hand, the tunneling technique requires the use of feedback circuits to follow large cantilever deflections and thermal drifts and this limits the available bandwidth. Also the contamination-induced instabilities of the tunneling junction makes its performance very unreliable. This is an important disadvantage of the electron tunneling detection. And the tunneling tip applies extraneous van der Waals and electrostatic forces on the cantilever. Actual force measurements can be affected because of these forces[**19**]. As a consequence of these problems, the tunneling detection method is not used widely today.

2.2.3.2 Capacitance detection

The capacitance detection was first used by Neubauer et al.[**19**] who used a simple parallel plate geometry. They used the back of the lever as one plate of a parallel plate capacitor and measured the change in capacitance due to the displacement of the lever. This technique proved more effective than the STM method. Also frictional force and load were determined simultaneously by measuring the capacitance change between the cantilever and two orthogonal plates. Optical techniques for AFM cantilever deflection are fundamentally limited by photon shot noise. There is no such a limitation for capacitance detection method. But there is another limitation problem arises from properties of capacitive detectors. Capacitance detection becomes more sensitive when large plates are used. But, AFM cantilevers must be as small as possible, because a high resonant frequency is required. If the plates are reduced in size, the gap must also be reduced to retain the same sensitivity, and if the gap is reduced, the alignment and flatness of the

plates become more critical. As a result, these problems limit the performance of small capacitive detectors.

Capacitive sensing is basically unsuitable for the AFM, because the plates cannot be made big enough to overcome the practical problems of a alignment and surface roughness.

2.2.3.3 Optical interferometry

An instrument based on a interferometer was developed [**22**], after the first papers on the AFM appeared, which used a tunneling sensor, because of its limitation problems. The light from the laser light source is polarized by the polarizing beam splitter and focused onto the back of the cantilever shown in Figure 2.4. The reflected light is collimated by the same lens and interferes with the reference beam reflected from an optical flat. Then the reference pattern is projected to on a photodiode. $\lambda/4 - plate$ is used to separate the reflected light from the incident light. The lever deflection is measured with the help of the interference pattern. The interference pattern is modulated by the oscillating cantilever. Interferometry is a well-established method for measuring small displacements. Therefore it was used in AFM measurements from an early stage, and a number of different types of interferometer have been implemented. The designs vary significantly, but can be divided into homodyne and heterodyne interferometers and optical fibre-based systems. The systems vary in performance, they are all capable in principle of high sensitivity and they all measure linear than angular displacement.

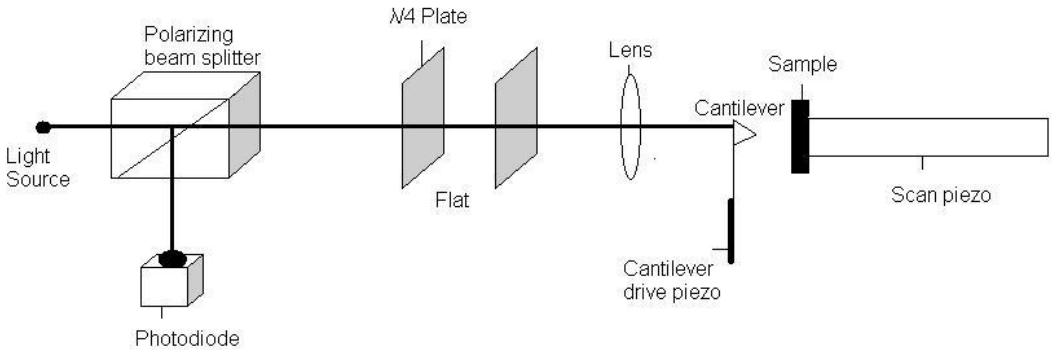

Figure 2.4: Schematic diagram of optical interferometry.

An instrument based on a interferometer was developed [**22**], after the first papers on the AFM appeared, which used a tunneling sensor, because of its limitation problems. The light from the laser light source is polarized by the polarizing beam splitter and focused onto the back of the cantilever shown in Figure 2.4. The reflected light is collimated by the same lens and interferes with the reference beam reflected from an optical flat. Then the reference pattern is projected to on a photodiode. $\lambda/4 - plate$ is used to separate the reflected light from the incident light. The lever deflection is measured with the help of the interference pattern. The interference pattern is modulated by the oscillating cantilever. Interferometry is a well-established method for measuring small displacements. Therefore it was used in AFM measurements from an early stage, and a number of different types of interferometer have been implemented. The designs vary significantly, but can be divided into homodyne and heterodyne interferometers and optical fibre-based systems. The systems vary in performance, they are all capable in principle of high sensitivity and they all measure linear than angular displacement.

In heterodyne interferometers light with frequency ω_0 is split into a reference path and a measurement path[**23**]. The light in the measurement path is frequency shifted to ω_1 by an acousto-optical modulator. The light reflected from the oscillating cantilever interferes with the reference beam on the detector It is one of the most sensitive deflection detection method.

The fiber optical interferometer is one of the simplest interferometers. The light from a laser source is sent to an optical fiber[**23**]. The light is split in a fiber-optic beam splitter into two fibers. One of the fiber is specially prepared not to receive any reflected light back in to the fiber. The other fiber is brought close to the cantilever and the light is partially reflected back into the fiber by the cantilever. The two reflected waves interfere with each other. The product is sent back to the fiber coupler and again split into two parts. One of is detected by the photodiode, the other half is fed back into the laser.

Clearly, interferometry has significant advantages over all the other methods discussed. The only real disadvantage is its complexity. In heterodyne

interferometers light with frequency ω_0 is split into a reference path and a measurement path[**23**]. The light in the measurement path is frequency shifted to ω_1 by an acousto-optical modulator. The light reflected from the oscillating cantilever interferes with the reference beam on the detector. It is one of the most sensitive deflection detection method.

The fiber optical interferometer is one of the simplest interferometers. The light from a laser source is sent to an optical fiber[**23**]. The light is split in a fiber-optic beam splitter into two fibers. One of the fiber is specially prepared not to receive any reflected light back in to the fiber. The other fiber is brought close to the cantilever and the light is partially reflected back into the fiber by the cantilever. The two reflected waves interfere with each other. The product is sent back to the fiber coupler and again split into two parts. One of is detected by the photodiode, the other half is fed back into the laser.

Clearly, interferometry has significant advantages over all the other methods discussed. The only real disadvantage is its complexity.

2.2.3.4 Optical beam deflection(OBD)

Meyer and Amer[**16**] developed the optical beam deflection technique which is the most common cantilever deflection detection system. In this system laser beam is dropped to the back of the cantilever, then reflected light from the back of the cantilever is sent to a two-cell photodiode. The light beam is set to hit the photodiodes in the middle of the two diodes. Forces on the tip cause the cantilever to bend, and any deflection of the cantilever will cause an imbalance of the number of photons reaching the diodes. Hence the electrical current in the photodiodes will be unbalanced too. The difference signal is amplified and it is the input signal to the feedback loop. This technique was later improved by the same authors in 1990[**22**], using a four-cell photodiode to measure lateral forces on the tip.

Figure 2.5 shows the diagram of a AFM with cantilever and OBD. The reflected laser beam is detected with a position sensitive photodetector(PSPD) which consists of two adjacent photodiodes ($PDA_A and PDB_B$) shown in Figure 2.6[**54**].

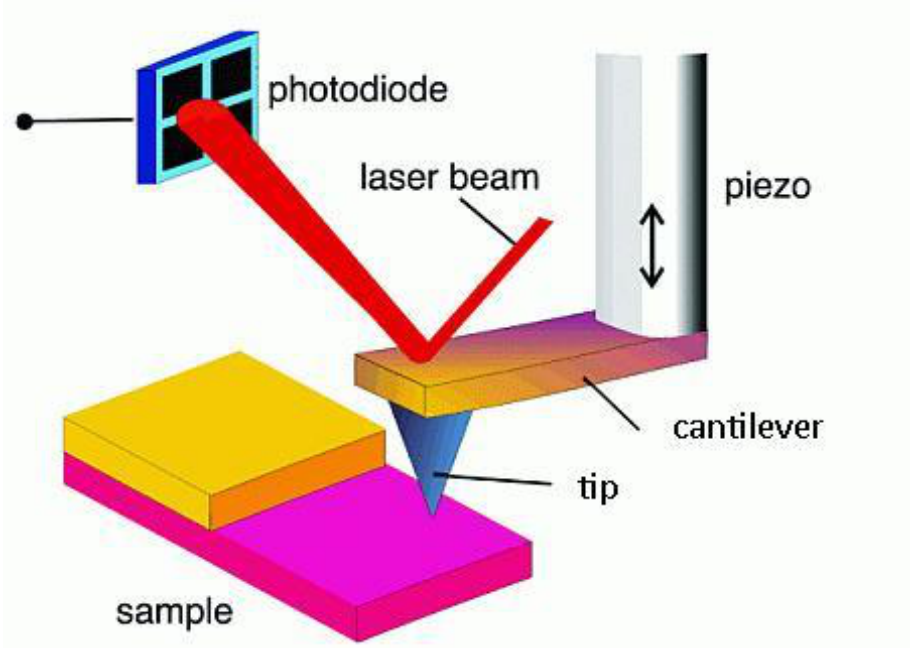

Figure 2.5: Diagram of a AFM with cantilever probe and optical beam deflection

The cantilever displacement Δz induces the cantilever deflection $\Delta\Theta$ given by,

$$\Delta\Theta = \frac{3}{2}\frac{\Delta z}{l} \tag{2.5}$$

where l is the cantilever length.

If the cantilever deflects $\Delta\Theta$, the laser beam deflects $2\Delta\Theta$. In this way, the PSPD displacement Δa is given by,

$$\Delta a = 3\frac{s}{l}\Delta z \tag{2.6}$$

where s is the distance between the tip and the PSPD.

The photocurrents ($i_A and i_b$) from the two photodiodes are independently detected with I-V convertors. The photocurrents are proportional to the intensity incident on the diode. The voltage signal (V_{A-B}) which is proportional to the current difference (i_{A-B}) is produced by a differential amplifier. In this way the variation of the cantilever deflection signal is given by,

$$\Delta V_{A-B} = \eta\alpha P\xi_{PD}R_{IV}\frac{3s}{la}\Delta z \tag{2.7}$$

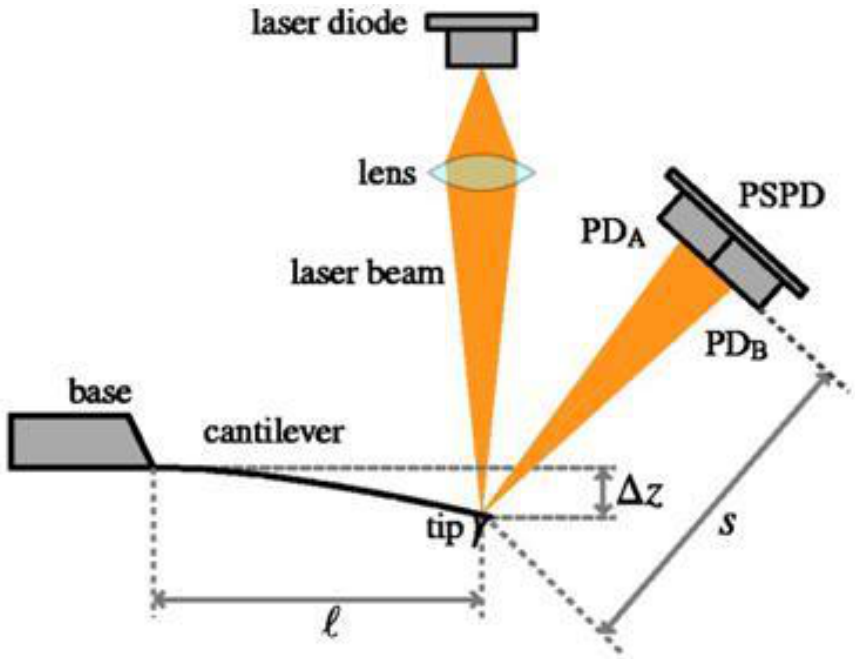

Figure 2.6: Typical experiment set-up for a cantilever deflection using OBD method[**54**]

η : The efficiency of the light-to-current conversion at the photodiodes.

α: The laser power attenuation coefficient in the optical path.

P: the output power of the laser diode.

ξ_{PD}: Frequency-dependent gain reduction factor

R_{IV}: The feedback resistor of the photodiode preamplifier.

This equation shows that the sensitivity can be increased by increasing the intensity of the light beam or by decreasing the divergence of the laser beam.

One of the major noise sources in OBD is the photodiode shot noise[**23**]. The voltage noise arising from the short noise is,

$$\delta v_s = \xi_{PD} R_{IV} \sqrt{2e\eta\alpha P B_{BPF}} \tag{2.8}$$

given, where e and B_{BPF} are the elementary charge and the band width of the band pass filter, respectively.

The effective cantilever deflection noise density caused by the shot noise is given by as following,

$$n_{zs} = \frac{\delta v_s/\sqrt{B_{BPF}}}{\Delta V_{A-B}/\Delta z} = \frac{la}{3s}\sqrt{\frac{2e}{\eta\alpha P}} \tag{2.9}$$

The other major noise source in OBD method is the John noise. It is occurred from the resistor R_{IV} used in the I-V converters. The voltage noise arising from the Johnson noise is given,

$$\delta v_j = \sqrt{4k_B T N_{PD} R_{IV} B_{BPF}} \tag{2.10}$$

where, k_B, T and N_{PD} are the Boltzman constant, temperature and the number of photodiodes used in the PSD, respectively. The effective cantilever deflection noise density is given by,

$$n_{zj} = \frac{\delta v_j/\sqrt{B_{BPF}}}{\Delta V_{A-B}/\Delta z} = \frac{la}{3s}\frac{1}{\eta\alpha P\xi_{PD}}\sqrt{\frac{4k_B T N_{PD}}{R_{IV}}} \tag{2.11}$$

In most of the OPD sensors n_{zs} is the predominant noise component. Thus, n_{zj} is smaller than n_{zs}.

The advantages of this detection system is that it is a very simple and convenient method, and also normal and lateral forces can be measured simultaneously. It is a widely used system and has been used especially in commercial instruments. Therefore we use the beam optical deflection to measure the cantilever deflection in our AFM supplied by Nanomagnetics Instruments Ltd.

2.2.3.5 Other deflection methods

There are other deflection methods such as piezoresistive and piezoelectiricity detection. Piezoresistive detection is an alternative detection system which is not used widely. Piezoresistive cantilever is based on the fact that the resistivities of certain materials which change with the applied stress, for instance Si. The resistance changes due to the mechanical deflection of the lever. Piezoelectricity detection is worked with the same principle. The cantilever deflection is measured by a characteristic changing of the electric potential when a stress is applied.

2.2.4 Piezo effect and piezoelectric scanners

An electric field applied across a piezoelectric material causes a change in the crystal structure, with expansion in some directions and contraction in others. Also, a net volume change occurs. Many scanning probe microscopes(SPM's) use the transverse piezo electric effect, where the applied electric field E is perpendicular to the expansion or contraction direction. The amount of expansion or contraction is;

$$\Delta L = L(E.n)d_{31} = L\frac{V}{t}d_{31} \tag{2.12}$$

L: the free length of piezo slab

n: direction of polarization

d_{31}: the transverse piezoelectric constant

V: the applied voltage

t: the thickness of the piezo slab

Piezo translators are used in SPM's to scan the sample or the tip. Especially piezo tube scanners are now widely used due to their simplicity and their small size. The piezo ceramic is shaped into a tube form. The outer electrode is separated into four segments and connected to the scanning voltage. Opposite sectors are driven by signals of the same magnitude but opposite sign. This gives two dimensional movement on a sphere. The inner electrode is normally driven by the z signal.

2.2.5 Principles of atomic forces

Many SPM variants have developed to detect the forces between the sample and the tip. A variety of tip-sample interactions can be measured by an atomic force microscopy depending on the separation between the tip and the sample. The interactions between the two atom or molecules can be classified as short-range or long-range interactions. If the distance between the atoms is smaller than the order of 2 or 3 Å, the interactions are short-range and always repulsive.

If the distance is larger than this typical interatomic spacing, the interactions are long-range and repulsive or attractive. In vacuum there are van-der-Waals, electrostatic and magnetic forces with a long range (up to 100 nm) and short-range chemical forces.

2.2.5.1 Short-range interactions

There are short-range chemical forces such as the Morse potential and the Lennard-Jones potential. They are strongly repulsive at a short distance and slightly attractive at a long distance. Thus the short-range repulsive attraction is more sensitive to a small change in the distance the long-range interaction. This provides the basis for a high-resolution surface imaging in contact-mode AFM.

$$V_{morse} = -E_{bond}(2e^{-\kappa(z-\sigma)} - e^{-2\kappa(z-\sigma)}) \quad (\mathbf{2.13})$$

$$V_{Lennard-Jones} = -E_{bond}(2\frac{\sigma^6}{z^6} - \frac{\sigma^{12}}{z^{12}}) \quad (\mathbf{2.14})$$

These chemical forces are more complicated and describe a chemical bond with bonding energy(E_{bond}) and equilibrium distance(σ). The Morse potential has an additional parameter: a decay length:κ

2.2.5.2 Long-range interactions

The fundamental interactions at long distances are the van der Waals(VDW) interactions, which are responsible for the formation of solids,wetting. etc. At distances of a few nanometers,van der Waals forces are sufficiently strong to move macroscopic objects such as AFM cantilevers. Van der Waals interactions consist of three components: polarization, induction, and dispersion. Polarization refers to permanent dipole moments such as exist in water molecules. Induction refers to the contribution of induced dipoles. Dispersion is due to instantaneous fluctuations of electrons, which occur at the frequency of light causing optical dispersion.

According to Lifshitz theory[**24**], the VDW forces are considered as dispersion forces associated with the electromagnetic fluctuations. This theory shows that

the forces between bodies interacting through a medium depend on the dielectric properties of the bodies and the medium, and they are generally attractive and but can also be repulsive. Measurements of the forces between bodies separated in the 50-250 nm range show that Lifshitz theory is in good agreement with experiment.

In a simple system, the van der Waals potential for two identical gas molecules, is given by,

$$U_{vdw} = (\frac{1}{4\pi\epsilon_0})^2(\frac{\mu^4}{3kT} + 2^{\mu}2\alpha + \frac{3}{4}^{\alpha}2\hbar\omega)\frac{1}{z^6} \qquad (\mathbf{2.15})$$

where μ is the dipole moment, T is temperature, k is the Boltzmann constant, α is the polarizability, ϵ_0 is the permittivity of free space and $\hbar\omega$ is the ground state energy of the electrons.

For a spherical tip with radius R next to a flat surface the van-der-Waals potential is;

$$U_{vdw} = -\frac{A_H R}{6z^2} \qquad (\mathbf{2.16})$$

A_H is the Hamaker constant which depends on the type of materials of the tip and sample and is of the order of 1 eV for most solids. z is the distance between the surface, R is the radius of the spherical tip. Long-range interactions usually act between the sample and the tip besides sort-range interactions. Electrostatic attraction or repulsion, current induced or static-magnetic interaction, and capillary forces due to the surface energy of water condensed between the sample and the tip are long-range interactions. When tip close to the sample van der waals forces are bigger than these interactions. When tip is far from the surface the van der waals interactions decreases rapidly and long-range forces become significant and contributes more to the signal.

On the basis of theory Hartmann[**25**] calculated the VDW interactions between a SiO_2 probe and a metal surface immersed in various liquids for the sip-sample interaction of $1 - 410^4$nm. Immersion of the tip or sample in highly polar liquids

is found to reduce the VDW forces, at small tip-sample distances, by up to more than two orders of magnitude with respect to the value ins vacuum. It is also found that VDW forces can be either attractive or repulsive by an appropriate choice of the immersion medium.

Between the tip and a homogenous surface there may be electrostatic and magnetic interactions. These forces take place in long-range interactions and given by,

$$F_{magnetostatic} = \nabla(m \cdot B_{sample}) \tag{2.17}$$

$$F_{electrostatic} = -\frac{1}{2}\Delta V^2 \frac{\partial C}{\partial z} \tag{2.18}$$

where ΔV is the potential difference between the sample and the tip, C is the tip-sample capacitance as a function of separation z, B_{sample} is the the magnetic field occuring from the sample surface, and m is the magnetic dipole of the tip.

Electrical forces are occurred by localized charge on the tip and insulating surfaces. The charge is deposited either by applying a voltage pulse to the microscope tip or by contact charging the insulator surface with the tip. While the charge can be stable for hours in the air, the charge in the vacuum can be stable for days. Electrical forces also can be occurred on the conductive tip and conductive surfaces. In this case, there should be potential difference between the tip and the surface. The tip-surface system can be compared to the capacitor with parallel plates. The electrical force becomes,

$$F_{electrostatic} = -\frac{1}{2}\Delta(V_{bias} - V_{CPD})^2 \frac{\partial C}{\partial z} \tag{2.19}$$

where V_{bias} is the applied potential between the tip and the surface, V_{CPD} is the contact potential between the tip and the surface. To minimize the electrostatic force, $(V_{bias} - V_{CPD})$ should be zero.

2.2.6 Modes of operation

2.2.6.1 Contact mode

The atomic force microscopy(AFM) measures the forces between a sharp tip and a surface with high sensitivity by recording the deflection of a small cantilever spring on which the tip is mounted. This deflection obeys Hooke's law

$$F = -kx \tag{2.20}$$

where F is the force, x is the displacement, and k is the stiffness of the cantilever. A feedback loop monitors the tip-sample force and adjusts the sample z-position to hold the force constant. The topographic image of the sample is then taken from the sample z-position data. The mode described is called contact mode, in which the tip is deflected by the sample due to repulsive forces, or contact. Thus contact mode is also known as repulsive mode. This mode was used in the earliest work in AFM[**7**].

To examine this mode in more detail, refer to the van der Waals curve in Figure 2.7[**56**]. As the atoms are gradually brought together, they first weakly attract each other. This attraction increases until electron clouds of atoms begin to repel each other electrostatically. This electrostatic repulsion weakens the attractive force as the separation between the atoms continues to decrease. The force goes to zero when the distance between the atoms reaches a couple of angstroms about the length of a chemical bond. When the total van der Waals becomes repulsive(positive), the atoms are in contact. Two other forces are present during contact mode in addition to the van der Waals force. A capillary force exerted by the thin water layer often present in an ambient environment and the force exerted by the cantilever itself.

To obtain high force sensitivity with this technique the simplest approach is to use a cantilever with a very low stiffness between $0.01 - 0.001$ N/m. Because the deflection of the cantilever should be significantly larger than the deformation of the tip and sample, the cantilever should be much softer than the bonds between

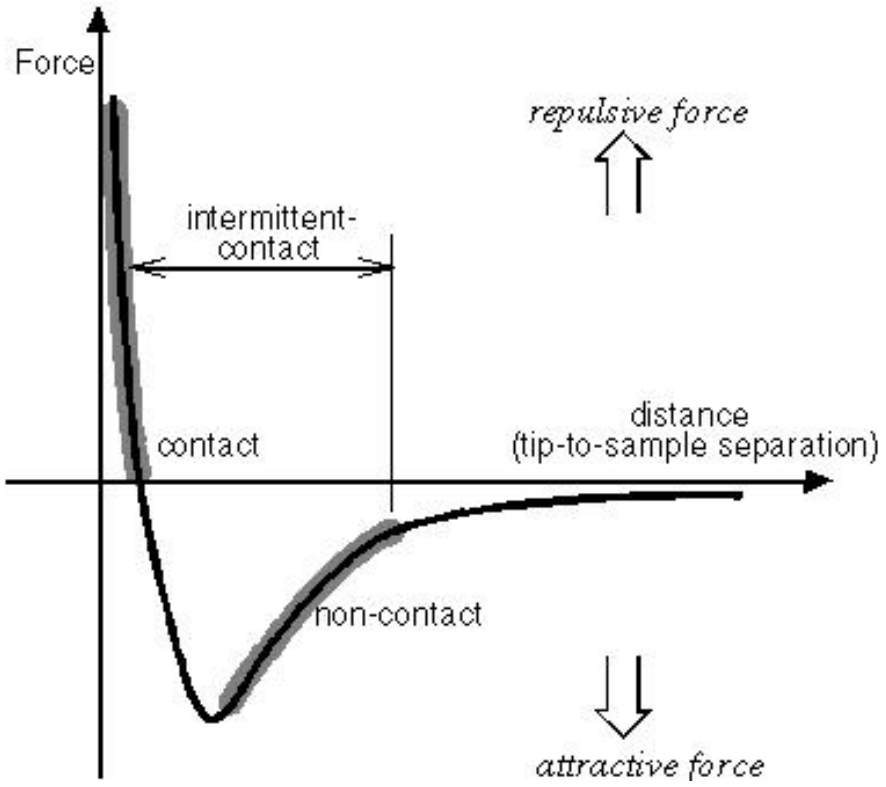

Figure 2.7: Force vs. distance curve[**56**]

the bulk atoms in the tip and sample. This mode is generally used for flat samples which can withstand lateral forces during scanning.

There are a number of problems with this technique. The first problem is that low stiffness cantilever has a low resonant frequency, and so it is a highly susceptible to vibrational noise[**7**]. The invention of micro fabricated cantilevers by Albrecht et al.[**13**] has greatly reduced this problem keeping the spring constant low by making the cantilever small. The other problem with this technique is that low stiffness cantilevers have a large thermal oscillation amplitude($x_{thermal}$)[**26**],

$$x_{thermal} = \sqrt{\frac{k_B T}{k}} \tag{2.21}$$

k_B is the Boltzmann constant and T is absolute temperature.

Also there is a more serious problem with this technique. If the tip is mounted on a soft cantilever, the initially attractive tip-sample forces can cause a sudden jump-to-contact when approaching the tip to the sample.

This instability occurs in the quasistatic mode if[**26**]

$$k < max(\frac{\partial^2 V_{ts}}{\partial z^2}) \tag{**2.22**}$$

where V_{ts} is the interaction potential between the tip and the sample. This problem can be avoided by increasing the cantilever stiffness to several tens of N/m, but this decreases the sensitivity of the contact mode so much that the weak attractive interactions can not be easily measured.

2.2.6.2 Intermittent-contact mode

Martin et al.[**11**] applied a new method which is called intermittent-contact mode or tapping mode to increase the force sensitivity and measure weak interactions.In the intermittent-contact mode during the surface scan, the cantilever assembly is sinusoidally vibrated by a piezo mounted above it, and the oscillating tip slightly taps the surface at the resonant frequency of the cantilever with a constant amplitude of oscillation. A feedback loop keeps the average normal force constant. This technique is also called as amplitude modulation of AFM(AM-AFM).

Martin et al. made the tip vibrated at the lever resonance frequency and recorded the vibration amplitude as a function of distance between the cantilever and surface(d). For large values of d, where the effect of the sample on the tip can be neglected, the tip vibration amplitude A as a function of the frequency w is Lorentzian of the form;

$$A = \frac{A_0(\omega_0/\omega)}{\sqrt{1 + Q^2(\omega/\omega_0 - \omega_0/\omega)^2}} \tag{**2.23**}$$

where $w_0 = c\sqrt{k}$ is the resonance frequency, c is a function of the lever mass, k is the spring constant, A is the amplitude at resonance and Q is the quality factor($Q \gg 1$).

$$Q \cong \frac{\omega_0}{\Delta\omega} \tag{**2.24**}$$

The change of amplitude δA for a small change of f' and $\delta f'$ is maximized and has the value

$$\delta A = \frac{\delta A}{\delta f'} \delta f' = \frac{2A_0 Q}{3\sqrt{3}(k - f')\delta f'} \qquad (\mathbf{2.25})$$

where f and f' is respectively the force between the sample and the tip and the magnitude of the force derivative as shown Figure 2.7.

The force imparted onto the sample by the cantilever can be very small because small shifts in the oscillation amplitude can be detected. The tapping mode allows delicate samples to be imaged with normal forces on the order of fractions of a nanonewton. The applied force is significantly lower than the force applied by the contact mode of operation. The lateral resolution in the tapping mode can be compared favorably to the contact mode of operation because high oscillation frequencies allow the tip to the contact the sample surface many times before it translates laterally by one tip diameter. Therefore the tip shape defines the lateral resolution in the tapping mode just as it does in the contact mode.

The tapping mode is used in topography measurements to minimize the effects of friction and other lateral forces to measure the topography of soft surfaces. It has been widely used in studying surface properties of biological material and polymers with great successes. But it is slow with cantilevers have high quality factors. However the use of cantilevers have high quality factors reduces noise. Thus Albrecht et al.[**27**] found a way to combine the benefits of high quality factor and high speed by introducing frequency modulation(FM) mode.

2.2.6.3 Non-contact mode

Albrecht et al.[**27**] developed a technique by modifying the technique applied by Martin et al.[**11**] They measured the change in resonant frequency directly with a Frequency Modulation(FM) circuit. Thus, this technique is also called as FM-AFM mode. It improves the bandwidth of measurements made with high quality factor(Q) cantilevers, so is particularly useful in ultrahigh vacuum(UHV).

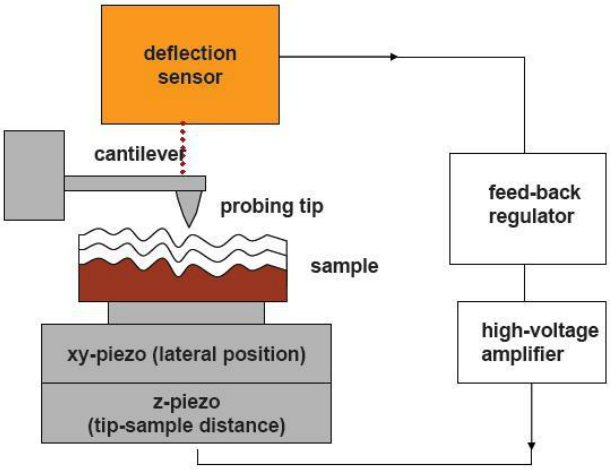

Figure 2.8: Schematic of tapping mode

Using the FM mode, the resolution was improved dramatically and finally atomic resolution was obtained by reducing the tip-sample distance and working in vacuum.

Three basic forces can be mapped across a sample in the non-contact mode by detecting the deflection of the cantilever under the influence of the desired force. These consist of electrostatic, magnetic and van der Waals forces, in the order of the complexity of the interaction. The first deals with monopoles, the second with dipoles, while the third requires a quantum mechanical treatment. These forces and their derivatives can be as small as 10^{-12} N and 10^{-14} N/m, respectively. They are much smaller than those encountered with the contact mode of AFM.

In non-contact mode the system vibrates a stiff cantilever near its resonance frequency with an amplitude of a few tens to hundreds of angstroms. Then it detects changes in the resonance frequency as the tip comes near the sample surface. The resonance frequency of the cantilever varies as the square root of its spring constant. In addition the spring constant of the cantilever varies with the force gradient experienced by the cantilever. Finally the force gradient which is derivative of the force versus distance curve shown in Figure 2.7, changes with the distance between the cantilever and sample. Thus, changes in the resonance frequency of the cantilever can be used as a measure of changes in the force gradient, which reflect changes in the cantilever-sample distance or sample

topography. The system monitors the resonance frequency of the cantilever and keeps it constant with the aid of a feedback system that moves the scanner up and down. By keeping the resonance frequency constant the system also keeps the average cantilever-sample distance constant. As in contact mode the motion of the scanner is used to generate the data set.

The oscillation frequency is the observable in non-contact mode and it is important to establish a connection between the frequency and forces acting between tip and sample. While the frequency can be calculated numerically, an analytic calculation is important for finding the functional relationships between operational parameters and the physical tip-sample forces. The motion of the cantilever can be described by a weakly disturbed harmonic oscillator. $q'(t)$ is the deflection of the tip of the cantilever. It oscillates with amplitude A at a distance of $q(t)$ from the sample. The closest point to the sample is $q = d$ and $q(t) = q'(t) + d + A$ The Hamiltonian for the cantilever is[28],

$$H = \frac{p^2}{2m^*} + \frac{kq'^2}{2} + V_{ts}(q) \tag{2.26}$$

where k is the spring constant, m^* is the effective mass, V_{ts} is the tip-sample potential and $p = m^* dq'/dt$

The unperturbed motion is given by

$$q'(t) = Acos(2\pi_f 0t) \tag{2.27}$$

and the resonance frequency f_0 of the free cantilever(tip far from the surface) is given by

$$f_0 = \frac{1}{2\pi}\sqrt{\frac{k}{m^*}} \tag{2.28}$$

If the force gradient $k_{ts} = \frac{\partial F_{ts}}{\partial z} = \frac{\partial^2 V_{ts}}{\partial z^2}$ is constant during the oscillation cycle, the calculation of the frequency shift is trivial;

$$\triangle f = \frac{f_0}{2k} k_{ts} \qquad (\mathbf{2.29})$$

However classically k_{ts} varies by several orders of magnitude during one oscillation cycle and a perturbation approach has to be employed to calculate the frequency shift. The first derivation of the frequency shift in non-contact mode was achieved in 1997[**22**] using canonical perturbation theory. The result of this calculation is

$$\Delta f = -\frac{f_0}{kA^2} < F_{ts} q' >= -\frac{f_0^2}{kA^2} \int F_{ts}[d + A + q'(t)] q'(t) dt \qquad (\mathbf{2.30})$$

The applicability of first-order perturbation theory depends on the magnitude of the perturbation, for example it depends on the ratio between V_{ts} and the energy $E = kA^2/2$ of the oscillating cantilever. E is typically in the range of several keV while V_{ts} is only a few electron volts and first order perturbation theory yields results for Δf with excellent precision.

Non-contact mode is desirable because it provides obtaining sample topography with little or no contact between the tip and the sample. Like contact mode it can be used measure the topography of insulators and semiconductors as well as electrical conductors. The low force between the cantilever and the sample is advantageous for studying soft or elastic samples. A further advantage is that samples like silicon wafers are not contaminated through contact with the tip. Also it provides high speed to avoid thermal drift problem.

2.3 Frictional Force Microscopy

The frictional force microscope (FFM, also called the lateral force microscope,LFM) is a modified force microscope that allows the simultaneous measurement of both normal and lateral forces. It can measure lateral deflections of the cantilever that arise from forces on the cantilever parallel to the plane of the sample surface.

Lateral deflections of the cantilever usually arise from two reasons; changes in surface friction and changes in slope. In the first case, the cantilever may encounter greater friction forces as it moves on another material of surface,

causing the cantilever twist more strongly. In the second case, it may twist because of a steep slope. To separate one effect from another, FFM and AFM images should be collected simultaneously.

The relative motion of tip and surface is realized by a scanner created from piezoelectric elements, which moves the surface perpendicularly to the tip with a certain periodicity. The normal force (F_N) applied to the surface is responsible for the deflection of the cantilever that supports to the tip. If F_N increases while scanning due to the local slope of the surface, the scanner is retracted by a feedback loop. And also if F_N decreases, the surface is brought closer to the tip by extending the scanner. In this way, the surface topography can be determined line by line from the vertical displacement of the scanner. Accurate control of such vertical movement is made possible by a light beam reflected from the back of the lever into a photodetector. The relative sliding of tip and surface is usually also accompanied by friction. A lateral force (F_L) which acts in the opposite direction to the scan velocity, hinders the motion of the tip. This force causes torsion in the cantilever, which can be observed along with the topography if the photodetector can detect also the lateral movement of the lever with the normal force deflection while scanning. In practice this is achieved using a four-quadrant photodetectors, as shown in Figure 2.9.

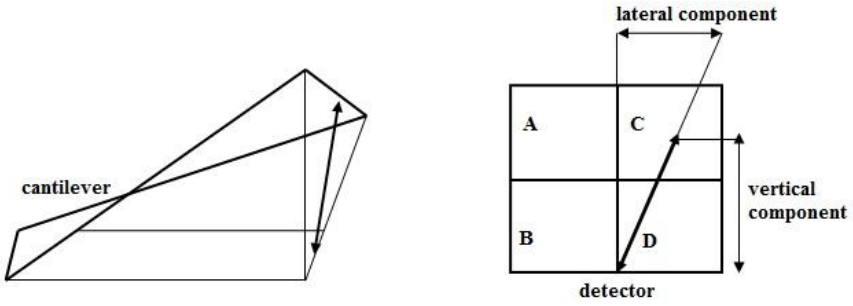

Figure 2.9: The photodetector for FFM

The FFM was first used by Mate et al.[**14**] in 1987. They observed atomic-scale features on the frictional force acting on a tungsten wire tip sliding on the basal plane of graphite surface at low loads $< 10^{-4}N$ They used optical interference for

measuring the deflection of a level with a known spring constant. Optical beam deflection was introduced later by Meyer and Amer[**16**].

3. ELECTROSTATIC FORCE MEASUREMENTS AND KELVIN PROBE FORCE MICROSCOPY (KPFM)

3.1 Introduction

In this section we will examine the measurement of electrostatic forces in the AFM. Then we will look in more detail the development, the theory and the applications of Kelvin probe force microscope(KPFM). The development of tapping mode by Martin et al.[**11**] allowed to detect weak long-range forces. Also electrostatic forces can be measured using this technique. Martin et al.[**17**] measured electric forces as small as 10^{-10} by applying an dc voltage between the tip and the sample. In 1988 Stern et al.[**29**] used this technique to detect the presence of electric charge on Polymethyl Methacrylate (PMMA) sample.

But electrostatic forces can not be distinguished from other long-attractive forces such as van der waals forces. In 1989-1990 Stern et al.[**19**] developed electrostatic force microscope(EFM) to develop their previous work on electric charge measurements on PMMA studied in 1988. In this technique, an ac voltage is applied during normal non-contact mode. When the tip scans above the surface of a sample, changes in the force gradient between the tip and the surface alters the effective spring constant of the lever, changing its resonance frequency. This is detected as a change in the amplitude of a oscillation of the tip by a lock-in amplifier and by an optical fiber-based interferometer. A feedback loop maintains a constant force gradient by adjusting the distance between the tip and sample. In the work of Stern et al.[**19**] in 1989 by applying ac voltage to the sample, images which differentiate between positive and negative charge could be obtained. The microscope's lateral resolution was better than other charge measurement techniques and this advantage of it can be used in investigating insulator charge distributions on smaller scale than previously possible.

An important development in EFM instrumentation was the development of Kelvin Probe Force Microscopy (KPFM) in 1991 by Nonnenmacher et al.[**21**]. Measurements of the contact potential difference(CPD) between different materials was performed for the first time using kelvin probe force microscopy. They achieved a high resolution for both the contact potential difference (better than 0.1 mV) and the lateral dimension (¡50 nm) and obtained contact potential difference images of gold, platinum, and palladium surfaces. The ac voltage between tip and sample was applied at the resonance frequency while the cantilever was vibrated by piezo above resonance. The signal change in the piezo-induced vibration amplitude while approaching the tip was used in the conventional way of AFM to control the distance between tip and sample. A second feedback loop was used to measure the CPD by minimizing the electric field between tip and sample.

In 1995 Kikukawa et al.[**30**] observed the surface potential of silicon pn junctions using a Kelvin probe force microscope whose sensitivity was about five times better than a conventional one. It was achieved by three major improvements: electrostatic force detection using the second cantilever resonance, cantilever Q-value enhancement by operating in a vacuum, and direct cantilever resonance frequency detection using the frequency modulation technique. Also in 1999 Sommerhalter et al.[**31**] lateral resolution was achieved by using the second resonance frequency of the cantilever to measure the electrostatic forces, while the first resonance frequency is used to simultaneously obtain topographic images by the frequency modulation technique.

Kitamura et al.[**32**] observed CPD images on Au deposited n-type and p-type Si(111) 7x7 surfaces with KPFM in ultrahigh vacuum conditions. The atomic scale potential difference between the Si(111) 7x7 surface and Au clusters did not reflect the work function, it was thought that it reflected the local electron density on the surface. On the other hand, the average potentials corresponding to the dc levels in each CPD image reflected the work function. If there are spatial variations in work function on the tip or sample surface, the measured values will not represent the work function at a point on the sample,the value at a point on

the sample will be weighted average. Because there is large contribution from the surface below the tip [**33**].

In 2003 Glatzel et al.[**34**] represented a comparison between the frequency modulation and the amplitude modulation detection mode of KPFM using measurements of gold islands on highly oriented pyrolytic graphite. The results in both detection modes show a strong dependence of the measured signal on the tip geometry. The main drawback of FM mode is the low sensitivity and therefore the necessity of high ac voltages. The AM-mode offers the possibility to use low ac voltages, which allows absolute work function measurements also on semiconductor surfaces.

KPFM has been used to study a wide range of properties and phenomena, such as voltage signals in integrated circuits[**20**] , self assembling monolayer films[**35**], surface potential variations in multilayer semiconductor devices[**36**] and characteristics of human hair[**37**]. Also in 2008 Filleter et al.[**38**] determined the work function difference between single layer and bilayer graphene grown epitaxially on 6H-SiC(001) by the Kelvin probe force microscopy. Bilayer films were found to increase the work function as compared to single layer films. This method showed a distinction obviously between interface layer, single layer, and bilayer graphene.

3.2 Electrostatic Force Microscopy

Electrostatic force microscopy(EFM) applies a voltage between the tip and the sample while the cantilever vibrates above the surface. When the voltage is applied between the tip and sample, because of the interaction between the sample and the tip, there will be a mobility in the conduction electrons or holes beneath the cantilever and an electrostatic force exerted on the tip. The electrostatic force resulting from electric charges in the sample consists of two oscillating components;F_w and F_{2w} and affects the vibration amplitude of the cantilever. The EFM has been used to map the electrical properties of the sample's surface. For instance, it can map the electric fields of a electronic circuit as the device is

turned on and off. The force sensitivity of the EFM suggests that the capacitive variations down to 10^{-21} F could be measured in a 1 Hz bandwith.

Stern and Terris et al.[**19**] deposited and imaged localized surface charge on insulators. The tip was oscillated near its resonant frequency. As the tip scanned above the surface of a sample, the resonance frequency was changed. This was detected as the change in the amplitude of oscillation of the tip by a lock-in amplifier and optical fiber-based interferometer. A feedback loop adjusted tip-sample separation by the help of changes in amplitude of oscillation of the tip to maintain a constant force-gradient. The tip was electrically isolated from the piezoelectric material so that a voltage could be applied to the tip for charging the sample surface. An electrode behind the sample could be used to provide an additional electrostatic force between the tip and the sample. Positive and negative charges were deposited onto the insulating sample by applying voltage to the tip. After charging, the sample was imaged with the tip electrically grounded.

3.3 Kelvin Probe Force Microscopy(KPFM)

Kelvin probe force microscopy(KPFM) is another scanning probe method measures the local surface potential or work function of different metals with high spatial resolution. It relies on the kelvin method takes its name from William Thomson, also known as Lord Kelvin who first introduced the method in 1898. In 1991 KPFM was developed by Nonnenmacher to look at different metal surfaces.

3.3.1 The Kelvin method

The Kelvin Probe Method is an old-age technique to measure the work function difference between the different metals. The work function of a metal is the minimum energy required to reject one electron from its surface.

$$\Phi = e \cdot \Psi - EF \tag{3.1}$$

Φ: work function

e: electron charge

Ψ: electrostatic potential

EF: Fermi energy level of the metal

The two metals are brought in to parallel and close position like a capacitor[**39**]. When they are unconnected, they have different fermi levels and different work functions (ϵ_1, ϵ_2) as shown in Figure 3.1(a). When they are in contact, electrons from the higher fermi level flows to the lower fermi level. In this way the fermi level of the new system must equalize. This movement of the electrons causes a potential difference which is called the contact potential difference(CPD) as seen in Fig 3.1(b). Contact potential difference is defined as the potential difference between dissimilar conductive materials whose mobile electrons are in thermal equilibrium. This contact potential difference is equal to work function difference,existing before the contact.To nullify the voltage occurred between the metals, a backing potential is applied as shown Figure 3.1(c) This applied backing potential is equal to contact potential difference, also equal to work function difference.

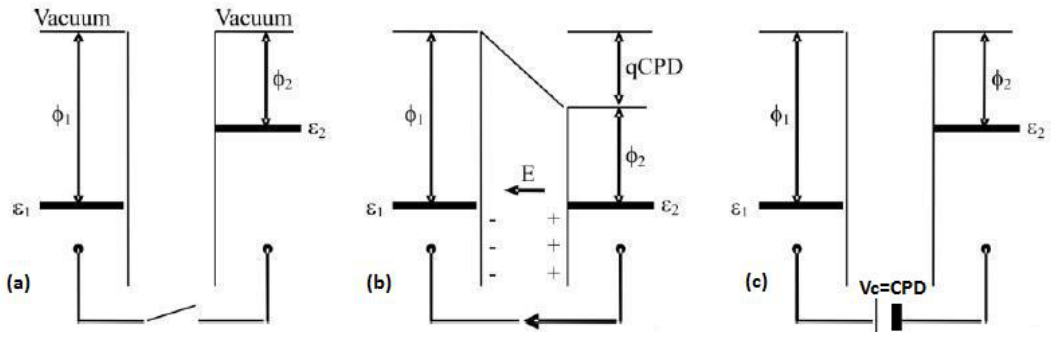

Figure 3.1: Schematic diagram of Kelvin method[**39**]

In this way, if the work function of one of metals is known , the work function of other metal can be measured. The principle of KPFM is similar to Kelvin method except measuring forces instead of currents.

In KPFM the work function of tested material which is surface of sample, is measured by the help of known work function of other material which is tip of the microscope. One of the materials is mechanically vibrated by an oscillation potential(V_{ac}) at frequency ω. The tip interacts electrostatically with the surface,

being attracted and repelled at the same frequency of V_{ac} as shown in Figure 3.2. Thus, an oscillation mode at a frequency ω appears on the cantilever. This oscillation is detected by the photodiode, which sends a signal through a lock-in amplifier to isolate the oscillation mode at ω. The oscillation amplitude at frequency ω is proportional to the surface-potential difference between tip and surface. To measure the exact work function of the sample, an additional feed back loop is acquired. This feed back loop applies a dc offset potential voltage(V_{dc}) to minimize the electrostatic interaction between the tip and surface.

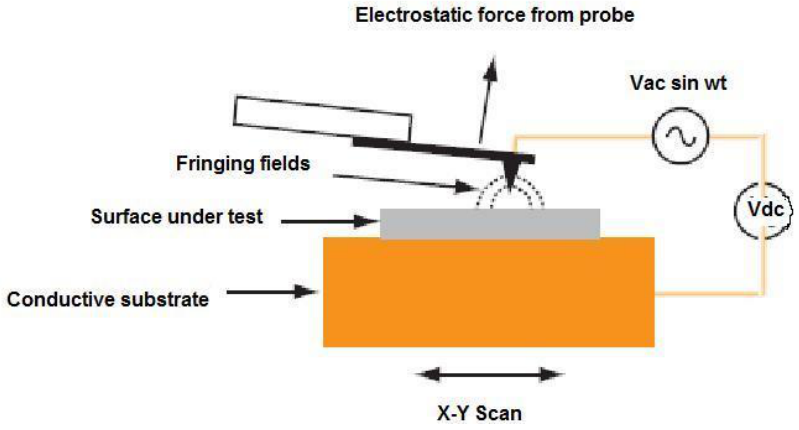

Figure 3.2: Kelvin probe method in an AFM

When an ac voltage is applied at an angular frequency ω between the tip and the surface, the resulting electrostatic force has a dc component and two oscillating components at angular frequencies, ω and 2ω. The force component oscillating at frequency ω is proportional to the contact potential difference (CPD) between the tip and the surface. If a dc voltage V_{dc} is applied the CPD is equal to $\frac{\Delta\phi}{e} + V_{dc}$, where $\Delta\phi$ is the work function difference between the tip and surface and e is the electronic charge.

We can show the resulting electrostatic force mathematically: An ac and a dc voltage are applied between the tip and sample.

$$V_{apply} = V_{dc} + V_{CPD} \tag{3.2}$$

The voltage between the tip and the surface can be written as,

$$\Delta V = V_{CPD} - V_{dc} + V_{ac}\sin(\omega t) \tag{3.3}$$

V_{CPD}:contact potential difference

V_{dc}:dc offset potential

V_{ac}: amplitude of the applied ac voltage signal

ω: frequency of the applied ac voltage signal

Assuming the geometry of the tip and the sample like the parallel plate capacitor geometry, the energy between the sample and the tip can be expressed as,

$$U = \frac{1}{2} C \Delta V^2 \tag{3.4}$$

where C:the local capacitance between the tip and the sample

The force is the derivative of energy with respect to tip-sample separation distance,

$$F = -\frac{\partial U}{\partial z} = -\frac{1}{2}\frac{\partial C}{\partial z}\Delta V^2 \tag{3.5}$$

$$= \frac{1}{2}\frac{\partial C}{\partial z}[V_{CPD} - V_{dc} - V_{ac}\sin(\omega t)]^2$$

$$= -\frac{\partial C}{\partial z}\frac{1}{2}(\Delta\phi - V_{dc})^2 - \frac{\partial C}{\partial z}(\Delta\phi - V_{dc})V_{ac}\sin(\omega t) - \frac{\partial C}{dz}[\frac{V_{ac}^2}{4} - \frac{V_{ac}^2}{4}\cos(2\omega t)]$$

$$= F_{dc} + F_{\omega} + F_{2\omega} \tag{3.6}$$

There are three different force signals;$F_{dc}, F_{\omega} and F_{2\omega}$

$$F_{dc} = -\frac{1}{2}\frac{\partial C}{\partial z}[(V_{CPD} - V_{dc})^2 + \frac{V_{ac}^2}{2}] \tag{3.7}$$

$$F_{\omega} = -\frac{\partial C}{\partial z}[(V_{CPD} - V_{dc})V_{ac}\sin(\omega t)] \tag{3.8}$$

$$F_{2\omega} = \frac{1}{4}\frac{\partial C}{\partial z}[V_{ac}^2\cos(2\omega t)] \tag{3.9}$$

According to equation **3.7**, **3.8** and **3.9** the electrostatic force consists of a static part and two contributions at ω and 2ω.

If $V_{CPD} = V_{dc}$ the ω component of the electrostatic force is zero. V_{CPD} is obtained by altering applied V_{dc} voltage by the feedback loop. V_{CPD} is the work function difference between the tip and the sample surface and the work function difference is exactly equal to eV_{dc}. This value of V_{dc} is sometimes called as 'Kelvin null

voltage'. In this way, variations in the work function of the sample surface can be measured quantitatively, relative to some reference material or to the tip.

There are two different KPFM modes commonly used.

One of them is two-pass technique[40].First scan collects topographic image,second scan records the kelvin probe signal at a larger constant tip-surface distant. So it is called as 'lift mode'. In the first scan no external voltage is applied to the tip or sample, topography of surface is determined by using the tapping mode of AFM as shown in Figure 3.3(a). Mentioned as before, in the AFM tapping mode the cantilever is resonated near its resonant frequency and the topography image is determined by keeping the oscillation amplitude constant with a feedback system. In the second scan the tip is lifted at a selected distance, then each line is scanned secondly using the topographic image recorded at first scan and the contact potential is measured as shown in Figure 3.3(b). In this scan a dc bias potential and an oscillating ac potential is applied to the sample. The ac potential is necessary to enhance the electrostatic force interaction between the tip and sample. There is a second feedback loop which adjusts the dc bias voltage to nullify the vibration amplitude of cantilever and hence the spectral component of F_ω. When the ω component of the electrostatic force is zero, V_{dc} is equal to the surface potential. The contact potential map is determined by recording these values of bias voltage makes the ω component of the electrostatic force zero and reversing the sign.

In the other mode, topographical signals and the kelvin probe signal are simultaneously detected at two different tip resonance frequencies. Thus topography of the surface and work function difference between the sample and tip are simultaneously determined. In this mode cantilever is excited by a signal contains more than one driven force. The output signal of the first resonance frequency is used to obtain topography image as used in intermittent-contact AFM mode. The output signal of the second resonance frequency is used to obtain the work function difference image of the sample. Exciting of the cantilever with the first and second resonance frequency can increase the sensibility of the measurement of force.

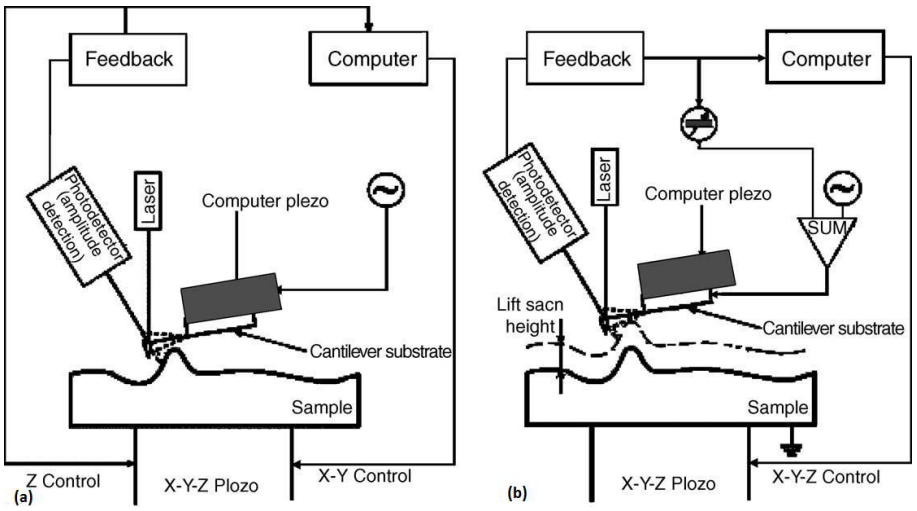

Figure 3.3: The topography measurement in tapping mode(a) and contact potential difference measurement in lift mode[**40**] (b)

These are the equations of motion for this mode:

$$F_{exc}(t) = F_1 cos(\omega_1 + F_2 cos(\omega_2 t) \tag{3.10}$$

$$m\ddot{z_1} = -k_1 z_1 - \frac{m\omega_1}{Q_1}\dot{z_1} + F_1 cos(\omega_1 t) + F_2 cos(\omega_2 t) + F_{ts}(z_1 + Z_2) \tag{3.11}$$

$$m\ddot{z_2} = -k_2 z_2 - \frac{m\omega_2}{Q_2}\dot{z_2} + F_1 cos(\omega_1 t) + F_2 cos(\omega_2 t) + F_{ts}(z_1 + Z_2) \tag{3.12}$$

where,

F_{ts} : The force between the tip and the sample.

ω_1: The first resonance frequency of the cantilever

ω_1: The second resonance frequency of the cantilever

F_1 : The amplitude of the first excitation

F_2 : The amplitude of the second excitation

k : The spring constant

Q : The quality factor of the cantilever

F_{ts} : The propelling force

This mode can be separated to two types in itself; amplitude detection mode(AM-KPFM) and frequency detection mode(FM-KPFM).

3.3.2 Amplitude Modulation of Kelvin Probe Force Microscopy (AM-KPFM)

In the AM-KPFM the amplitude of the cantilever oscillation at ω induced by the electrostatic force is measured directly[**34**]. It is measured by direct detection of the lever deflection by a lock-in amplifier referenced to ω. For determining the CPD, a feedback loop alters the detected amplitude to zero by adjusting V_{dc} to $\Delta\Phi/e$. AM-KPFM is sensitive to the force. This mode requires soft cantilevers with low resonant frequencies and large modulation amplitudes to obtain sufficiently large and detectable mechanical deflection.

3.3.3 Force modulation of Kelvin probe force microscopy (FM-KPFM)

The frequency modulation method (FM-KPFM) detects the resonance frequency shift(Δf) induced by the bias voltage applied between tip and sample[**41**]. The parabolic dependence of Δf on the bias voltage is recorded and used to evaluate the CPD between tip and sample. FM-KPFM is sensitive to the force gradient. Hence a higher lateral resolution is expected in FM-KPFM than for the force-sensitive AM-KPFM method.

The frequency modulation method (FM-KPFM) detects the resonance frequency shift(Δf) induced by the bias voltage applied between tip and sample[**41**]. The parabolic dependence of Δf on the bias voltage is recorded and used to evaluate the CPD between tip and sample. FM-KPFM is sensitive to the force gradient. Hence a higher lateral resolution is expected in FM-KPFM than for the force-sensitive AM-KPFM method.

Kitamura et al.[**42**] operated this method to measure CPD and topography simultaneously. The gradient of electrostatic force was detected as frequency shift of cantilever resonance frequency. The amplitude of the ω component was detected by using a lock-in amplifier where the output of the lock-in amplifier became zero when a V_{dc} corresponding the $\Delta\phi$ was applied. When the output of the lock-in amplifier was zero, the applied V_{dc} was the CPD for the the tip. CPD images were obtained from a feedback loop that maintained the lock-in output

at zero. CPD images with a resolution of less than 10 meV were observed in this mode.

The resonance frequency of the cantilever is given by

$$f_0 = \frac{1}{2\Pi}\sqrt{\frac{k}{m^*}} \tag{3.13}$$

All long-range forces including the electrostatic force shift the resonance frequency f_0 to f_0':

$$f_0' = \frac{1}{2\pi}\sqrt{\frac{k - \frac{\partial F}{\partial z}}{m^*}} \approx f_0(1 - \frac{1}{2k}\frac{\partial F}{\partial z}) \tag{3.14}$$

The mechanical resonance of the cantilever is frequency-modulated with frequencies f_{mod} and $2f_{mod}$. The Figure 3.4 shows shows a schematic frequency spectrum of the cantilever oscillation[**40**]. The peaks at f_{mod} and $2f_{mod}$ originate from the electrostatic force. The peaks at $f_0 \pm f_{mod}$ and $f_0 \pm 2f_{mod}$ show the frequency modulation of f_0. This frequency modulation is produced by the oscillating electrostatic force gradient. FM-KPFM nullifies the signal at $f_0 \pm f_{mod}$ by applying a bias voltage V_{dc} which is equal to the $\Delta\Phi$. In this way, this provides $V_{dc} = \frac{\Delta\Phi}{e}$.

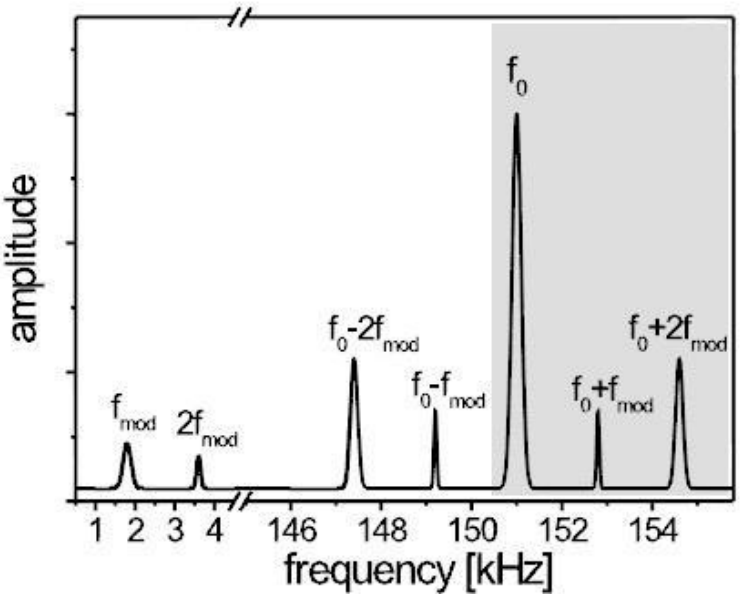

Figure 3.4: Schematic frequency spectrum of the tip oscillation[**41**]

3.4 Instrumentation

3.4.1 Experimental set-up

We modified the Atomic Force Microscope at Sabancı University supplied by NanoMagnetics Instruments Ltd to the Kelvin Probe Force Microscope as shown in Figure 3.5. In our first experimental set-up an extra PLL(Phase Locked Loop) was used. Since for the AFM only one driven frequency is used and hence there is only one PLL in the electronic system of the AFM. But either the first and the second resonant frequency were used for The KPFM. To separate the information concerning the each resonant frequency a high pass filter and low-pass filter and high pass filter were used. Figure 3.6 shows the experimental set-up we used first.

Figure 3.5: The KPFM modified in Sabancı University

3.4.1.1 Phase-locked loop(PLL)

Phase-Locked Loop is a closed loop frequency control system that synchronizes the frequency of the output signal generated by an oscillator with the frequency of a reference signal by the help of the phase difference of the two signals[**43**]. In the electronic of Atomic force Microscopy supplied by NanoMagnetics Instruments Ltd., there is a phase-lock loop card that generates the excitation signal applied

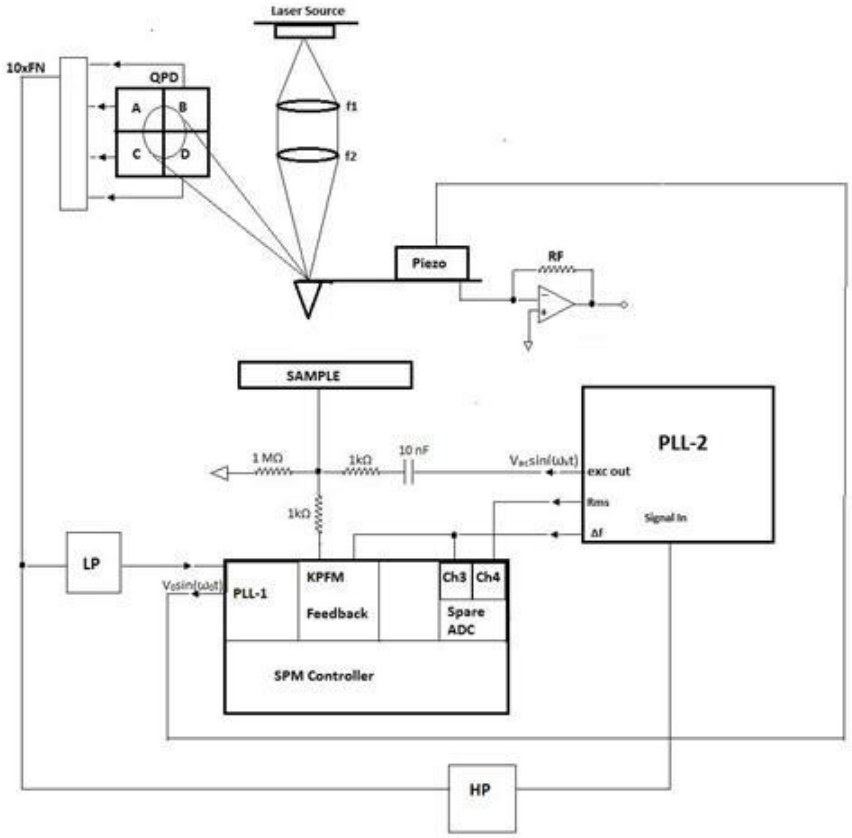

Figure 3.6: Schematic of the first experimental-set up

to the dither piezo. The PLL card adjusts the frequency/phase of the oscillator to set the system into resonance and the digital Phase Locked Loop measures the frequency shifts(Δf) in the non-contact mode. The PLL Card can also be used for tapping mode AFM, as a Dual Channel Lock-in, where amplitude and phase of input signal is measured[**44**]. Due to employing the second resonance frequency of the cantilever for kelvin probe force microscope, an extra PLL is used for this system. The second PLL sets the system into second resonance.

3.4.1.2 High-pass filter

High-pass filter offers easy passage to high-frequency signals but reduces the amplitude of low-frequency signals. It reduces the amplitude of frequencies lower than the filter's cut-off frequency. Cut-off frequency is the value of frequency that shows from which point of value the difficult passage starts.

Cut-off frequency is given by,

$$f_c = \frac{1}{2\pi\tau} = \frac{1}{2\pi RC} \tag{3.15}$$

where τ is the time constant, R is the resistance,C is the capacitance.

Figure 3.7 shows the first-order electronic of high-pass filter which is formed by placing an input voltage across the series combination of a capacitor and a resistor and using the voltage across the resistor as an output.

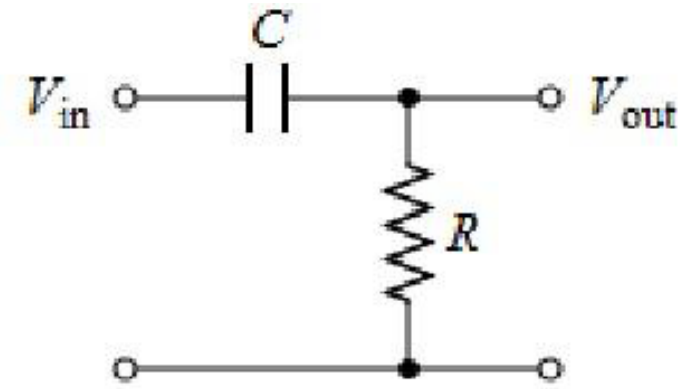

Figure 3.7: The electronic schematic of the first order high-pass filter

For our system we used a high-pass filter which has $350kHz$ cut-off frequency. This filter passes the signals with frequencies higher than $350kHz$. Thus, the signal at the second resonance frequency which is around $400 - 450kHz$, can be used for contact potential images.

3.4.1.3 Low-pass filter

Low-pass filter's task is opposite of the high-pass filter. It passes low frequency signals but attenuates signals with frequencies higher than the cut-off frequency.

The first order electronic of low-pass filter is shown in Figure 3.8 that is occurred by placing an input voltage across the series combination of a resistor and capacitor and an output voltage across the capacitor.

A low-pass filter with $100kHz$ cut-off frequency was used in our system.

The low pass filter passes the signals with frequencies lower than $100kHz$. In this way, the signal at the first resonance frequency which was about $60 - 70kHz$, can be used for topography image.

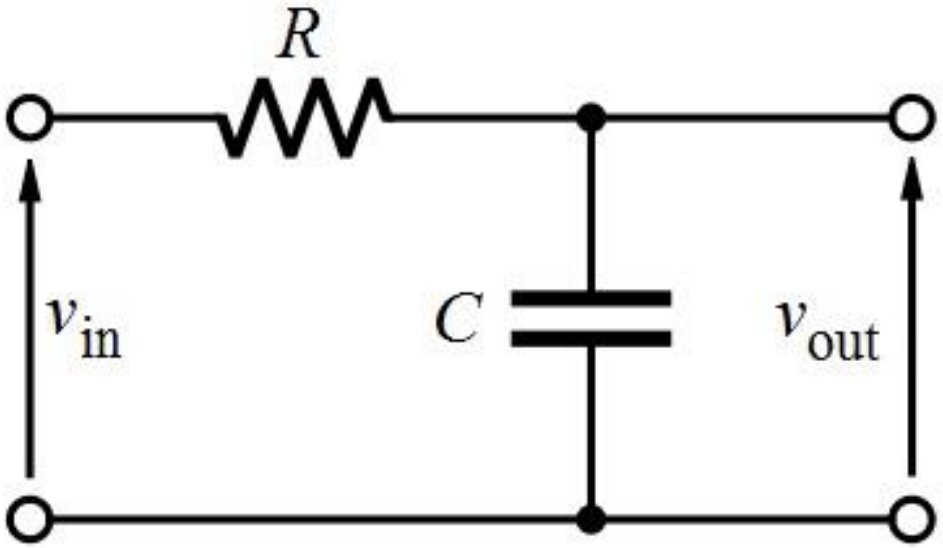

Figure 3.8: The electronic schematic of the first order low-pass filter

The cantilever deflection is detected by the optical beam deflection system. The light source is a red laser diode, the wavelength of laser light is $650nm$. The laser beam is focused on the cantilever surface, and the reflected beam is directed to a position sensitive photodiode. The first and the second resonance signals are separated from each other using low-pass and high-pass filters. The first resonance signal is used to obtain topography image with controlling by the first feedback loop for tip-height control. The topography feedback loop maintains a constant oscillation at the forced oscillation frequency by changing the tip-sample distance. The first oscillation frequency is detected using the first phase-locked loop(PLL). In the non-contact mode PLL measures the frequency shift. The second PLL adjusts the frequency of the oscillator to sets the system into second resonance. The first resonance frequency is around 70-80 kHz. The second resonance frequency is about 400-450 kHz.($f_2 \approx f_1$) The second feedback loop adjusts the dc bias between tip and sample until the ac vibration of the tip at the second resonance frequency is nullified.

A lock-in amplifier was used instead of the second phase-locked loop in the second experimental set-up which was shown in the Figure 3.9 to be able to measure very small amplitudes of oscillation. The second resonance frequency and amplitude can be adjusted manually by the digital lock-in amplifier. A mixture of dc and ac voltages ($V_{dc} + V_{ac}sin(\omega t)$) are applied between the sample and the tip. The

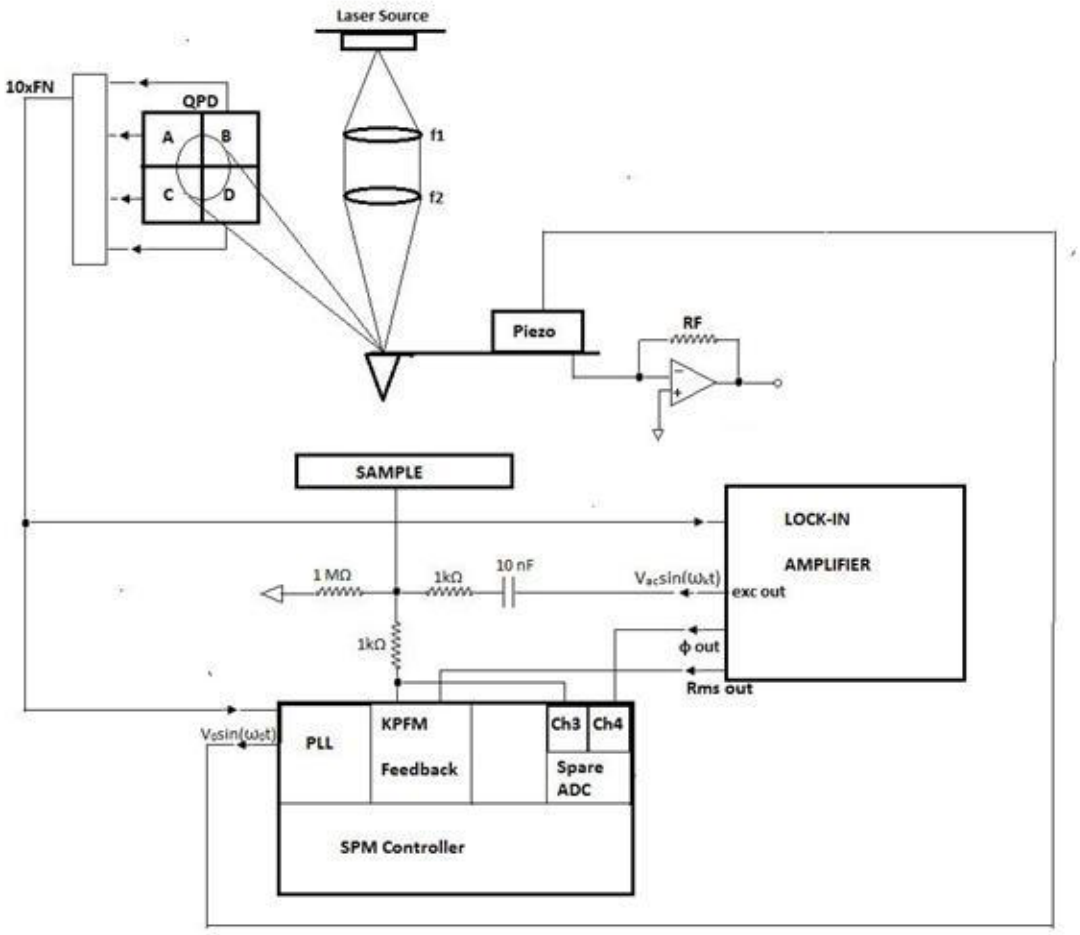

Figure 3.9: Schematic diagram of the second experimental-set up

amplitude of the ω component is detected by lock-in amplifier. The output of the lock-in amplifier becomes zero when a V_{dc} which is equal to the $\Delta\phi$ is applied. Contact potential difference images are obtained from the second feedback loop maintains the lock-in output at zero.

3.4.1.4 Lock-in amplifier(LIA)

Lock-in Amplifier is a system used to detect and measure very small ac signals, even if the signal and noise frequencies are very close to each other. The principle of the lock-in method consists of noise signal rejection at all frequencies except at a reference frequency by using phase-sensitive detection (PSD), which allows to select a specific component of the signal with a given frequency and phase.

For instance, an experiment is excited at a fixed frequency from an oscillator or function generator and the lock-in amplifier detects the response from the

experiment at the reference frequency[**45**]. Lock-in amplifier measurements require a reference frequency. If the output signal from a function generator is the reference wave, the response signal from the experiment is the signal wave and the internal reference signal generated by lock-in amplifier and locked by a phase-locked loop to external reference is the lock-in wave as shown in Figure 3.10, V_{PSD} is given,

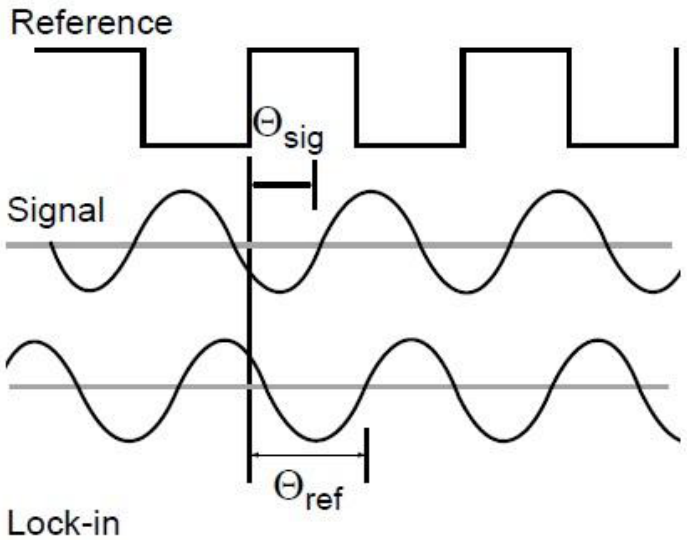

Figure 3.10: The signal of the reference, the signal of the response from the experiment and the signal of the lock-in's reference[**45**]

$$V_{PSD} = V_{sig}V_L sin(\omega_r + \theta_{sig})sin(\omega_L t + \theta_{ref}) \quad \textbf{(3.16)}$$

$$= \frac{1}{2}V_{sig}V_L cos([\omega_r - \omega_L]t + \theta_{sig} - \theta_{ref}) - \frac{1}{2}V_{sig}V_L cos([\omega_r + \omega_L]t\theta_{sig} + \theta_{ref}) \quad \textbf{(3.17)}$$

where V_{sig} is the signal amplitude, ω_r is the signal frequency,θ_{sig} is the signal's phase, V_L is amplitude of the lock-in's reference , ω_L is the frequency of lock-in's reference and θ_{ref} is the phase of lock-in's reference.

The lock-in amplifies the signal and then multiplies it by the lock-in reference using a phase-sensitive detector or multiplier. The PSD output is two AC signals, one of them is at the difference frequency and the other is at the sum frequency.

4. RESULTS

4.1 Results by Atomic Force Micrsocope

First experiments were made by Atomic Force Microscopy(AFM) to understand the principle of microscopy and make the calibration of the system to obtain high quality images from Kelvin Probe Force Microscopy(KPFM). These experiments were made with different modes of AFM, with different parameters with different samples. For tapping and non-contact modes of AFM, single crystal silicon cantilevers with 300 kHz resonance frequency and 40 N/m force constant, also with 150 kHz resonance frequency and 7.4 N/m force constant were used. For contact mode of operation single crystal silicon cantilevers with 0.2 N/m were used.

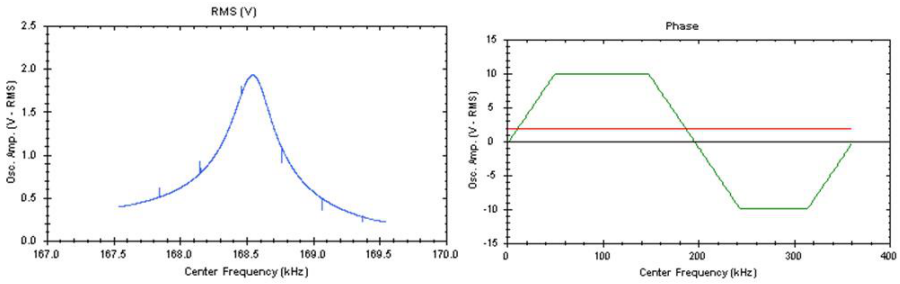

Figure 4.1: Graph of center frequency vs oscillation amplitude of cantilever

Before imaging, initially the natural resonance frequency of the cantilever used should be determined by the software. To determine the natural resonance frequency of the cantilever, the cantilever is oscillated by the dither piezo. The frequency value which is corresponding to maximum oscillation amplitude is called as the resonance frequency of the cantilever. After determining the resonance frequency of the cantilever, the reference phase is determined. The changes in the phase are monitored by means of the reference phase and then the phase shifts are converted to the image. In the Figure 4.1 the graph shows the frequency values versus oscillation amplitude of cantilever. The software calculates the quality factor of cantilever. The quality factor is the ratio of given

energy to the system to dissipation energy. Also we calculated the quality factor with the parameters of software by exporting them to another programme. We drew a graph with the frequency and oscillation amplitude values and fit them to Lorentz curve as shown in Figure 4.2. Quality factor was calculated as 316.191 from this graph with the formula of $Q = \frac{\omega^0}{\Delta\omega}$.

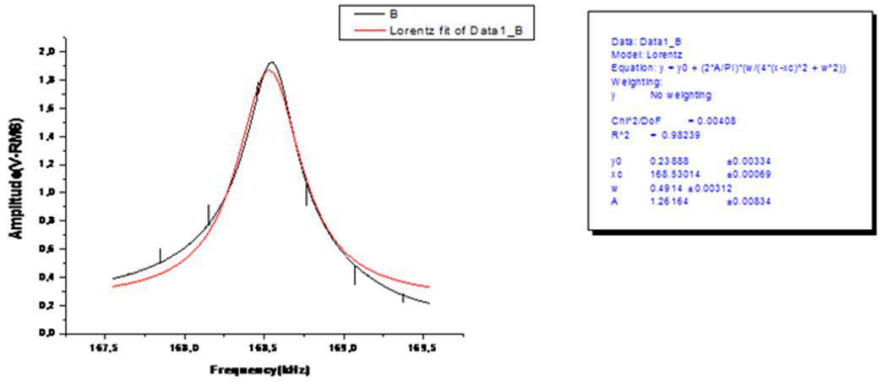

Figure 4.2: Center frequency versus oscillation amplitude graph drew by another program and fit to Lorentzian curve.

The images in the Figure 4.3 are the forward images of blu-ray disk obtained by tapping mode of AFM. The images are phase, RMS(root mean square of amplitude) and topography images respectively. We get different information about the surface by comparing values of parameters from feedback system with the reference values. For instance,in the Figure 3a the phase difference during scanning with respect to the reference phase is shown. The Figure 4.4 shows the images of backward scanning. For these images the scan speed was 2 μ/sec, the image size was $256x256$ pixels.

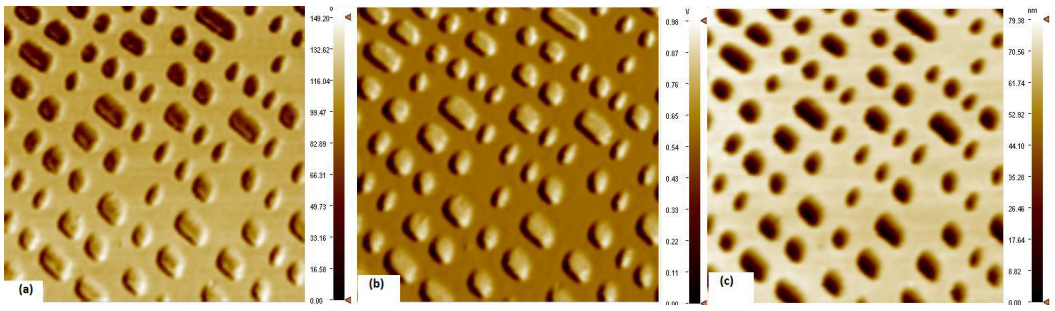

Figure 4.3: Tapping mode AFM forward images of blu-ray disk. (a)Phase imageof forward scanning. (b) Rms image of forward scanning (c) Topography image of forward scanning.

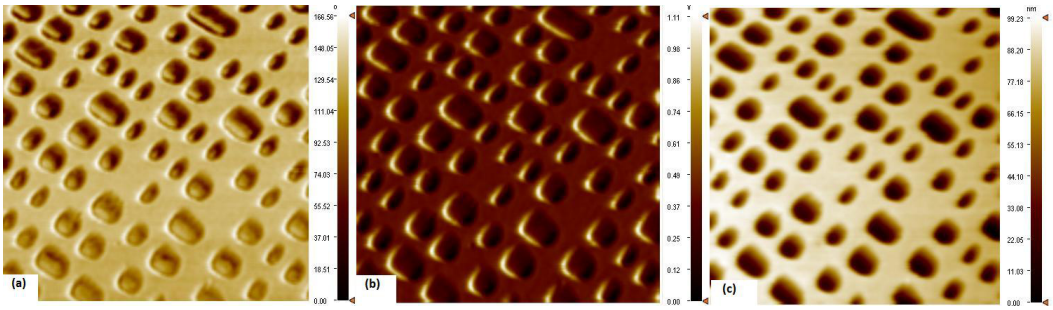

Figure 4.4: Tapping mode AFM backward images of blu-ray disk. (a)Phase image of backward scanning. (b) Rms image of forward scanning (c) Topography image of backward scanning.

On CD and DVD disks the information is written by indentation of a nickel stamp on a poly carbonate surface, resulting pits in the surface. A new medium was developed for rewritable data storage based on a phase-change optical recording[**47**]. A localized laser spot hits a thin layer of material, resulting in a phase transition from crystalline to amorphous. These small amorphous areas define data marks that have a different reflectivity from the crystalline material. On blu-ray discs such marks are now written on 300 nm wide tracks which is shown in Figure 4.5. This track width is less than half the width of DVD.

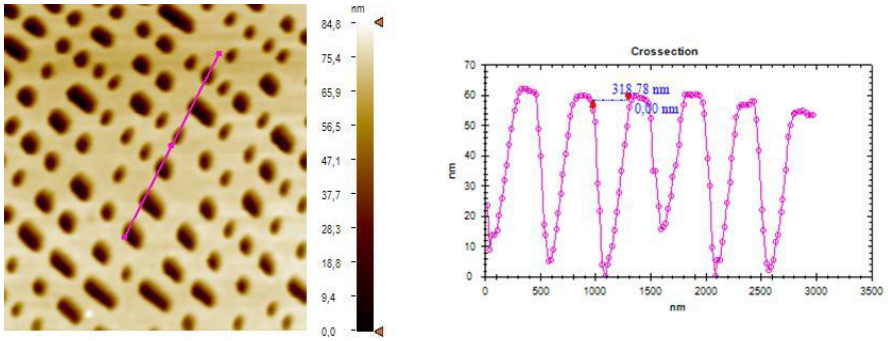

Figure 4.5: The measurement of blu-ray track width on the cross of AFM scan

We made several experiments with different parameters to find the highest working performance of the AFM. We changed laser intensity and excitation amplitude values on imaging blu-ray disk. The first test was made to find the best operating range for laser intensity. Initially laser intensity was adjusted as 8% and F_T which shows the amount of light dropped on the photo diode was read as 0.650 V. Secondly laser intensity was changed to 17% and F_T was increased to 1.300 V while other parameters were not changed. Finally the laser intensity was adjusted to 25% so as to increase F_T above 2V. The Figure 4.7(a) shows the

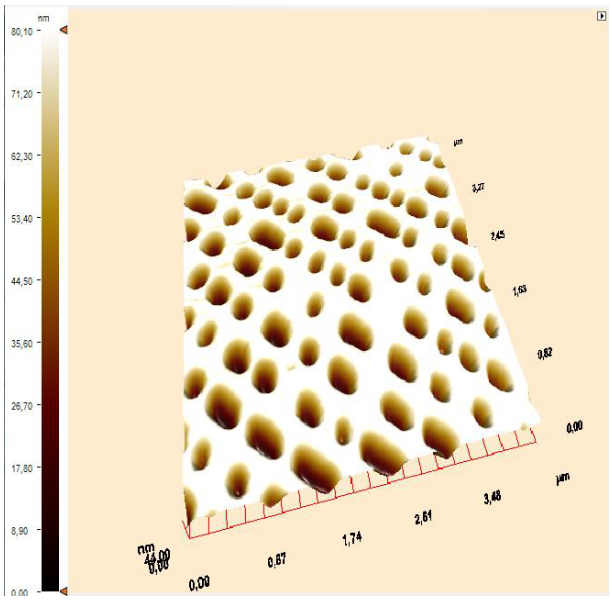

Figure 4.6: The 3 dimensional view topography image of blu-ray disk.

topography image with the parameter of 8% laser, the Figure 4.7(b) shows the image with the parameter of 17% laser. The quality of image was increased when the F_T was increased to 1.3V. The figure 4.7(c) shows the topography image with the parameter of 25% laser. The quality of image was decreased when the F_T was increased to nearly 3V. It can be said that the best operating range of F_T is between 1V and 2V for the highest quality of image.

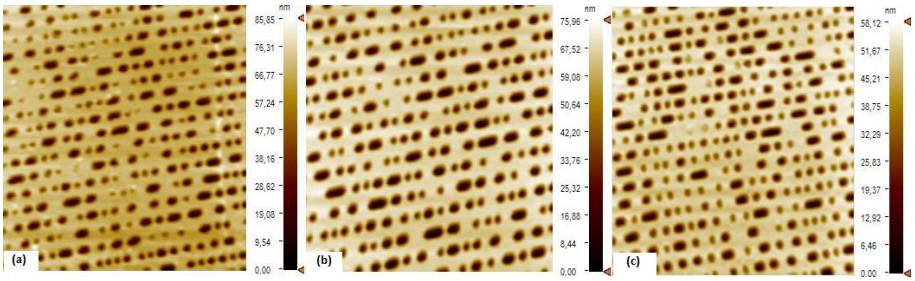

Figure 4.7: (a) The topography image of blu-ray disk(F_T=0.650V) (b) The topography image of blu-ray disk(F_T=1.300V) (c)The topography image of blu-ray disk(F_T=2.850V)

The second test was to find the best operating range of excitation amplitude of cantilever. When the magnitude of excitation amplitude was adjusted to 7%, the RMS(the root mean square of maximum oscillation amplitude) value was approximately 1V and the amplitude was approximately 250 mV. When the magnitude of excitation amplitude was adjusted to 17%, the RMS value was increased to 2V and the amplitude was increased to 400mV. Finally when the the

magnitude of excitation amplitude was increased to 20%, the RMS was increased to above 3V and the amplitude was changed to 600mV. The Figure 4.8 shows the topography images of bu-ray disk with the values of amplitude 250mV, 400mv and 600mV, respectively. We can say that the best operating range of RMS is between 2 and 3 volt.

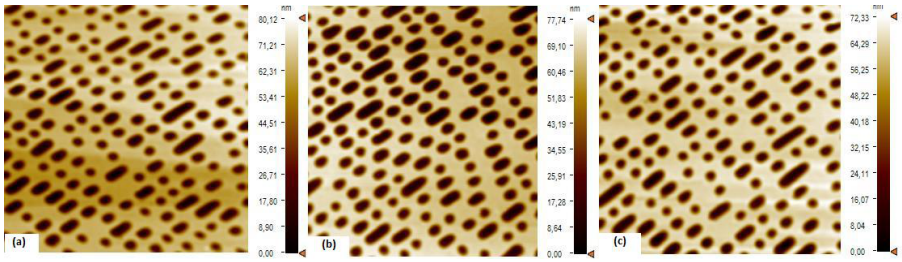

Figure 4.8: (a) The topography image of blu-ray disk(RMS=1V) (b) The topography image of blu-ray disk(RMS=2V) (c)The topography image of blu-ray disk(RMS=3.5V)

We also imaged CD disk by operating the AFM in different modes. For the images in the tapping mode, contact mode and non-contact mode the typical scan speed was 2μ m/s, the scan area was 10x10 μ and the scan size was 256x256 pixels. In the tapping mode we obtained V_z shown in Figure 4.9(a) and RMS image shown in Figure 4.9(b).

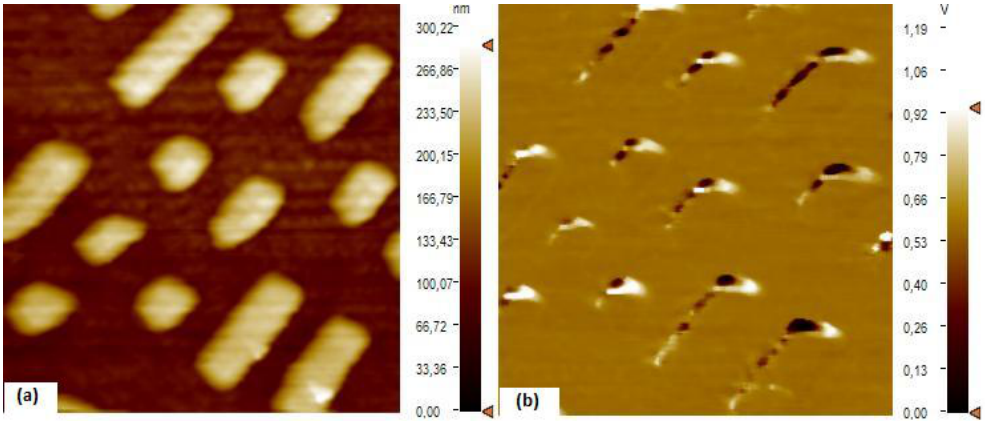

Figure 4.9: (a) The topography image of CD disk in tapping mode (b) The RMS image of CD disk by operating in tapping mode

In the contact mode we obtained V_z shown in Figure 4.10(a) and F_N image shown in Figure 4.10(b). In the contact mode a set F_N is used as a reference signal to obtain images from changes around the reference F_N instead of the changes in the amplitude in the tapping mode.

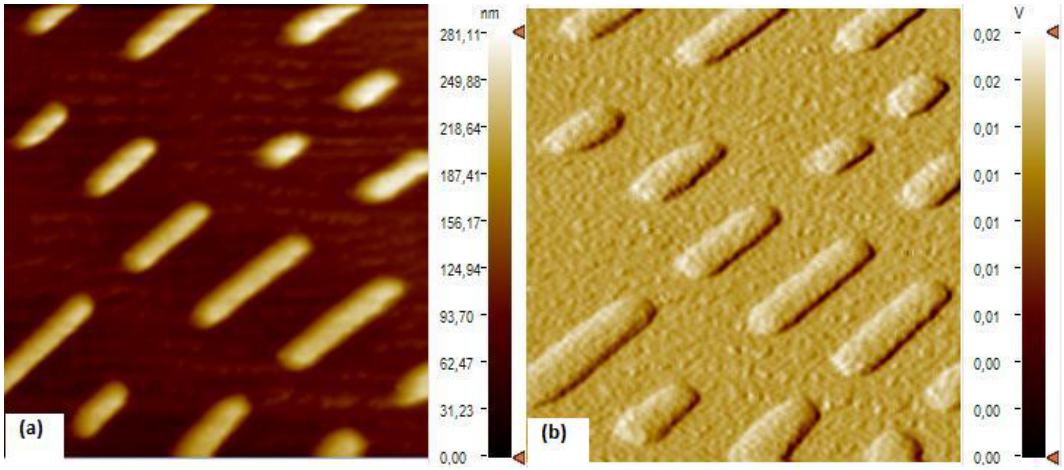

Figure 4.10: (a) The topography image of CD disk in contact mode (b) The F_N image of CD disk by operating in the contact mode.

Also in the non-contact mode the resonance frequency shift is used by the feedback loop during the surface-tip interaction. In this way in the non-contact mode besides the topography image shown in Figure 4.11(a), the resonance frequency shift (Δf) image shown in Figure 4.11(b) is obtained.

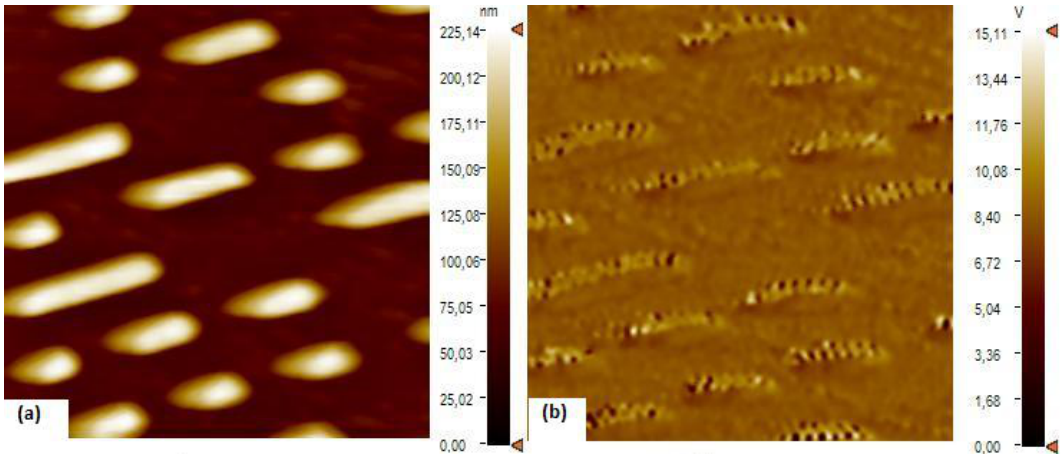

Figure 4.11: (a) The topography image of CD disk in non-contact mode (b) The frequency shift image of CD disk in non-contact mode.

In the non-contact mode even small information can be seen in the topography image because of higher resolution in the non-contact mode than the other modes. The Figure 4.12 shows the height of the small and large bits by the cross-section of topography image of CD disk.

The Figure 4.13 shows the topography of AFM scan of DVD disk. The AFM operated in the contact mode. The scan speed for this image was 2 (2μ m/s).

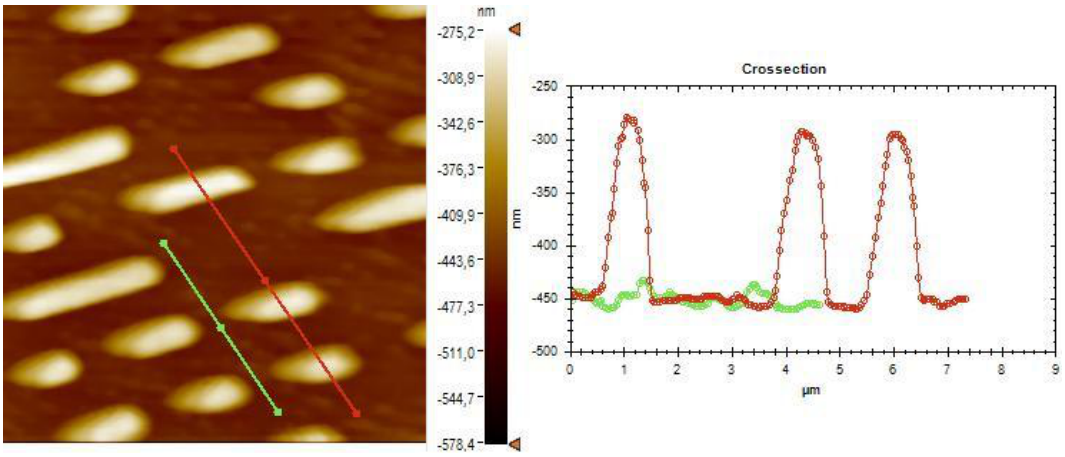

Figure 4.12: Cross section of non-contact AFM scan of CD disk on the topography image

The scan area was 10x10 μm and the image size was 256x256 pixels. As mentioned before DVD disk has twice larger track width than the blu-ray disk.

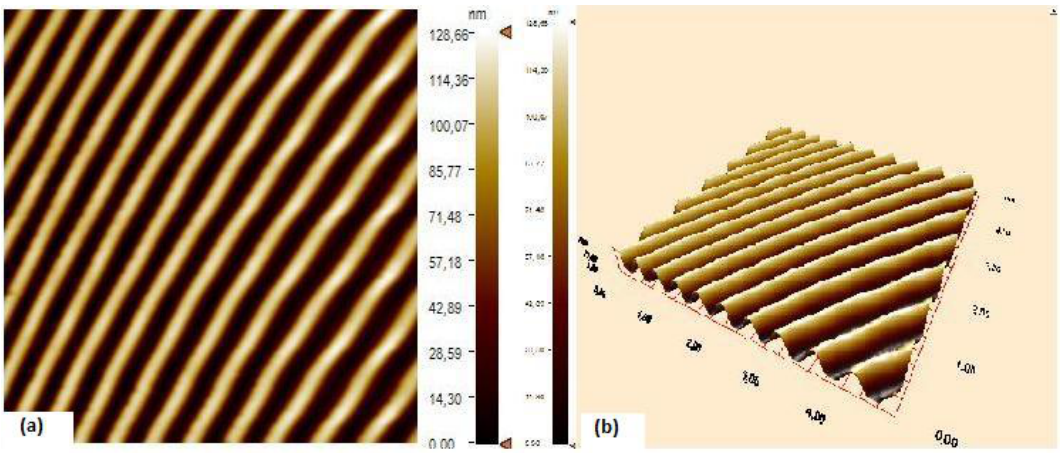

Figure 4.13: The topography image of DVD disk.

With the same parameters and the same operation of mode the CD was imaged and the topography image of it is seen in the Figure 4.14. It can be seen that on the CD disk the track widths are larger than the DVD disk.

6H-SiC(100) was imaged by AFM in the tapping mode. The scratches and shakes occured by production mistakes were established in the 5x5 μm topography image of AFM shown in Figure 4.15.

After etching hydrogen 6H-SiC(100) was imaged by AFM again in the tapping mode. The 4x4 μm topography image shown in Figure 4.16(a) shows a rough region of steps with their height of $\approx$ 0.75 nm and width of $\approx$ 100 nm.

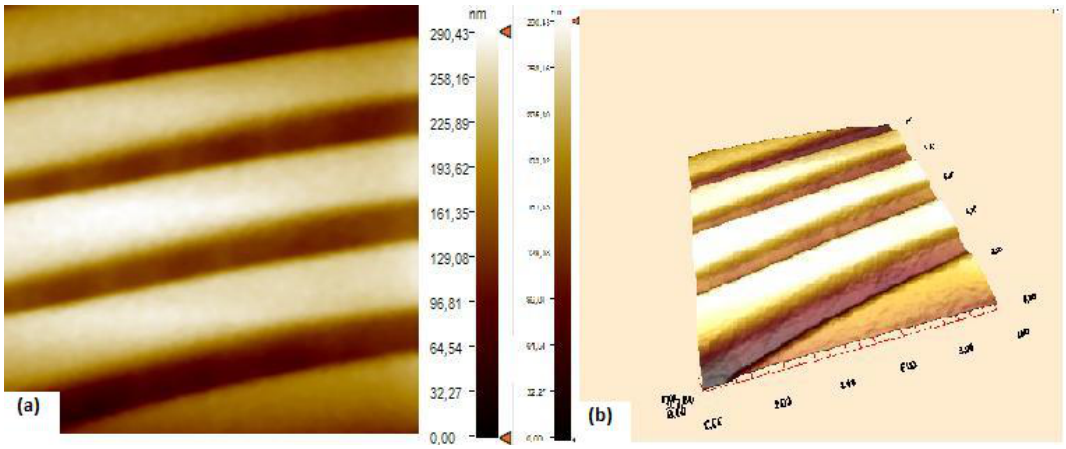

Figure 4.14: The topography image of CD disk.

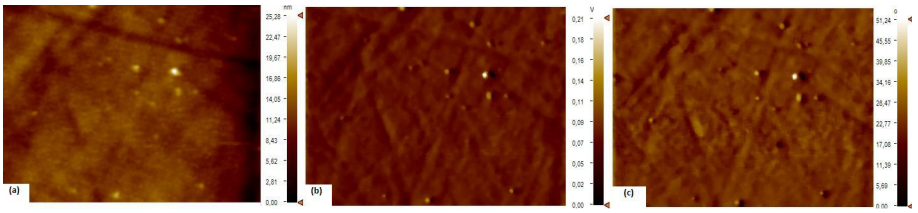

Figure 4.15: (a)The topography image of 6H-SiC (b) RMS image of 6H-SiC (c) Phase image of 6H-SiC . (The scan speed=2μm)

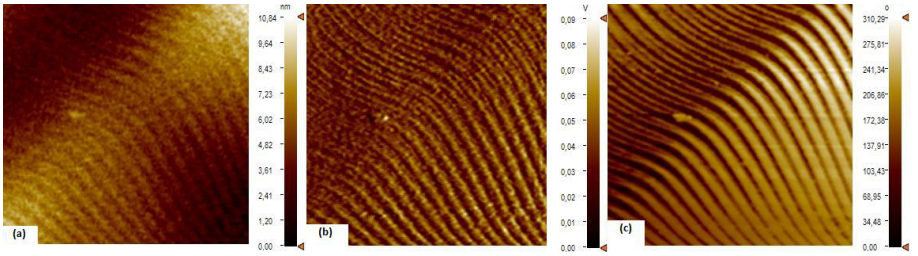

Figure 4.16: (a) The topography image of hydrogen-etched 6H-SiC (b) RMS image of hydrogen-etched 6H-SiC (c) Phase image of hydrogen-etched6H-SiC. (The scan speed=2μm)

4.2 Results by Frictional Force Microscope

4.2.1 Measuring the lateral forces of difference thickness of graphene layers

Graphene is a mono layer of sp^2 bonded carbon atoms packed into a two-dimensional (2D) honeycomb lattice. It can be stacked into 3D graphite, rolled into one dimension nanotubes or wrapped up into zero- dimensional (0D) fullerenes, as shown in figure 1[**46**]. Until recently, it has been known to exist only in the one, zero dimensional form and its three dimensional structure like graphite

which comprise graphene sheets. Since it was known that two dimensional crystals were thermodynamically unstable,[**48,49**] it was presumed that graphene didn't exist in the free state. However, graphene was first prepared via mechanical exfoliation of graphite crystals by Professor Andre Geim's research group at the University of Manchester[**50**]. Since, not only graphene has unique electrical and mechanical properties, but also the thinnest material ever fabricated, it has recently attracted attention of the research communities.

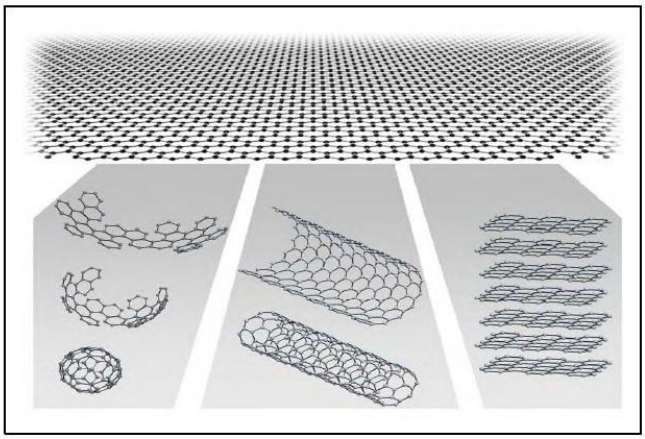

Figure 4.17: Structure of different graphitic forms. On the top of figure, graphene, one atomic thick layer, is shown. In the bottom middle, carbon nanotubes are shown. On the bottom right, a stack of graphene layers called graphite is shown. On the bottom left, buckyball model is given.

In the graphene characterization, graphene thickness is crucial point to distinguish monolayer, bi-layer and few layer of graphene. For this purpose , low energy electron diffraction,(LEDD), phonon-electron spectroscopy, Raman spectroscopy, optic microscope and atomic force microscope can be used. In this work, frictional forces of graphene layers will be determined by using frictional force mode in the atomic force microscopy supplied by NanoMagnetics Instruments Ltd.

Graphene is prepared by using method called mechanical exfoliation in this work. For this method , 15mm of flake graphite (larger than 0,850 mm) was placed to plastic sticky tape with tweezers, then pressed slowly and tape was peeled apart. This process can be repeated until graphite is thin enough. Finally, cleaved graphene sample was transferred into 300 nm SiO_2 on Si substrates. First characterization is done by optical microscope benefitting from optical contrast.

In Figure 4.18, optical image of graphene flakes with different thicknesses is shown. As seen in the figure there are four layers with different thicknesses. Figure 4.19 shows the measurements of these graphene flakes.

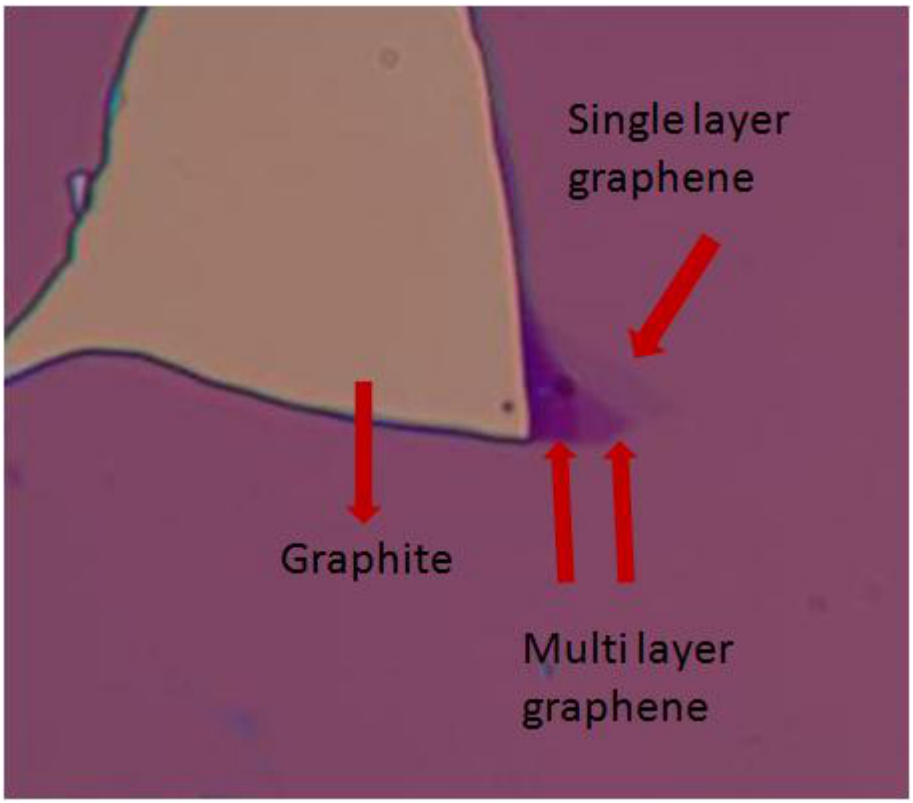

Figure 4.18: Optical image of graphene with magnification X100.

Then lateral forces of graphene layers with difference thicknesses were measured by frictional force microscopy. In frictional force microscopy mode, topography and lateral force images are obtained simultaneously. First the thickness of graphene and graphite layers were measured on topographic images. Secondly frictional forces were evaluated by means of the lateral forces images of graphene flakes.

To calculate the lateral forces of graphene layers with difference thicknesses, first the lateral spring constant which is dependent to geometric properties of cantilever. The lateral spring constant is given by,

$$c_L = \frac{Gwt^3}{3h^2l} \tag{4.1}$$

where G is the shear modulus, w is the width of the cantilever, t is the thickness

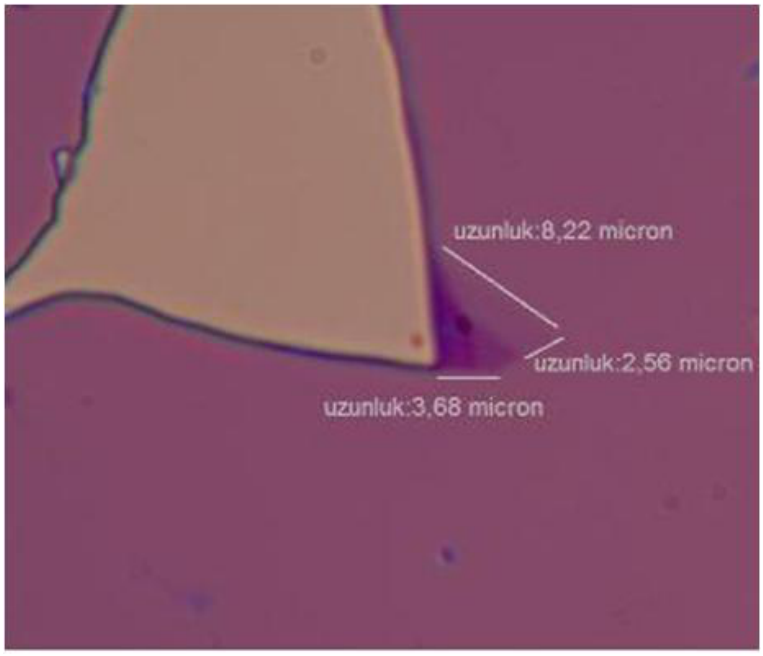

Figure 4.19: Measurements of graphene flakes on optical image with magnification X100.

of the cantilever,l is the length of the cantilever and h is the height of the tip. For silicon $G = 0,510^{11}N/m^2$. The cantilever used is single crystal silicon cantilever. For this cantilever $w = 50\mu m$, $t = 2\mu m$,$h = 17\mu m$, $l = 450\mu m$. c_L was calculated as 51.3 N/m. After calculating the lateral constant spring, by using this constant and cross section of lateral force images the lateral forces of graphene layers were calculated with given formula,

$$F_L = \frac{3}{2} c_L \frac{h}{l} S_z V_L \qquad (\mathbf{4.2})$$

where S_z is the sensitivity of photodiode,V_L is the the difference voltage between the horizontal signals. V_L was calculated as the average of lateral voltage values in the cross section graphic from lateral force image. The sensitivity of photodiode used in our AFM is 0.43 A/W. Frictional forces on four graphene layers with different thicknesses were calculated.

Figures 4.20, 4.21, 4.22 and 4.23 show the topography images of graphene layers and lateral force images in the simultaneously scan and also cross section of this two images. For these images contact mode cantilever which has 0.2 N/m force constant is used. The scan speed and the image size was 2 μ m/s and 256x256 pixels, respectively.

The Figure 4.20 (b) shows the topographic images of graphene, from this image the thickness of graphene was measured as 1,05 nm. By using the formula 2, the lateral force of this single layer graphene was calculated as 7,8 pN.

In the Figure 4.21 (a), the thickness of few layer graphene was measured as 4,90 nm from the cross section of the topography image. The lateral force of this layer was calculated as 7,7 pN.

In the Figure 4.22 (a), the thickness of multi layer graphene was measured as 6,08 nm. The lateral force of this layer was calculated as 7,5 pN. In the Figure 4.23 (a), the thickness of graphite was measured as 164,92 nm. The lateral force of this layer was calculated as 0,48 pN.

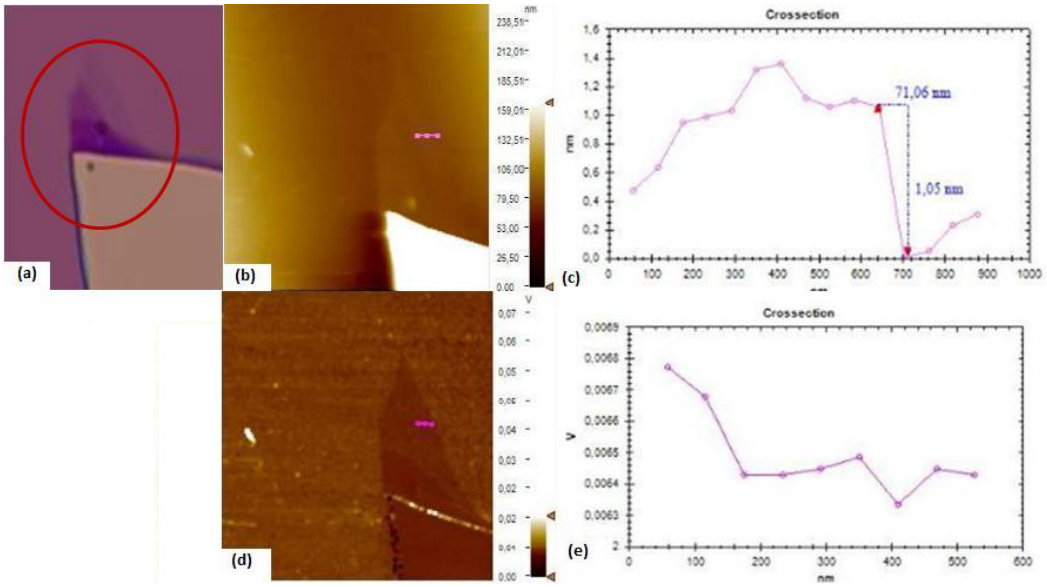

Figure 4.20: (a)Optic microscope image of graphene flakes imaged by FFM (b) The topograpy image of the graphene layer.(c)The crosssection of the topography image.(d) The lateral force image of the same graphene layer (e) cross section of the lateral force image.

The frictional forces values of graphene layers with respect to thickness of graphene layers were graphed with the help of origin programme by fitting to the first order exponential curve as shown in Figure 4.24. The graphic shows that the frictional force on graphene is larger than on graphite (multilayer of graphene).

As seen from the cross section of lateral force image in Figure 4.25 the frictional force on graphene is smaller than on SiO_2. Also the contrast difference between

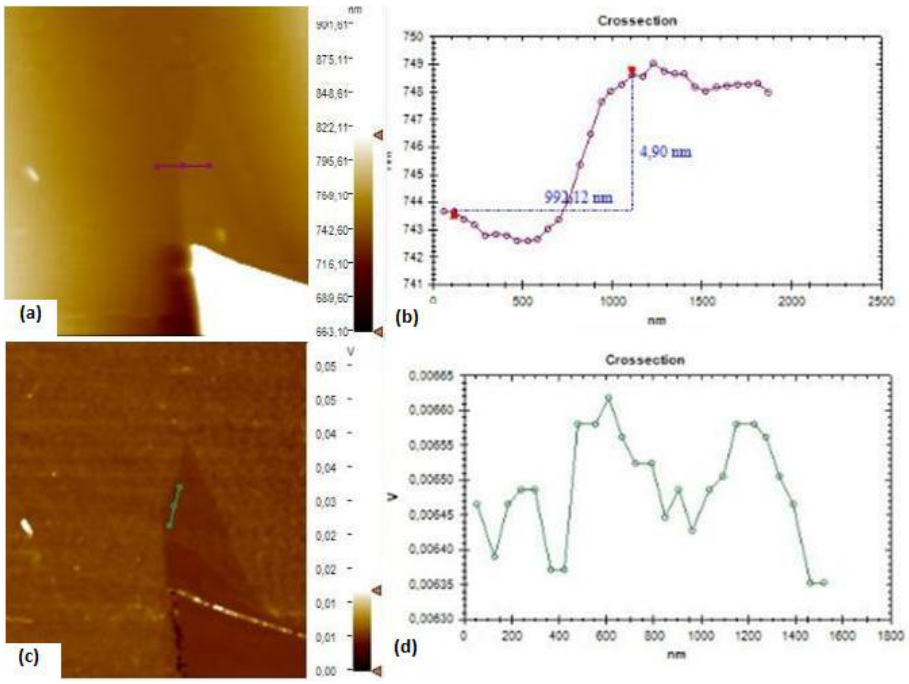

Figure 4.21: (a) The topograpy image of the graphene layer.(b)The cross section of the topography image. (c) The lateral force image of the same graphene layer (d) cross section of the lateral force image.

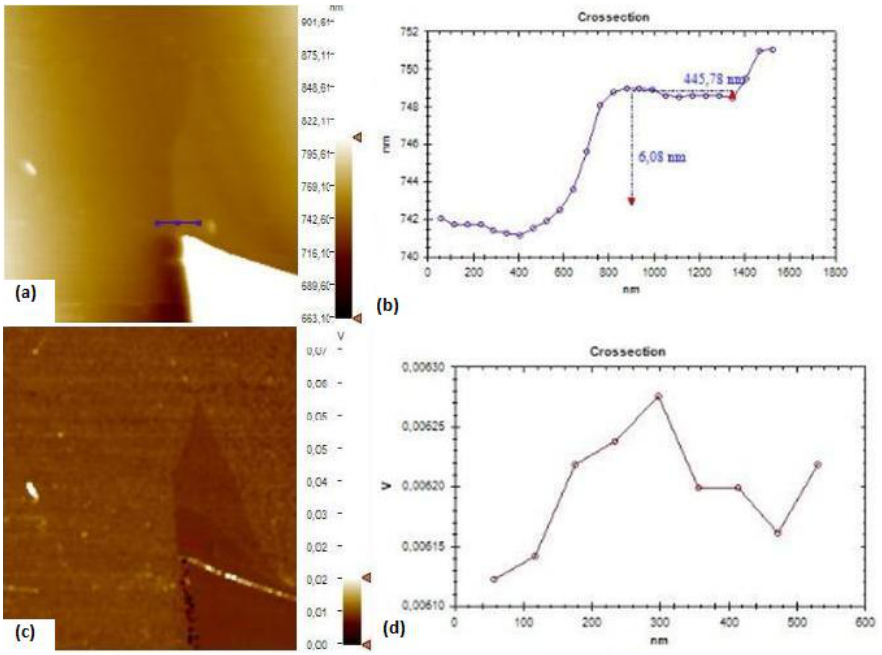

Figure 4.22: (a) The topograpy image of the graphene layer.(b)The cross section of the topography image. (c) The lateral force image of the same graphene layer (d) cross section of the lateral force image.

the graphene layers with different thicknesses can be seen from the lateral image and cross section.

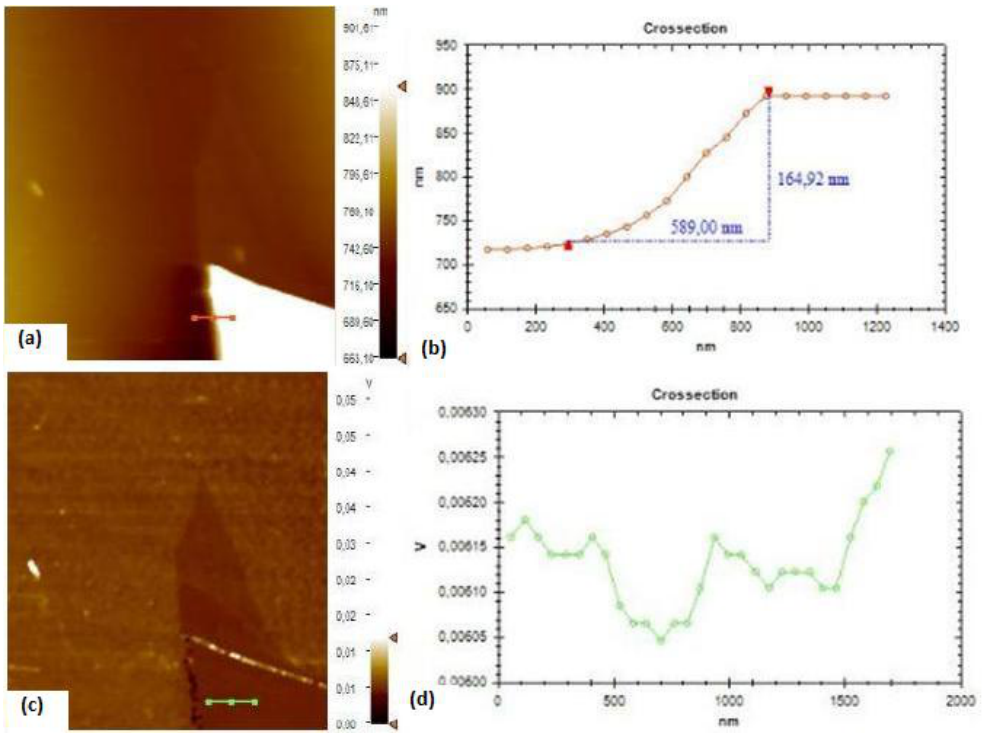

Figure 4.23: (a) The topograpy image of the graphene layer.(b)The cross section of the topography image. (c) The lateral force image of the same graphene layer (d) cross section of the lateral force image.

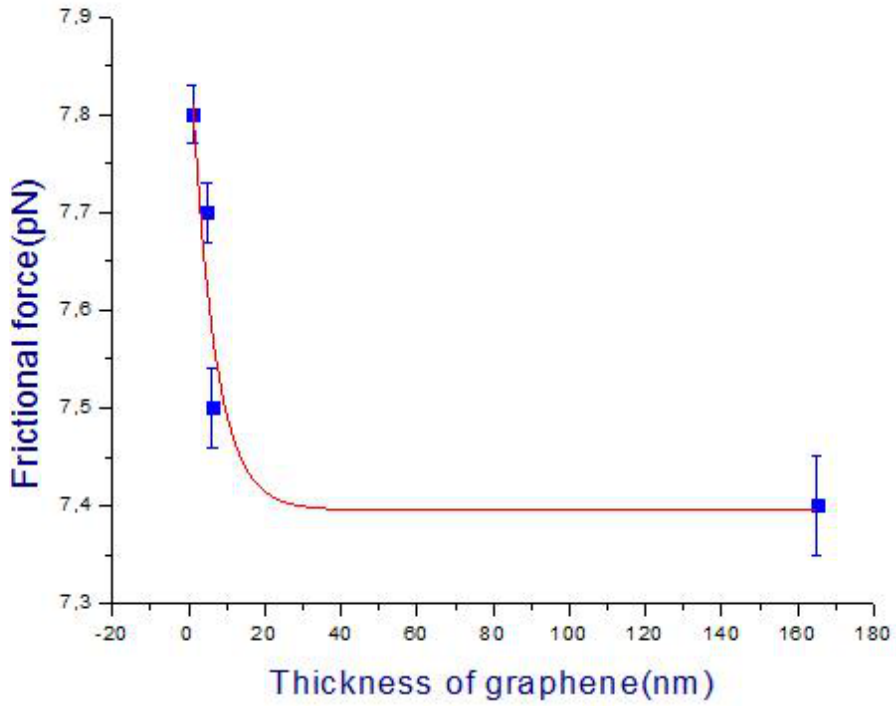

Figure 4.24: The frictional forces were measured as a function of the thickness of the graphene and graphite.

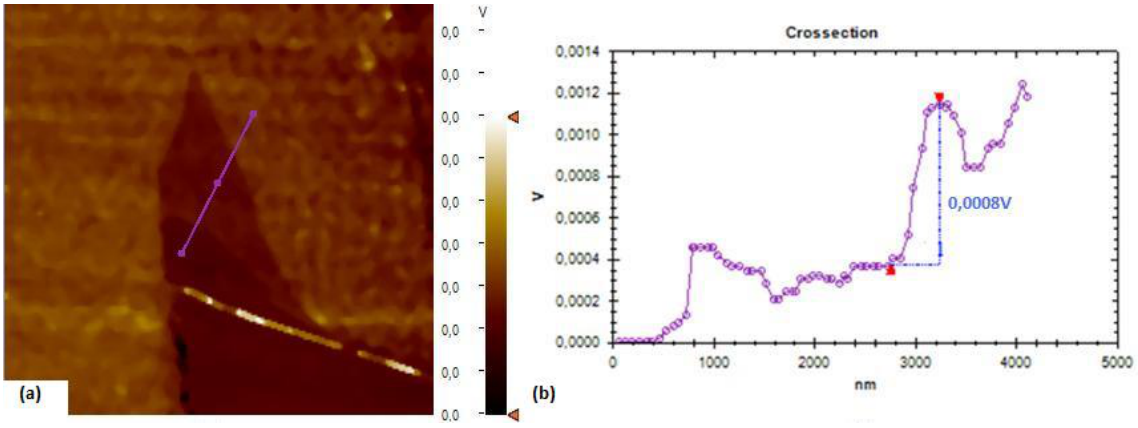

Figure 4.25: (a)The lateral force image of graphene. (b) The cross section of lateral force image.

4.3 Results by Kelvin Probe Force Microscopy(KPFM)

4.3.1 Operating KPFM in AM method and FM method

We obtained the first images by KPFM with the first experimental set-up with the phase-lacked loop mentioned before. The cantilevers we used for the first images were single crystal silicon tips used for Electrostatic Force Microscopy with 75 kHZ resonance frequency and 3 N/m force constant. These tips are electrically conductive by means of coating of 5 nm Chromium and 25 nm Platinum on both sides of the cantilever.

On CD, DVD there is a layer of approximately 1.7 mm thick which is made from poly carbonates. This layer is prepared by injection molding and in the printed CD and DVD they molded to form the bumps and pits. After these bumps and pits are molded, the data storage surface is coated with aluminum by sputtering. Hence when applied to the laser the molded bumps creates pits on the aluminum surface and data is read depending on the reflected light from the aluminum surface bumps. Blu-ray disc is also an optical disc storage medium. But as mentioned before its data storage is based on a phase-change optical recording. We imaged the blu-ray disk by AM-KPFM. We obtained simultaneously topography and contact potential images shown in Figure 4.26. Because of the difference metals of the surface and the bits, work function difference between the surface and the bits was seen in the contact potential image shown in Figure 4.27.

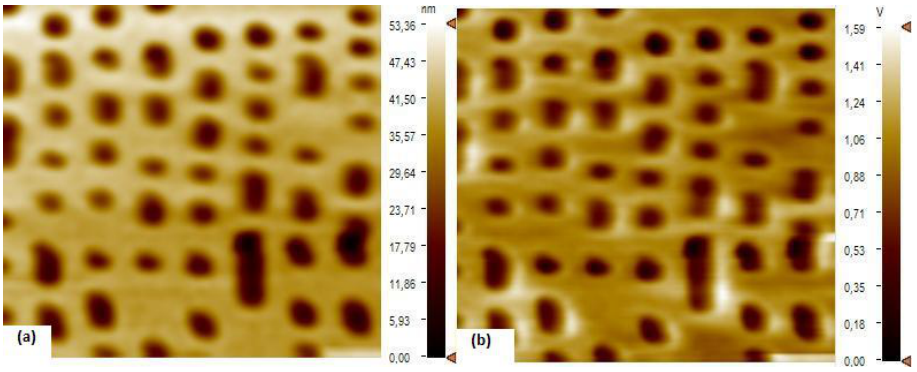

Figure 4.26: (a)The topography image of blu-ray disk by AM-KPFM. (b) The contact potential image of blu-ray disk by AM-KPFM.

For these images the first resonance frequency was 63 kHz. The second resonance frequency used for contact potential image was 407 kHz. The set dc was a value between 0.1 V and 0.2 V. The scan area and the image size was 5 μ m x 2.44 μ and 256x256 pixels, respectively. The scan speed was 1 μ m/s.

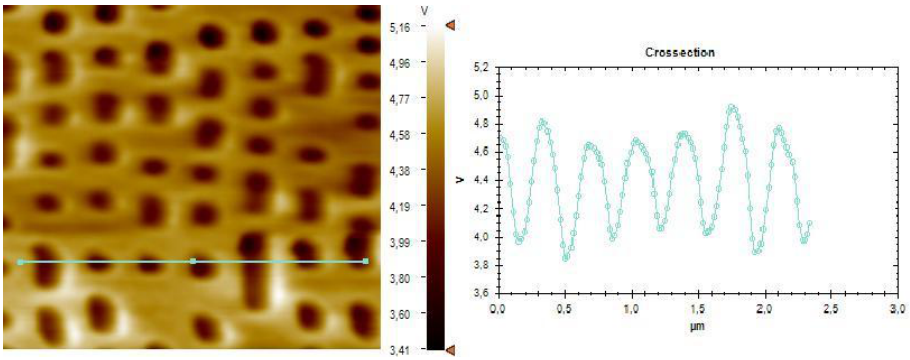

Figure 4.27: Cross section of AM-KPFM scan of blu-ray disk on the contact potential image

After imaging blu-ray disk by the experiment set-up with PLL, lock-in amplifier was used instead of PLL to obtain images with higher resolution and to operate KPFM also in Force Modulation(FM) method. The Figure 4.28 shows contact potential, phase and topography images obtained by operating in AM-KPFM, respectively. For these images the first resonance frequency was 62 kHZ. The second resonance frequency used for contact potential can be adjusted by lock-in amplifier. By the lock-in amplifier it adjusted to 10 kHz. Generally the second resonance frequency is adjusted to be six or seven times smaller than the first resonance frequency. The scan speed and the scan area was 1 μ/m and $3\mu m$x$3\mu m$.

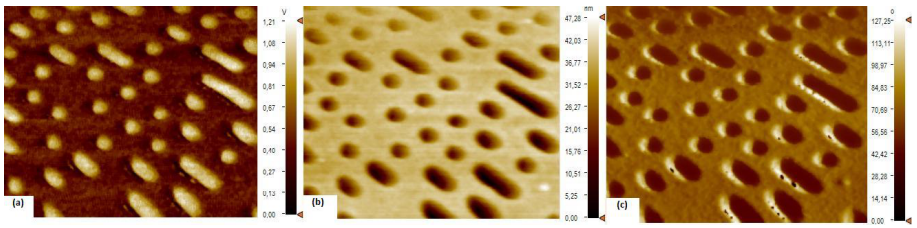

Figure 4.28: (a)The contact potential image of AM-KPFM scan (b) The topograph image of AM-KPFM scan (c) The phase image of AM-KPFM scan.

The cantilevers used for EFM could not work to operate KPFM in FM method because of its spring constant. To operate in FM-KPFM the force constant of cantilever should be larger. We have a cantilever which spring constant are 40N/m for non-contact imaging but it is single crystal silicon tip which is not electrically conductive. We decided to use HF acid for oxide etching on the silicon tip. At 20^oC the cantilevers were held for a minute in the etchant prepared as 10:1 HF(10 H_2O:1 48 HF). With these cantilevers the images shown in Figure 4.29 were obtained.

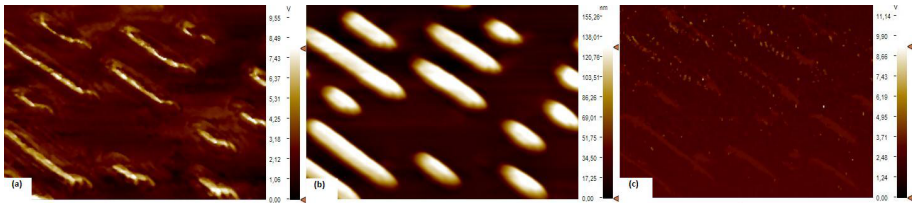

Figure 4.29: (a)The contact potential image of cd disk operating in FM-KPFM. (b) The topograph image of cd disk operating in FM-KPFM.(c) The frequency shift(Δf) image of cd disk operating in FM-KPFM.

Because of oxidation of silicon in a short time and low quality images by etched cantilevers, electrically conductive was decided to make by metal coating method. The cantilevers used for non-contact and tapping imaging with resonance frequency of 300 kHz and force constant of 40N/m were coated with 5nm Cr and 20 nm Au, respectively by evaporator coating system(shown in Figure 30). The SEM images of cantilevers before coating and after coating in Figure 4.31 and 4.32. The resonance frequency of cantilevers were decreased to 272 kHz because of totally 25 nm metal coating.

With the cantilevers coated with 25 nm metal CD disk was imaged in AM-mode and FM-mode and these images are shown in Figure 4.33.

Figure 4.30: The evaporator coating system in our laboratory

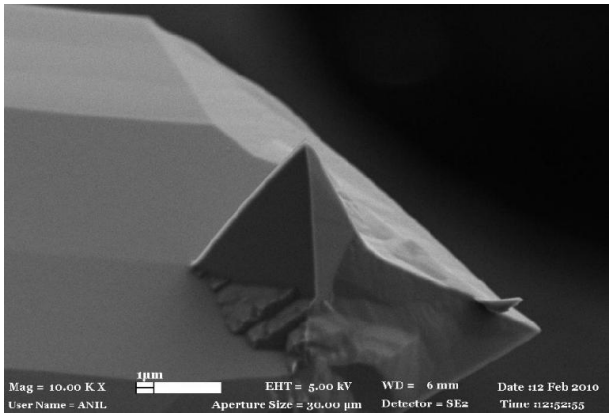

Figure 4.31: The SEM image of the single crystal silicon cantilever before coating

The scan speed and the scan area was 2 μ m/s and 10μ mx10 μ m. For two modes the same cantilever which the first resonance frequency was 272 kHz and the force constant was 40N/m was used. The second resonance frequency was adjusted to 40 kHz. For the AM-mode the AC voltages of amplitude around 0.5V were used. For the FM-mode the AC voltages of amplitude around 5V were used. The work function image in the AM-mode in the Figure 4.34(a) shows that the variations of work function were measured as only 0.17V, whereas($\Delta\phi = 0.17V$) the variations of work function in the FM-mode were measured as 0.34V($\Delta\phi = 0.34V$) in Figure 4.34(b). In the AM detection the contrast in the work function images

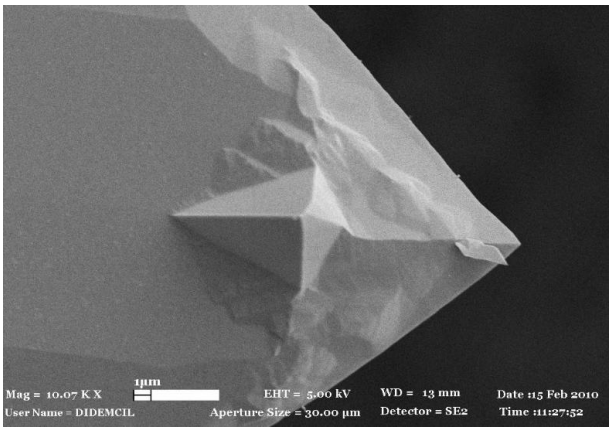

Figure 4.32: The SEM image of the single crystal silicon cantilever after coating

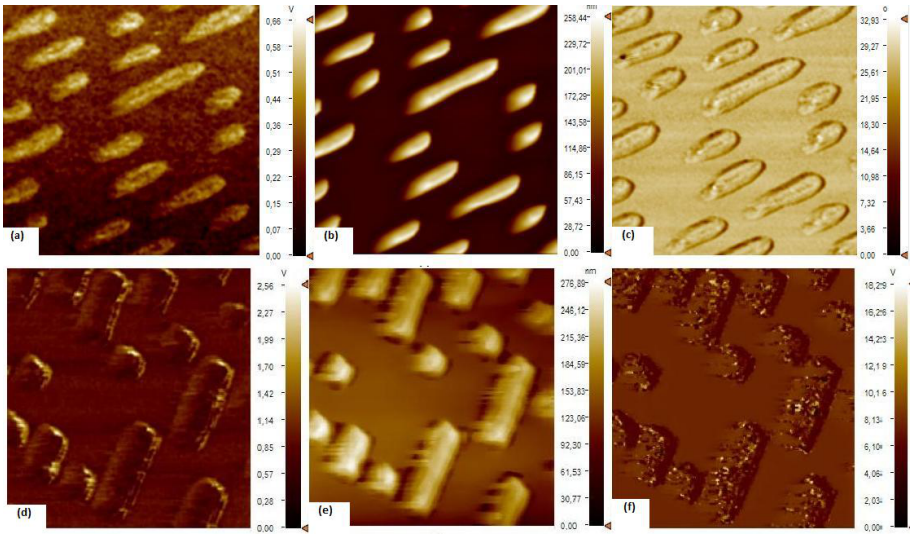

Figure 4.33: (a) The contact potential image of CD disk operating in AM-KPFM. (b) The topograph image of CD disk operating in AM-KPFM (c) The phase image of CD disk operating in AM-KPFM (d) The contact potential image of CD disk operating in FM-KPFM. (e) The topograph image of CD disk operating in FM-KPFM. (f)The phase image of CD disk operating in FM-KPFM

was observed as lower than the detection in the FM-mode. The advantage of AM-mode is the possibility to use low AC voltages.

Also we imaged hall probe by AM-KPFM. On the hall probe there are different metals as seen optic microscope image in the Figure 4.35.

This scan was with conductive cantilever used for EFM with resonance frequency of 75 kHz and force constant of 3 N/m. The scan speed and scan area was

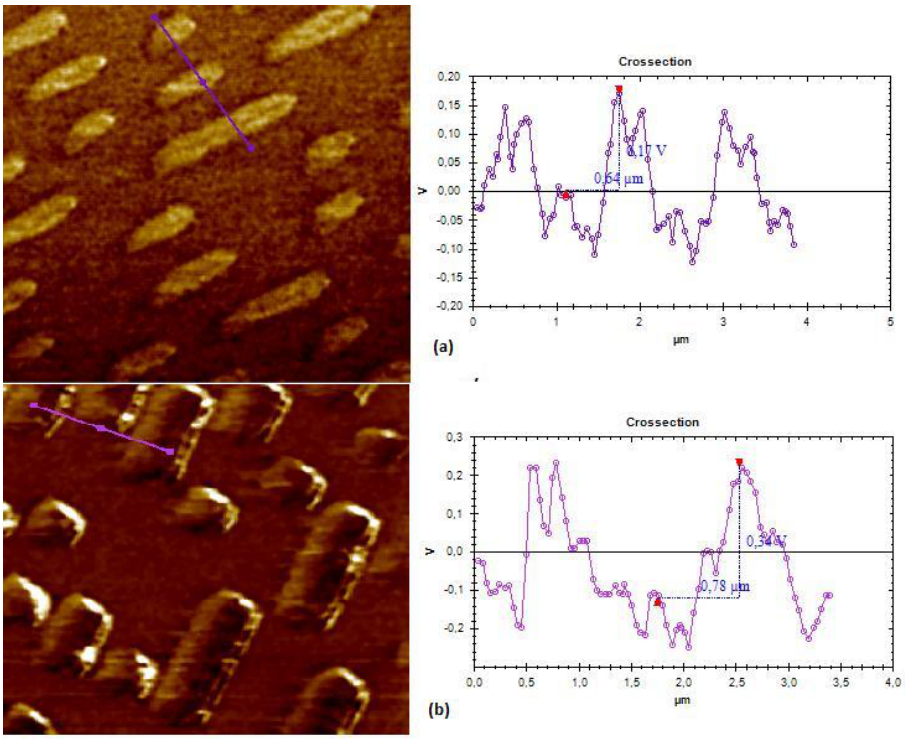

Figure 4.34: (a)Cross section of AM-KPFM scan of cd disk on the contact potential image (b)Cross section of FM-KPFM scan of blu-ray disk on the contact potential image

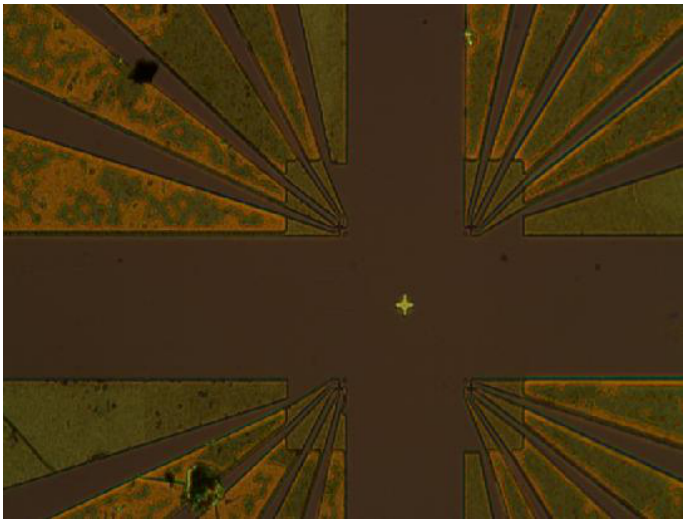

Figure 4.35: Optic microscope image of hall probe with x20 magnification

2 μ m/s and 20μ mx20 μ m. In the Figure 4.36 optic microscope image shows the area of the KPFM scan.

In the Figure 4.37 the cross section of scan is shown on the contact potential image. The cross section line begins from Au part of the hall probe to Ge part

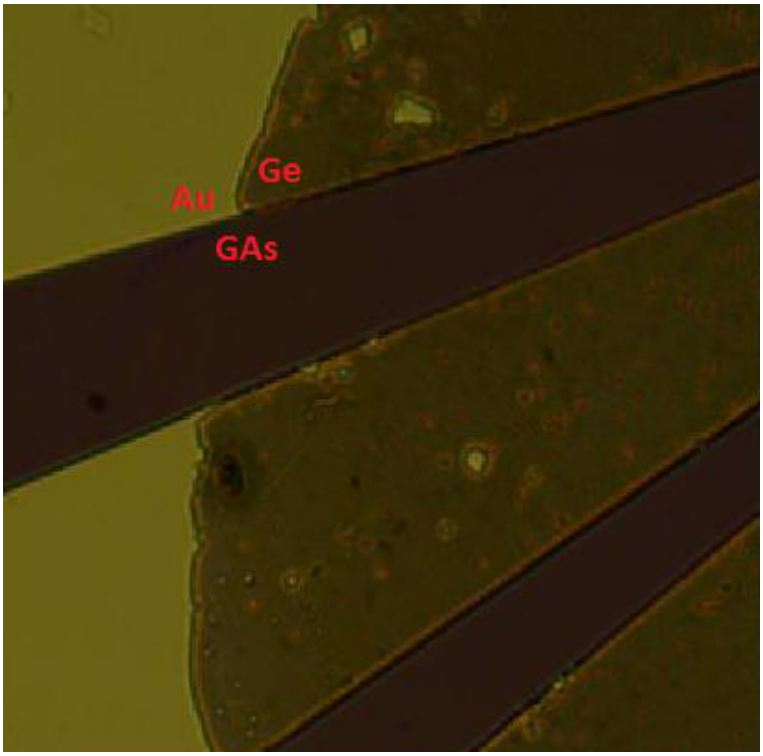

Figure 4.36: Optic microscope hall probe image of scan area of AM-KPFM with x5 magnification

of the hall probe. The work function of Au varies from 5.1 to 5.47 eV. The work function of Ge is 4.83 eV. As seen on the graph the work function should be decrease while the cross section line reaches to Ge part of the hall probe. And the work function difference between the Ge and Au should vary from 0.2 V to 0.6V. In the Figure 4.37 the work function difference between the Au and Ge was measured as 0.6 V.

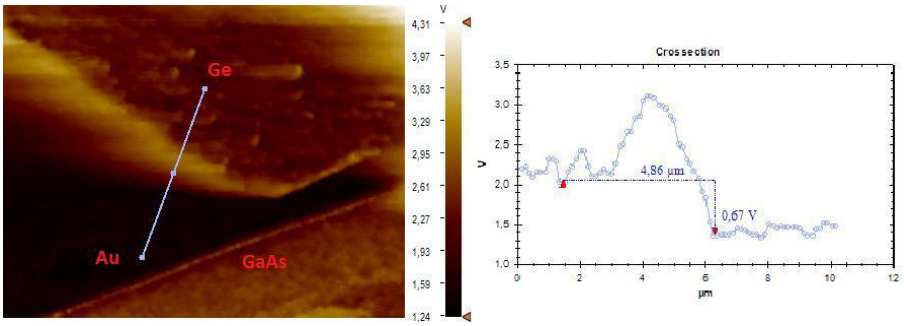

Figure 4.37: Cross section of AM-KPFM scan of hall probe on the contact potential image

4.3.2 Measuring work function difference of graphene, graphite and SiO_2 surfaces using KPFM

In this section the graphene was analyzed by KPFM. We predict that we can determine the work function difference between graphene and SiO2, graphite and SiO2 and also graphene and graphite. We prepared graphene with the same mechanical exfoliation method described in the section 4.2. The prepared graphene was characterized by the optical microscope. Figure 4.38 shows the optical microscope image of prepared graphene. To characterize by KPFM, sample should be electrically conductive. We obtained the electrical conductivity by using silver paint. Silver paint contacts taken from graphene sheet as shown in Figure 4.39. Benefitting from optical contrast some layers of graphene were expected to be single layer graphene shown in Figure 4.38. The prepared graphene was characterized with Raman Spectroscopy to be sure about the thickness of graphene layers.

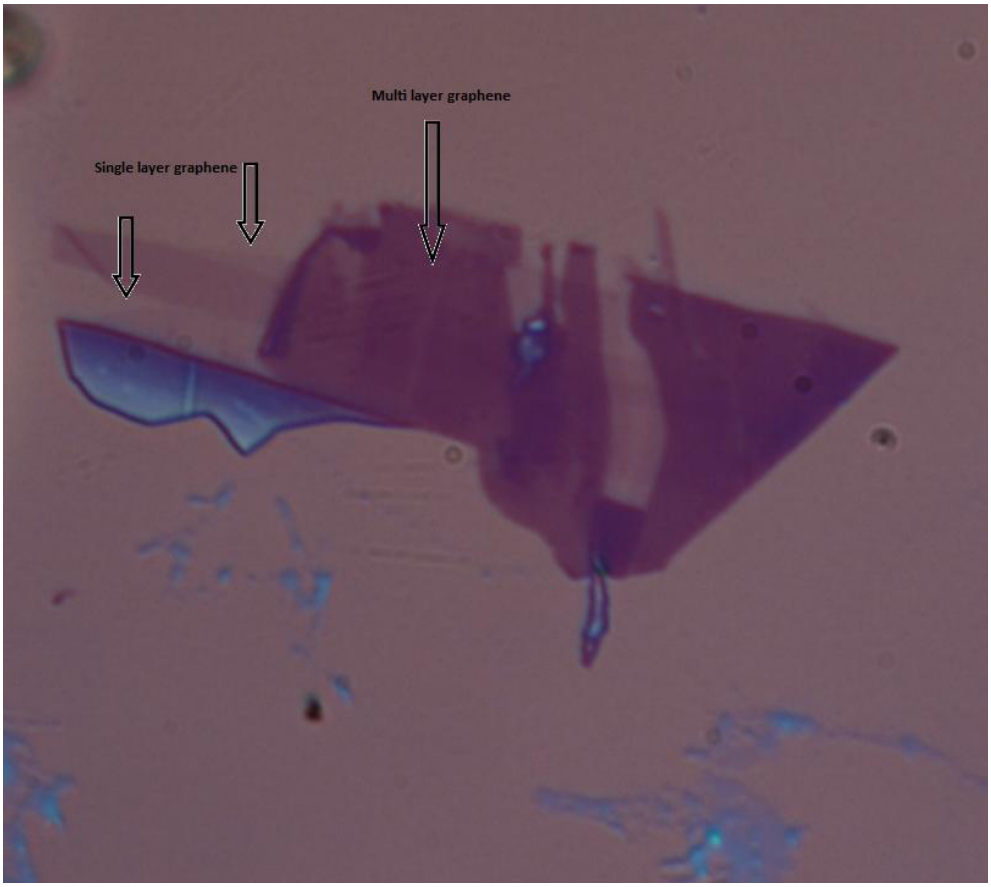

Figure 4.38: Optical microscope image of graphene with magnification x100

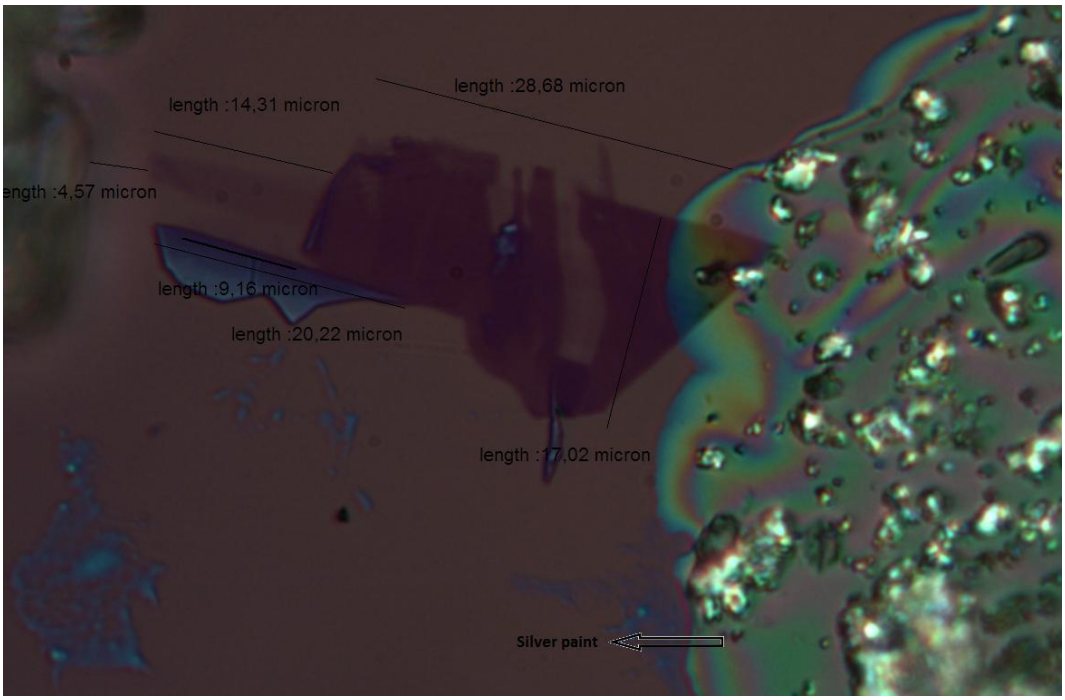

Figure 4.39: Optical microscope image of graphene layer taken contact by silver paint with magnification x100.

Raman spectroscopy has historically been used to probe structural and electronic characteristics of graphite materials, providing useful information on the defects (D band), in-plane vibration of sp^2 carbon atoms (G band) as well as the stacking order (D'band)[**51**].The D peak is related to the finite crystallite size, shows the structural quality and disappears for perfect crystals. The integrated G line signal is correlated with the thickness of graphitic flake and is shifted upward in frequency for double and single layer graphene compared to that of bulk graphite. The D' band is used used as a simple and efficient way to confirm the presence of single layer graphene. The peak width of the D' line shows a strong contrast between single and few layer graphene[**52**]. Also the intensity of G line versus D' line increases from single layer to multi graphene.

We examined our prepared graphene with a Renishaw In via Reflex Raman Microscope System of Prof. Dr. Mustafa Çulha's laboratory at Yeditepe University. We used a 514 nm wavelength green argon ion laser with a 25 mW maximum power. The numerical aperture of the objective lens was 0.8. Figure 4.40, 4.41, 4.42 and 4.43 shows raman spectroscopy of different graphene layers on prepared graphene. As seen in the figures the width of the peak of D' decreases

from double layer shown in Figure 41 to single layer graphene shown in Figure 4.42 and 4.43. Also the instensity of G line versus D' line increases from single layer graphene shown in Figure 43 to multi layer graphene shown in Figure 40.

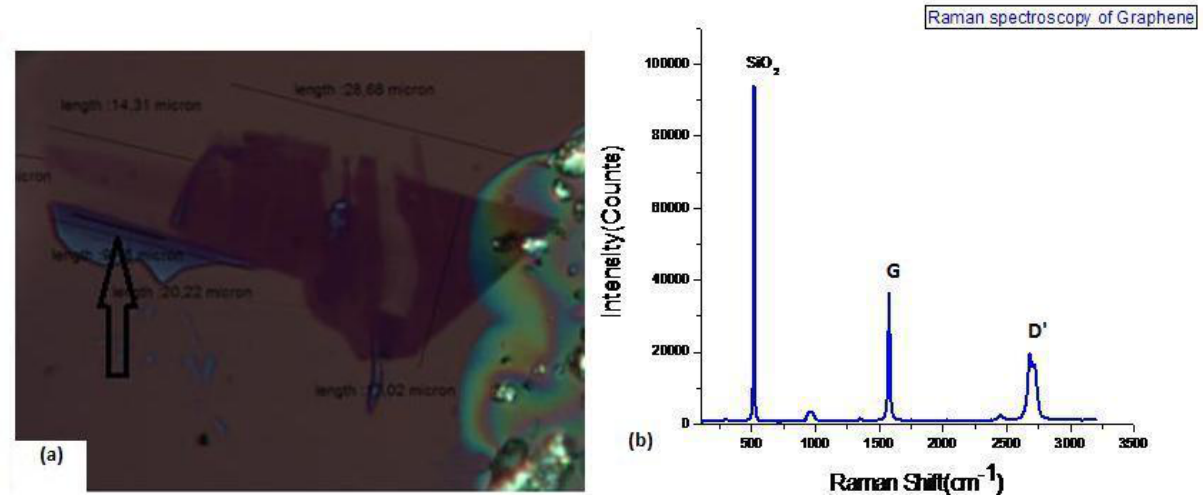

Figure 4.40: (a)Optical microscope image of graphene sheet characterized by Raman spectroscopy (b)Raman Spectroscopy of multi layer graphene

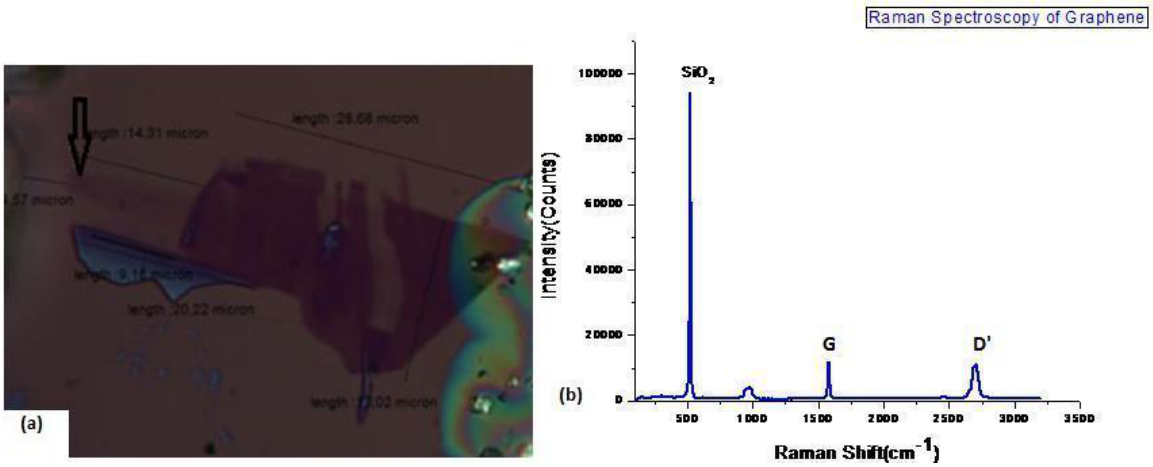

Figure 4.41: (a)Optical microscope image of graphene sheet characterized by Raman spectroscopy (b)Raman Spectroscopy of few layer graphene

After characterization by optic microscope and raman spectroscopy, prepared graphene was analyzed by KPFM. KPFM operated in AM-KPFM. We used single crystal silicon cantilevers coated with 5nm Cr and 20 nm Au with first normal resonant frequencies ranging between 250-300 kHz. For first scan of KPFM we apply an ac voltage with an amplitude of 5V and a kelvin frequency of 40 kHz.

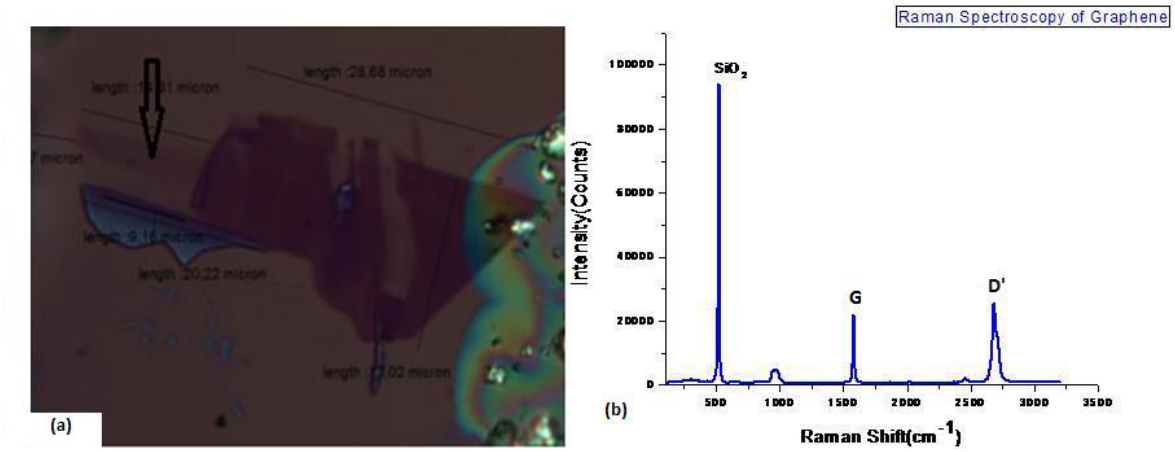

Figure 4.42: (a)Optical microscope image of graphene sheet characterized by Raman spectroscopy (b)Raman Spectroscopy of single graphene

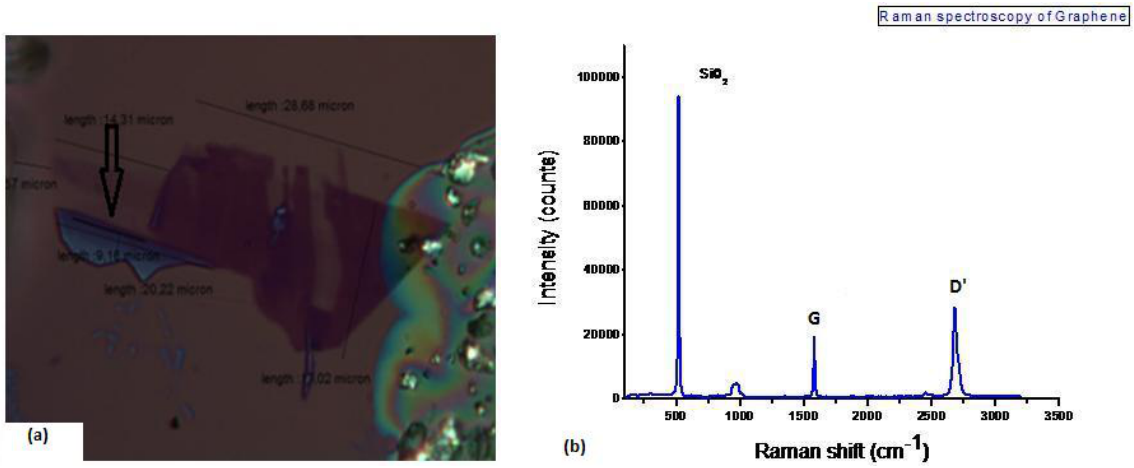

Figure 4.43: (a)Optical microscope image of graphene sheet characterized by Raman spectroscopy (b)Raman Spectroscopy of single graphene layer.

The scan speed and the scan area was 2μ m/s and 20μx20μ. The images of AM-KPFM scan are given by Figure 4.44 and 4.45.

Figure 4.46 shows the thickness of single layer graphene sheet.The thickness of single graphene was measured as 1.03 nm. In this measured thickness of graphene there are also the electric dipole of residues left from the adhesive tape during graphene preparation and the dipole moments of water molecules adsorbed on top of graphene. Figure 4.47 shows the thickness of few-layer graphene It was measured as 3.2 nm. In Figure 4.48 the work function of SiO_2 was measured

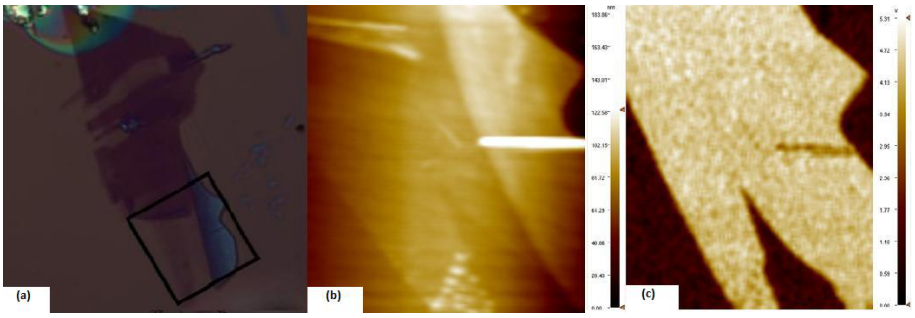

Figure 4.44: (a)The graphene sheet characterized by AM-KPFM was marked on the optical microscope image.(b)The topography image of graphene by AM-KPFM scan. (c)The contact potential image of graphene by AM-KPFM scan.

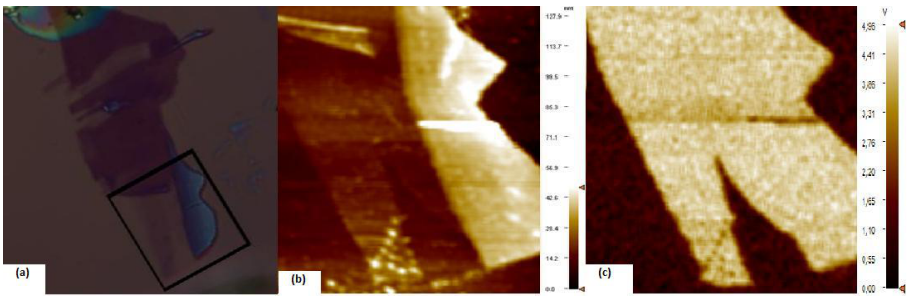

Figure 4.45: (a)The graphene sheet characterized by AM-KPFM was marked on the optical microscope image.(b)The topography image of graphene by AM-KPFM scan. (c)The contact potential image of graphene by AM-KPFM scan.

1.79 V lower than the graphite. Also it is theoretically lower than the work function of graphite.

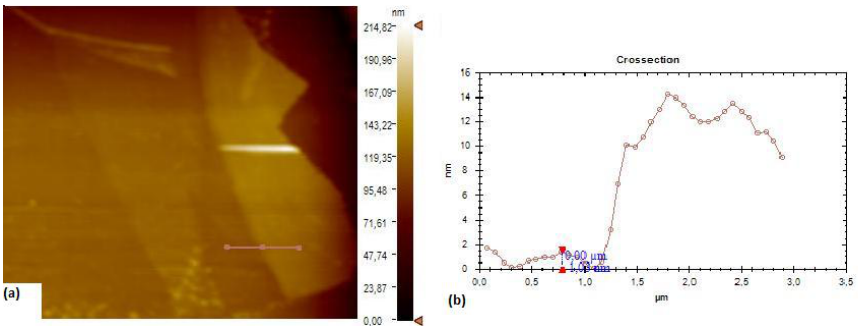

Figure 4.46: Cross section of AM-KPFM scan of single layer of graphene on the topography image

In the second scan of KPFM, kelvin probe resonance frequency was decreased to 25kHz and the oscillation amplitude of kelvin probe was changed to 0.5 V while the other parameters were not changed. In the images shown in Figure 4.49 the contrast in the contact potential image was changed. When we change the

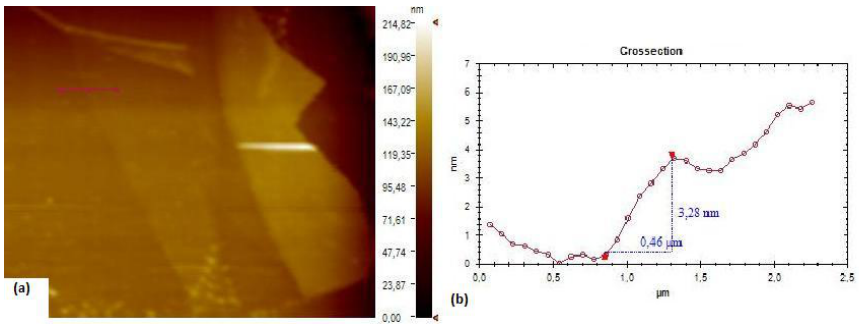

Figure 4.47: Cross section of AM-KPFM scan of few-layer of graphene on the topography image

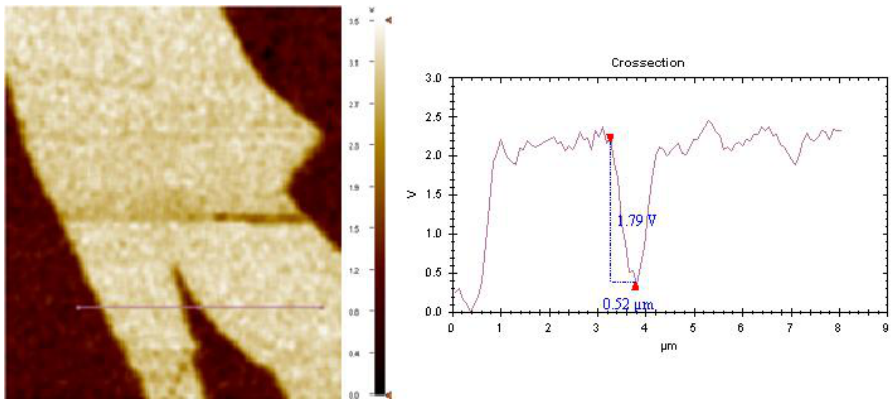

Figure 4.48: Cross section of AM-KPFM scan of graphene on the contact potential image

amplitude of kelvin probe and the kelvin probe frequency, the values of contact potential change.

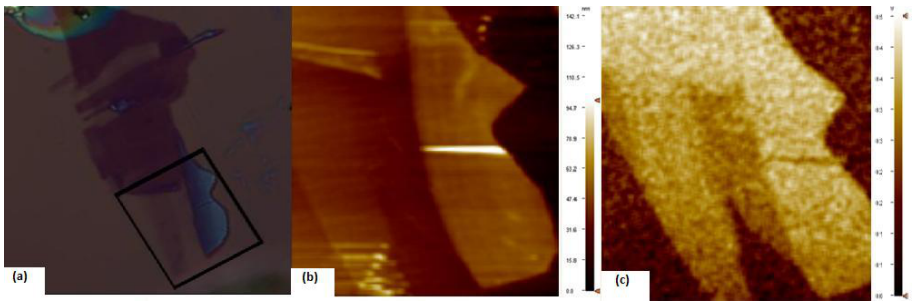

Figure 4.49: (a)The graphene sheet characterized by AM-KPFM was marked on the optical microscope image.(b)The topography image of graphene by AM-KPFM scan.(c)The contact potential image of graphene by AM-KPFM scan.

In the contact potential image between the single layer of graphene and multi layer of graphene(graphite) and also single layer of graphene and few layer of graphene a contrast difference was occured. Shown in the Figure 4.50 between the multilayer graphene and single layer graphene, 0.07 V work function difference

was measured. The work function of single layer graphene is smaller than the work function of graphite. Also 0.03 V work function difference was measured between the single layer graphene and the few-layer graphene shown in Figure 4.51. The work function of single layer graphene is reduced by 30 mV as compared to double layer graphene. The central result of our experiments is that the work function of graphene varies with the thickness of graphene. The work function of single layer graphene was reduced as compared to double layer graphene.

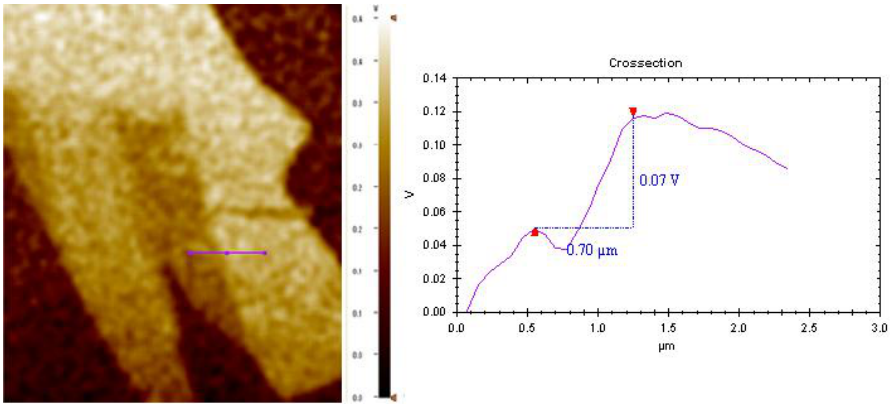

Figure 4.50: Cross section of work function difference between the single layer graphene and graphite

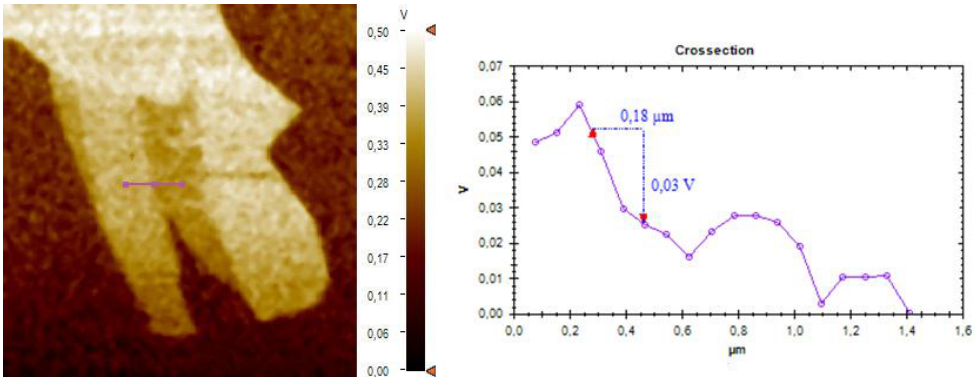

Figure 4.51: Cross section of work function difference between the single layer graphene and few-layer graphene

4.3.3 Measuring work function difference of HOPG and Au by KPFM

To calibrate the system in AM-KPFM mode we measured the work function difference between Au and HOPG. The work function values change with the amplitude of kelvin probe and kelvin probe frequency. To find the convenient

amplitude and frequency value we imaged HOPG coated with 0.5 nm Au.We observed Au islands on HOPG after coating on SEM images shown in Figure 4.52.

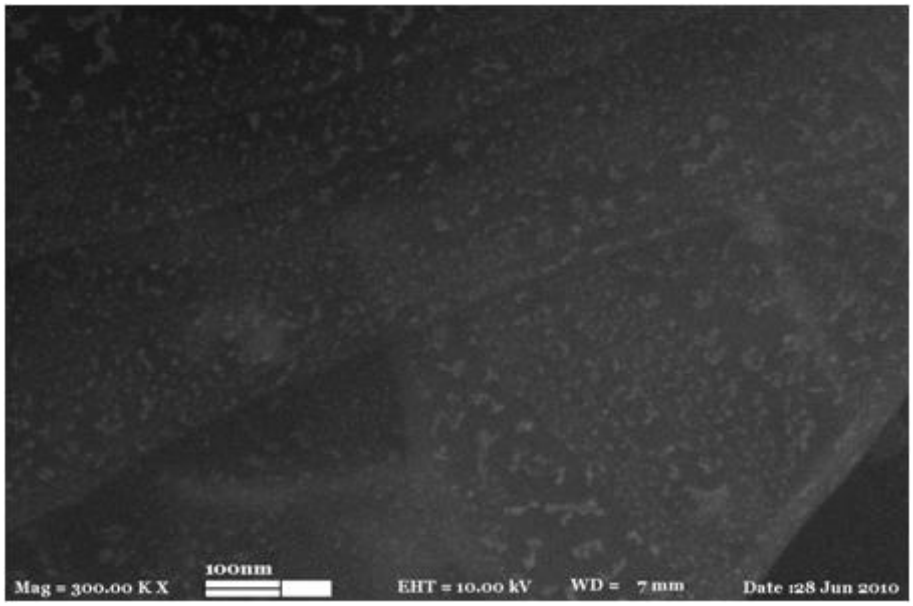

Figure 4.52: SEM image of Au islands on HOPG

We observed Au islands on HOPG also on topography image of AM-KPFM scan shown in Figure 4.53(a) and contrast difference between Au and HOPG on contact potential image shown in Figure 4.53(b). In theory, the work function difference between Au and HOPG is approximately 0.4 eV. We observed the work function difference value fits to the theoretical value (shown in Figure 4.54) at 25 kHz of kelvin probe frequency with the kelvin probe amplitude of 1.5V. The scan speed, the scan area and the images size were 2 μ m/s, 0.5 μ m x 0.5 μ and 256x256 pixels, respectively.

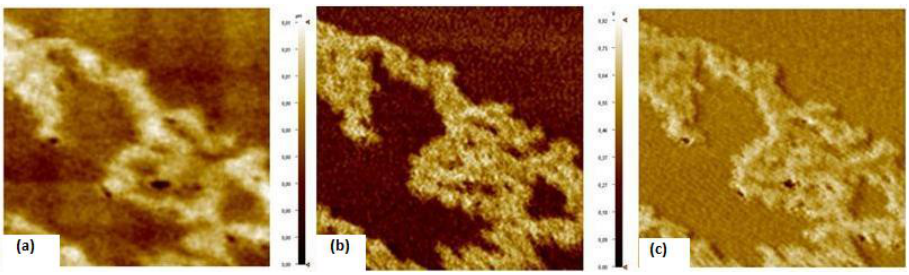

Figure 4.53: (a)Topography image (b)Contact potential image (c)Phase image of Au islands on HOPG

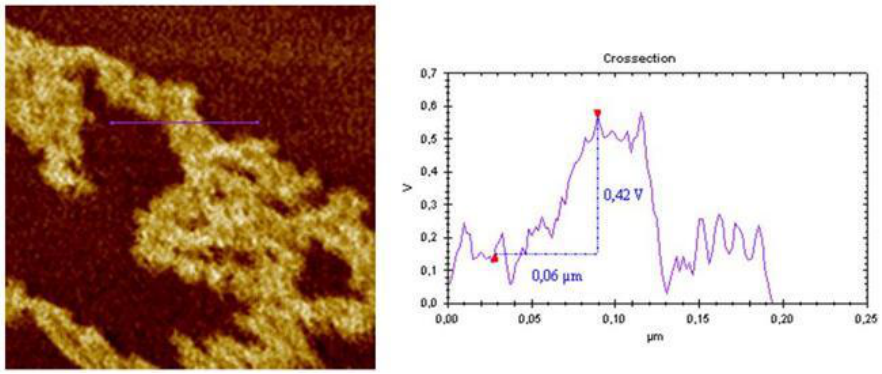

Figure 4.54: Cross section on contact potential image of Au islands on HOPG.

4.3.4 Imaging a sample prepared by electron beam lithography using KPFM

We prepared a sample by electron beam lithography to characterize by KPFM.

E-beam lithography is identical to optical or any other lithographies[**53**]. In e-beam lithography the substrate is coated with a thin layer of resist, which is chemically changed under exposure to the electron beam(shown in Figure 4.55). Thus the exposed areas can be dissolved in a specific solvent.(Dissolving in a specific solvent process called as development) This is called as 'positive lithography'. If the non-exposed areas are dissolved, this is called 'negative lithograph'.

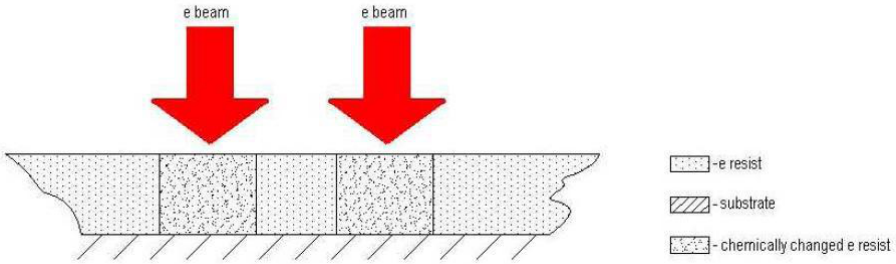

Figure 4.55: Resist cross section[**53**]

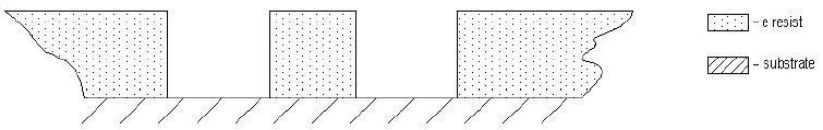

Figure 4.56: Resist cross section.Only the chemically changed e resist can be dissolved in a specific solvent in positive lithography[**53**].

After development process, a thin metallic layer is deposited on the substrate. On the areas exposed to the electron beam the deposited metal sticks to the substrate, while on the unexposed areas the metal sticks to the resist surface.

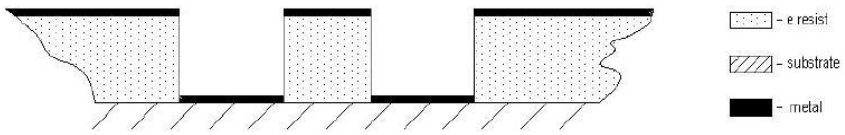

Figure 4.57: Resist cross section after metal deposition[**53**]

After metal deposition the remaining resist is dissolved in an solvent. This process is called 'lift off'. In lift off only the metal sticking to the substrate remains(shown in Figure 4.58).

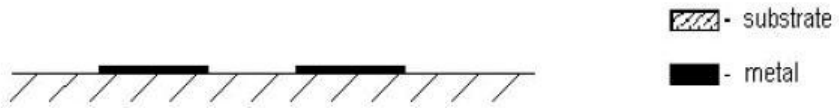

Figure 4.58: Final result cross section[**53**].

After cleaning 300 nm SiO_2 on Si substrates, they were coated with Cr to provide the electrically conductivity. After coating Cr the samples were covered 95-100 nm by C_2 PMMA ((Poly(methyl methacrylate)) which is a positive e-beam resist. After that samples were written by e-beam. The pattern was consist of squares in different sizes. This pattern was designed by Design Cad. After writing by e-beam, in development process the exposed areas were dissolved by solvent which is formed of 3 IPA: 1 MIBK. After development, 3nm Cr and 30 nm Au were deposited on samples by evaporator coating system. After metal deposition lift off process was implemented. In lift off process Au with the remaining resist on the spacing of squares is dissolved, Au sticking to the substrate on insides of squares remained. In this work, different dosage tests were done between 80-600 $\mu C/cm^2$.

The pattern is consist of 5 square arrays with different sizes and a hall probe array as shown in Figure 59. There are square arrays with size of 0.5 μm, 0.2

μm, 0.1 μm and 50 nm. Also there is a hall probe array with size of 0.01 μm. This square arrays were characterized by KPFM. Topography, phase and contact

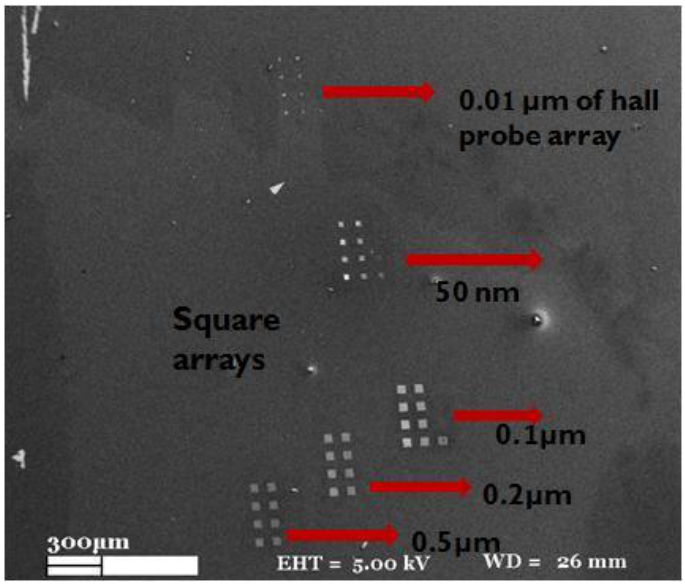

Figure 4.59: SEM image of sample after e-beam lithography.

potential images were obtained simultaneously. The cantilevers used were 5nm Cr and 20 nm Cr coated single crystal silicon cantilevers with the resonance frequency 278 kHz and 40 N/m. f_{KPFM}, A_{KPFM}, the scan speed and the scan size were 25kHz, 1.5V, $2\mu m/s$ and 256x256 pixels, respectively.

Initially, the square array with the size of 0.5 μm and with the dosage of 401 $\mu C/cm^2$ were characterized by AM-KPFM. This array of SEM image(Figure 4.60(a)) and KPFM images(Figure 4.60(c) and 4.60(d)) were given below respectively.

The period of this arrays is 1 μm as shown in the cross section of topography image in Figure A.1(a)

As mentioned before in the end of e-beam lithography in the pattern the spacing of squares are coated with Cr, insides of squares are coated with Au. Hence, in the contact potential image, we should see the work function difference between Cr and Au. The work function of Au varies from 5.1 eV to 5.47 eV. The work function of Cr is 4.5 eV. In Figure 62, the work function difference between Au and Cr was measured 0.56 V, the expected work function difference is between 0.6V and 1V.

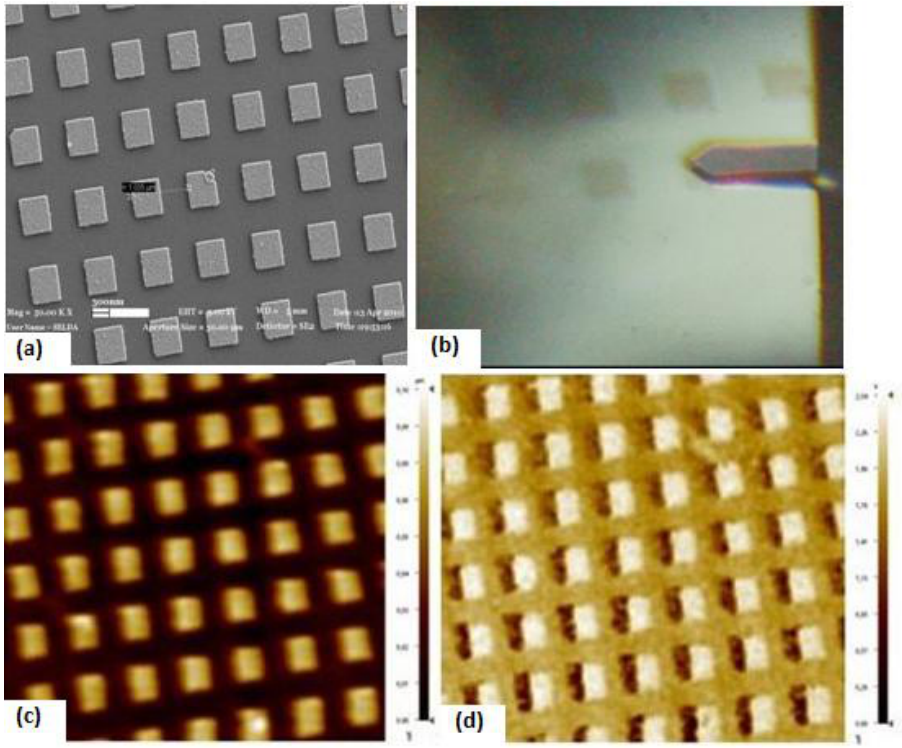

Figure 4.60: (a)SEM image (b)CCD AFM camera image (c)Topography image and(d)CPD image of the square array with the size of 0.5 μm and with the dosage of 401 $\mu C/cm^2$

Secondly, the square arrays with the size of 0.2 μm was imaged. The dosage of the square array with the size of 0.2 μm was 268 $\mu C/cm^2$. The images of SEM and KPFM are shown below.(Figure A.2)

5. CONCLUSION

In this work, the principle of Atomic Force Microscopy and Kelvin Probe Force Microscopy which is modified version of AFM was studied. Understanding the principle of KPFM is important as much as understanding the principle of AFM which is very important for many science researches by giving atomic resolution of materials. Because KPFM is an extremely powerful technique that permits the characterization of electronic properties of materials. It also provides simultaneous high resolution imaging as well as electrical characterization. This technique is performed in many scientific areas on variety of materials such as encompassing metals, classical semiconductors, organic and biological materials etc. Also because of its high voltage resolution it permits the study of surface potential differences with many thin films, including which has poor conductive properties.

Initially in this work, AFM was optimized to obtain the highest quality of images from KPFM. The optimization values of excitation amplitude of cantilever and laser intensity were searched. To achive this, many experiments were made with different parameters and with many kinds of samples.

this work, with Frictional Force Microscopy was also studied. By FFM, the frictional force images of graphene, graphite and SiO_2 were obtained. By calibration of lateral forces, frictional forces of graphene and graphite were calculated and compared. According to results, the frictional force on graphene was larger than on graphite. Also the frictional force on graphene was smaller than on SiO_2.

Amplitude modulation of KPFM and Frequency Modulation of KPFM were compared in this work. When the sample sample was imaged by both of methods, in the AM method the contrast in the work function images was observed as lower

than the FM method. The advantage of AM-mode is the possibility to use low AC voltages.

The work function difference of graphene, graphite and SiO_2 were measured by AM-KPFM. Also work function difference between the single layer graphene and double layer graphene was observed. Also in this experiment it is observed that when the amplitude and frequency of kelvin probe are changed, the work function values are changed. Thus, to calibrate the system and to find the optimized frequency and amplitude of kelvin probe, Au islands on HOPG were imaged with KPFM.

Also from the experiments in AM-KPFM method, it appeared that when the amplitude of AC voltages are decreased, the resolution of contact potential images is increased.

Finally a sample prepared by Electron Beam Lithography was characterized by AM-KPFM in this work. Work function differences of different metals(Au and Cr) on the pattern of sample was measured.

REFERENCES

[1] **Hertz, H.**, 1882. On the Contact of Elastic Solids, *In Jones and Schott Editors*

[2] **Hund, F.**, 1927.*Z. Phys.* **40**, 742.

[3] **Lee-Desaultels, R.**, 2005. Theory of van der waals forces as applied to pParticlate materials.

[4] **Young, R.,Ward, J. and Scire, F.**,1972. The topografiner: An instrument for measuring surface microtopography, *Rev. Sci. Instrum.* **43**, 999-1011.

[5] **Binnig, G. and Rohrer, H.**,1986. Scanning tunneling microscopy, *IBM Journal of Research and Development* **34**, 4.

[6] **Eigler, D.M. and Schweizer, E.K.**, 1990. Positioning single atoms with a scanning tunneling microscope *Nature*, **344** 524.

[7] **Binnig, G., Quate, C.F and Gerber, Ch.**, 1986. Atomic force microscope, *Phys. Rev. Lett.* **56**, 930.

[8] **Giaver I.**, 1960. Energy gap in superconductors measured by electron tunneling, *Phys. Rev. Lett.* **5**, 147-148.

[9] **Binnig, G. and Rohrer H.**, 1987. Scanning tunneling microscopy-from birth to adolescence, *Rev. Mod. Phys.* **59**, 615-625.

[10] **Binnig, G., Gerber, Ch., Stoll, E., Albrecht, T.R. and Quate, C.F**, 1987. Atomic resolution with atomic force Microscope*Europhys. Lett.***3**, 1281.

[11] **Martin, Y., Williams, C.C. and Wickramasinghe, J.**, 1987. Atomic force microscope-force mapping and profiling on a sub 100-$\mathring{A}$ scale *Appl. Phys. Lett.* **61**, 4723.

[12] **Marti, O. Drake, B. and Hansma, P.K.**, 1987. Atomic force microscopy of liquid-covered surfaces: Atomic resolution images.*Appl. Phys. Lett.* **51**, 484.

[13] **Albrecht, T.R., Akamine, S. Carver, T.E. and Quate, C.F.**, 1990. Microfabrication of cantilever styli for the atomic force microscope *J. Vac. Sci. Technol. A.* **8**, 3386

[14] **Mate, C.M., McClelland, G.M., Erlandsson, R., and et al.**, 1987. Atomic-scale friction of a tungsten tip on a graphite surface *Phys. Rev.Lett.* **59**, 1942.

[15] **Neubauer, N., Cohen, S.R. and McClelland G.M.**, 1990. Nanomechanics of a Au-Ir Contact Using a Bidirectional Atomic Force Microscope,*J. Vac. Sci. Technol. A.* **8**, 3449

[16] **Meyer, G. and Amer, N.M.**, 1990. Simultaneous measurement of lateral and normal forces with an optical-beam-deflection atomic force microscope *Appl. Phys. Lett.* **57**, 2089-2091.

[17] **Martin, Y., Williams, C.C. and Wickramasinghe, J.**, 1988. High-resolution capacitance measurement and potentiometry by force microscopy Appl. Phys. Lett. **52**, 1103.

[18] **Erlandsson, R., McClelland, G.M.,Mate, C.M. and Chiang S.**, 1988. Atomic force microscopy using optical interferometry *J. Vac. Sci. Technol. A* **6**, 266.

[19] **Terris, B.D., Stern, J.E., Rugar, D. and Mamin, H.J.**, 1989. Contact electrification using force microscopy *Phys. Rev.Lett.* **63**, 2669

[20] **Weaver, J.M.R. and Abraham, D.W.**, 1991. High resolution atomic force microscopy potentiometry*J. Vac. Sci. Technol. B* **9**, 1559.

[21] **Nonnenmacher, M., O'Boyle and Wickramasinghe, H.K.**, 1991. Kelvin probe force microscopy *Appl. Phys. Lett.* **58**, 2921.

[22] **Binnig, G., Quate, C.F. and Gerber, Ch.**, 1986. Atomic Force Microscopy,*Physic. Rev. Lett.* **56**, 930-933.

[23] **Bhushan, B.(Ed.)**, Springer Handbook of Nanotechnology(2nd Edition), 616-621.

[24] **Lifshitz, E.M.**, 1956. The theory of molecular attractive forces between solids *Soviet Phys.* **2**, 73.

[25] **Hartmann, U.**, 1991. van der Waals interactions between sharp probes and flat sample surfaces *Phys. Rev. B* **43**, 2404.

[26] **Burnham, N. and Colton, R.J.**, 1989. Measuring the nanomechanical and surface forces of materials using an atomic force microscope *J. Vac. Sci. Technol A* **7**, 2906-2913.

[27] **Albrecht, T. R.,Grutter, P.,Horne, H. K. and Rugar, D.**, 1991. Frequency modulation detection using high-Q cantilevers for enhanced force microscope sensitivity *J. Appl. Phys.* **69**, 668-673.

[28] **Bhushan, B.(Ed.)**, Springer Handbook of Nanotechnology(2nd Edition), 684.

[29] **Stern J.E., Terris B.D., Mamin H.J.,Rugar D.**, 1988. Deposition and imaging of localized charge on insulator surfaces using a force microscopy *Appl.Phys. Lett.* **53**, 2717.

[30] **Kikukawa, A., Hosaka, S., and Imura, R.**, 1995. Silicon pn junction imaging and characterizations using sensitivity enhanced Kelvin probe force microscopy *Appl. Phys. Lett.* **66**, 25.

[31] **Sommerhalter, Ch.,Matthes, Th. W., Glatzel, Th. and et.al.**, 1999. High-sensitivity quantitative Kelvin probe microscopy

by noncontact ultra-high-vacuum atomic force microscopy *Appl.Phys. Lett.* **75**, 2.

[32] **Kitamura, S., Suzuki, K., Iwatsuki, M. and Mooney, C.B.**, 1999. Atomic-scale variations in contact potential difference on Au/Si(111) 7x7 surface in ultrahigh vacuum *Appl. Surface Sci.* **157**, 222-227.

[33] **Burnham, N.A.,Colton, R.J. and Pollock, H.M.**, 1992. Work-function Anisotropies as an Origin of Long-Range Surface Forces. *Phys. Rev. lett.* **69**, 144.

[34] **Glatzel, Th., Sadewasser, S. and Lux-Steiner, M.Ch.**, 2003. Amplitude or frequency modulation-detection in Kelvin probe force microscopy *Appl. Surface Sci.* **210**, 84-89.

[35] **Lu, J., Guggisberg, B., Luthi, R., Kubon, M., Scandella, L., Gerber, C., Meyer, E. and Guntherodt, H.J.**, 1998. Surface potential studies using Kelvin force spectroscopy *Appl. Phys. A* **66**, S-273.

[36] **Leveque, G., Girard, P., Skouri, E. and Yarekha, D.**, 2000. Kelvin probe force microscopy using near-field optical tips *Appl. Surface Sci.* **157**, 251.

[37] **Seshadri, I.P. and Bhushan, B.**, 2008. Effect of rubbing load on nanoscale charging characteristics of human hair characterized by AFM based Kelvin probe *J. of C. and Int. Sci.* **325**, 580-587.

[38] **Filleter, T., Emtsev, K. V.,Seyller Th. and Bennewitz, R.,**, 2008. Local work function measurements of epitaxial graphene *Appl. Phys. Lett.* **93**, 133117.

[39] **Palermo, V., Palma, M. and Samori, P.**, 2006. Electronic Characterization of Organic Thin Films by Kelvin Probe Force Microscopy *Adv Matter* **18**, 145-164.

[40] **de Wit, J.H.W.** , 2004. Local potential measurements with the SKPFM on aluminium alloys *Electrochimica Acta* **49**, 2841-2850.

[41] **Zerweck, U.,Loppacher, C., Otto, T., Grafström, S. and Eng, L.M.**, 2007. Kelvin probe force microscopy of C60 on metal substrates: towards molecular resolution *Nanotechnology* **18**, 084006.

[42] **Kitamura, S., Suzuki K. and Iwatsuki, M.**, 1999. High resolution imaging of contact potential difference using a novel ultrahigh vacuum non-contact atomic force microscope technique *Appl. Surface Sci.* **140**, 265-270.

[43] **Encinas J.**,1993. Phase Lock Loops *Springer*

[44] **Münir Dede**,2008. PhD thesis of development of nano hall sensors for high resoulution scanning hall probe microscopy

[45] Stanford Research Systems, Application Note 3.

[**46**] Philips Research,From CD to Blu-ray.

[**47**] **Novoselov, K.S and Geim, A.K.**, 2007. The rise of graphene. *Nature materials* **6**, 183-191.

[**48**] **Peierls, R.E.**, 1935. Quelques proprietes typiques des corpses solides. *Ann. I. H. Poincare* **5**, 172-222.

[**49**] **Landau, L.D.**, 1937. Zur Theorie der phasenumwandlungen II. *Phys. Z. Sowjetunion* **11**, 26-35.

[**50**] **Novoselov, K.S., Geim, A.K., Morozov, S.V., Jiang, D., Zhang, Y., Dubonos, S.V., Grigorieva, I.V. and Firsov, A.**, 2004. Electric Field Effect in Atomically Thin Carbon Films *Science* **306**, 666-669.

[**51**] **Zhenhua, N., Yingying, W., Ting, Y. and Zexiang, S.**, 2008.Raman Spectroscopy and Imaging of Graphene *Nano Res* **1**, 273-291.

[**52**] **Graf, D., Molitor, F.,Ensslin, K., Stampfer, C., Jungen ,A., Hierold, C. and Wirtz, L.**, 2007. Spatially Resolved Raman Spectroscopy of Single adn Few-Layer Graphene*Nano Letters* **7**, 238-242.

[**53**] **Bostjan Bercic** Introduction to Electron Beam Lithography

[**54**] **Fukuma, T., Kimura, M., Kobayashi, K., Matsushige, K. and Yamada, H.** 2005. Development of low noise cantilever deflection sensor for multi environment frequency-modulation atomic force microscopy *Rev. Sci. Instrum.* **76**, 053704

[**55**] **Kelvin, L.** 1898. On Contact Electricity of Metals*Phil. Mag.* **46**, 82-120.

[**56**] A Practical Guide to Scanning Probe Microscopy *Park Scientific Instruments*

APPENDICES

APPENDIX A.1: Figures

APPENDIX A.1

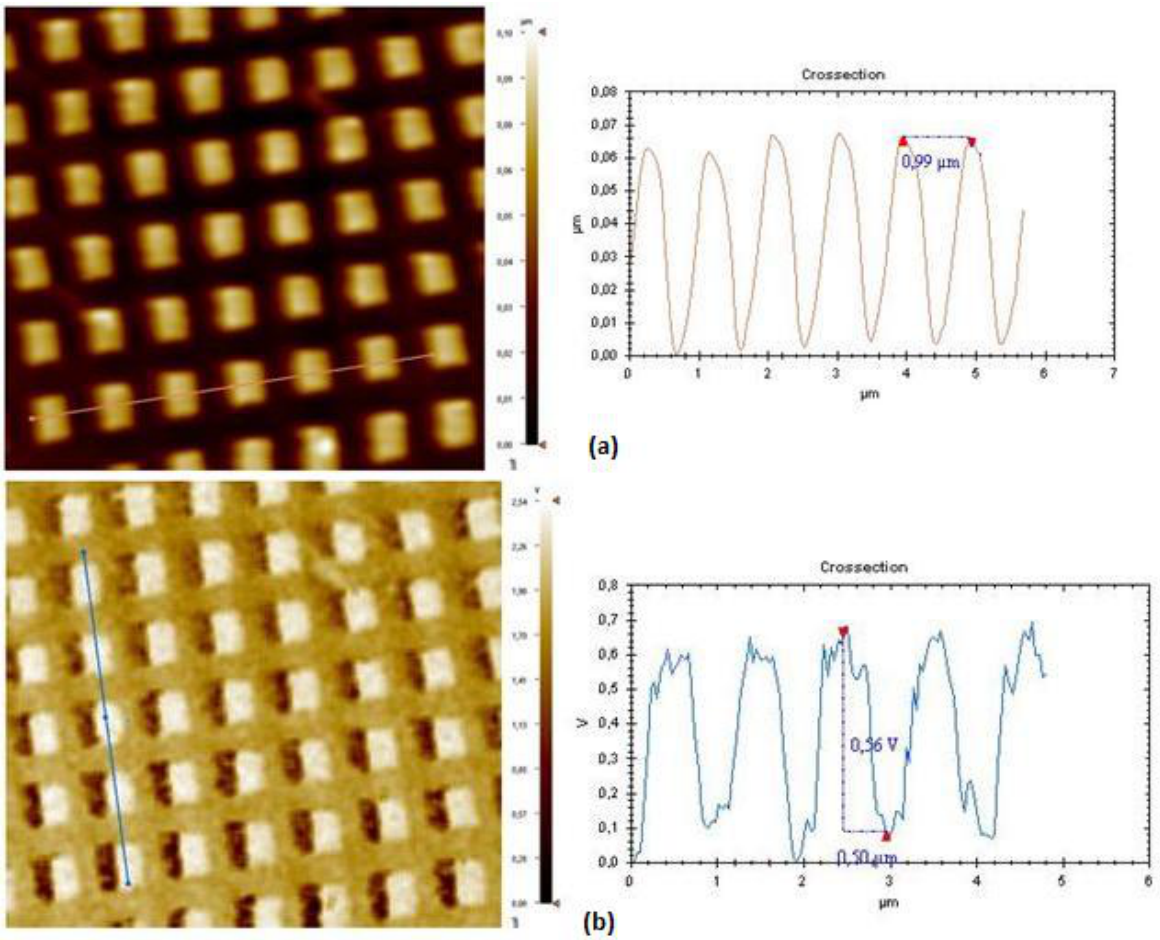

Figure A.1: (a)Cross section on topography image of AM-KPFM scan of the square array with the size of 0.5 μm and with the dosage of 401 $\mu C/cm^2$ on topography image (b) Cross section on CPD image of AM-KPFM scan of the square array with the size of 0.5 μm and with the dosage of 401 $\mu C/cm^2$

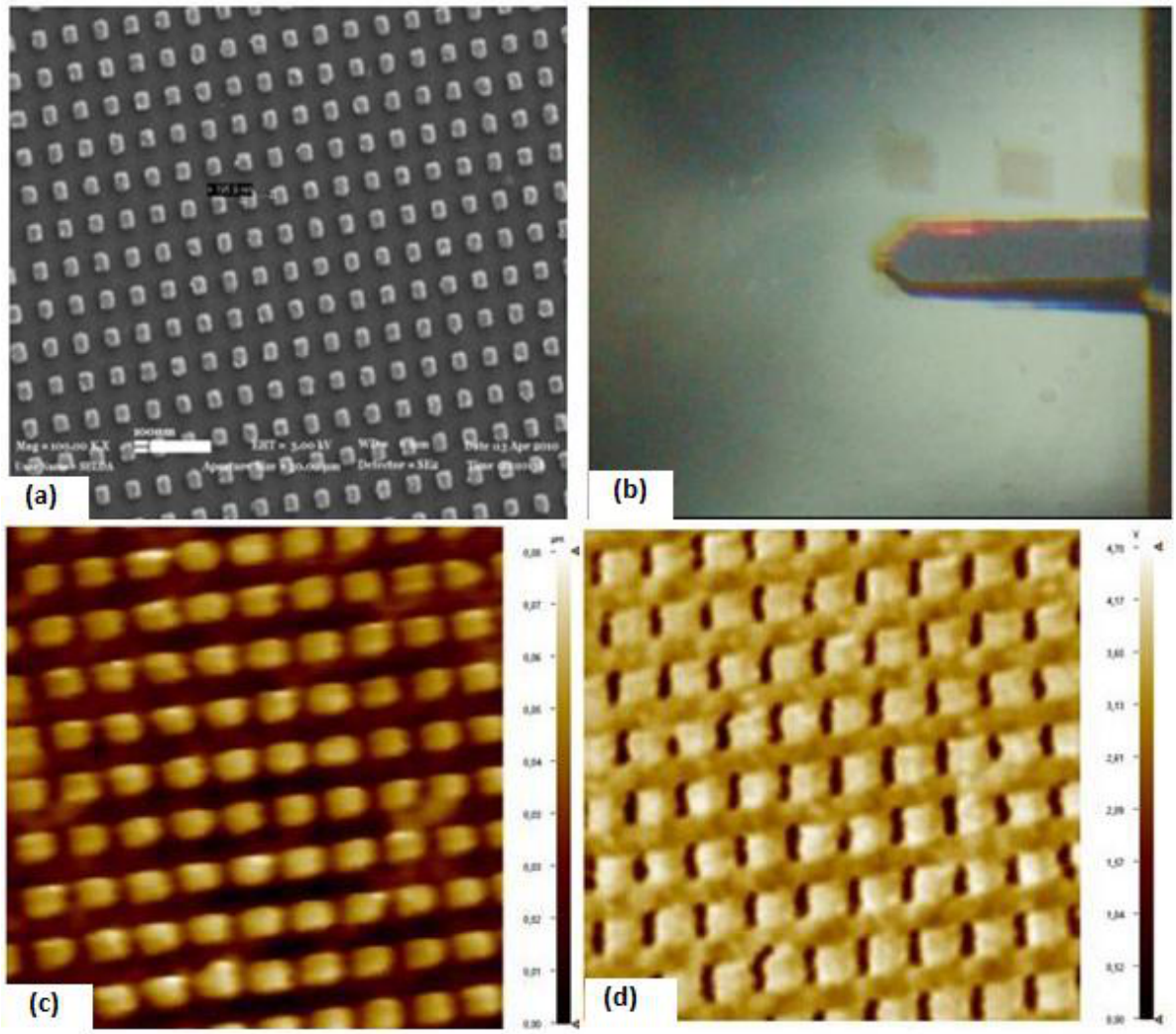

Figure A.2: (a)SEM image (b)CCD AFM camera image (c)Topography image and(d)CPD image of the square array with the size of 0.2 μm and with the dosage of 268 $\mu C/cm^2$

CURRICULUM VITAE

Candidate's full name: Nihan ÖZKAN

Place and date of birth: Edirne, 23.08.1984

Universities and Colleges attended:

2002-2010 Physics Engineering Master of Science-İstanbul Technical University

2002-2007 Physics Education-Dokuz Eylül University

1994-2002 H.F.Z. Anotalian High School